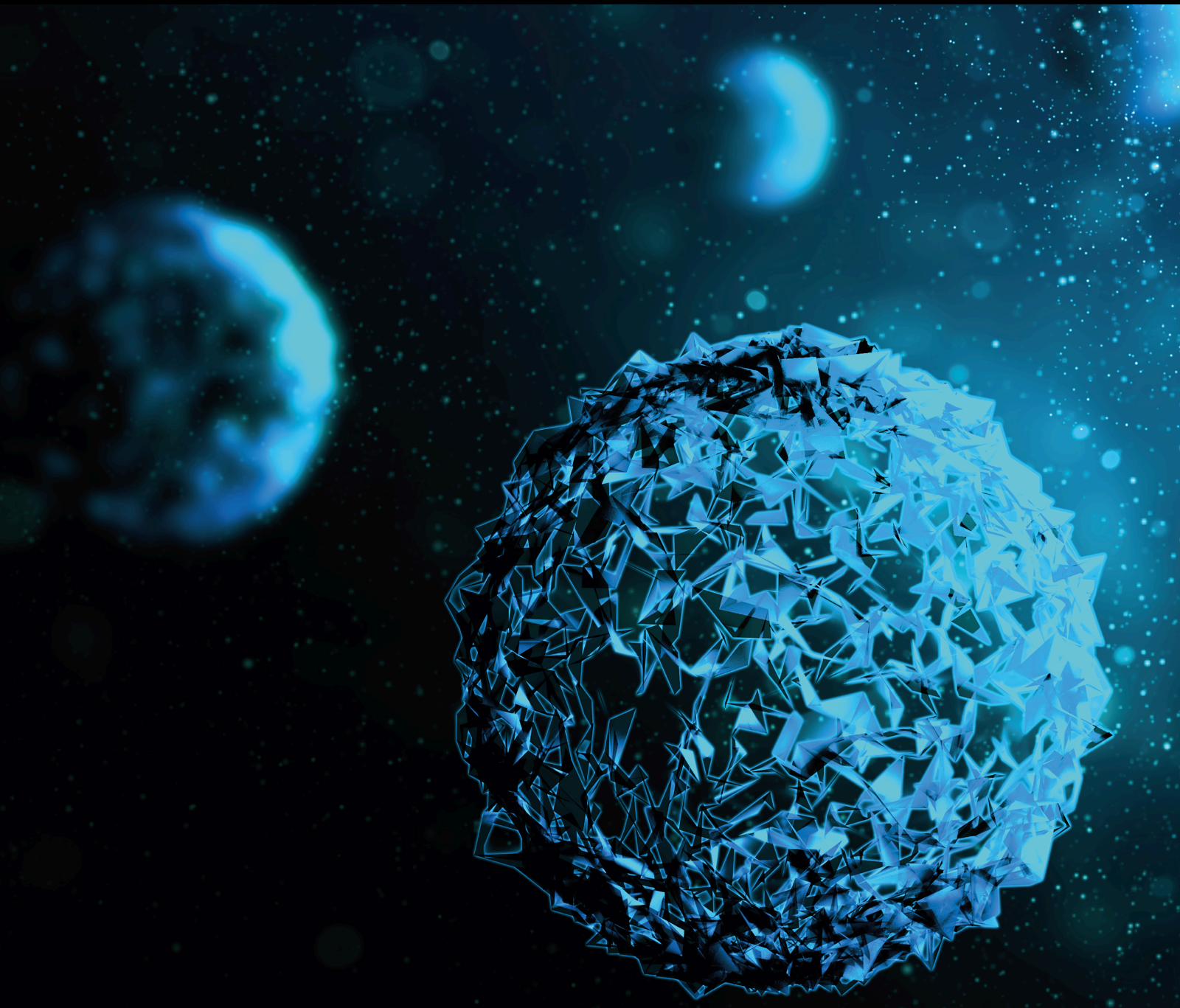


# Redox Imbalance in Chronic Inflammatory Diseases

Special Issue Editor in Chief: Ziqing Li

Guest Editors: Dongliang Xu, Xinhua Li, Yilun Deng, and Chaohong Li



---



# **Redox Imbalance in Chronic Inflammatory Diseases**

BioMed Research International

---

## **Redox Imbalance in Chronic Inflammatory Diseases**

Special Issue Editor in Chief: Ziqing Li

Guest Editors: Dongliang Xu, Xinhua Li, Yilun  
Deng, and Chaohong Li



---

Copyright © 2022 Hindawi Limited. All rights reserved.

This is a special issue published in "BioMed Research International." All articles are open access articles distributed under the Creative Commons Attribution License, which permits unrestricted use, distribution, and reproduction in any medium, provided the original work is properly cited.

## **Editorial Board**

Aziz A. Chentoufi, Saudi Arabia  
Shtaywy S. Abdalla, Jordan  
Saheem Ahmad, Saudi Arabia  
Juan-Manuel Anaya, Colombia  
Paul Ashwood, USA  
Shuai Chen, China  
Michele Rosario Colonna, Italy  
Clara Crescioli, Italy  
Urszula Demkow, Poland  
Mirosława Ferens-Sieczkowska, Poland  
Silvia Gregori, Italy  
Thomas Griffith, USA  
ganesh ingavle, India  
Ziqing Li, China  
Jun Lu, China  
Prasanth Manohar, China  
Marija Mostarica-Stojković, Serbia  
Kanury V S Rao, India  
Yves Renaudineau, France  
FJ Sánchez-García, Mexico  
Harry W. Schroeder, USA  
Arif Siddiqui, Saudi Arabia  
João S. Silva, Brazil  
Hannes Stockinger, Austria  
Asmaa M. Zahran, Egypt  
Zi-Ji Zhang, China

## Contents

### **Redox Imbalance in Chronic Inflammatory Diseases**

Ziqing Li , Dongliang Xu, Xinhua Li, Yilun Deng, and Chaohong Li  
Editorial (3 pages), Article ID 9813486, Volume 2022 (2022)

### **Video-Assisted Health Education Promotes Rehabilitation Training of Total Knee Arthroplasty Patients and Reduces Stress and Burnout in Nurses Compared to Oral Education**

Ping Li , Xing Li , Hua Meng , Ling Huang , Li Zhang , Shuang Wang , and Shaohua Chen   
Research Article (6 pages), Article ID 5058899, Volume 2021 (2021)

### **Therapeutic Applications of Nanozymes in Chronic Inflammatory Diseases**

Haojue Wang, Zichen Cui, Xuan Wang, Shui Sun, Dongsheng Zhang, and Chuanyun Fu   
Review Article (9 pages), Article ID 9980127, Volume 2021 (2021)

### **A Study on COMP and CTX-II as Molecular Markers for the Diagnosis of Intervertebral Disc Degeneration**

Dong-Duo Qi , Zhong-Han Liu , De-Sheng Wu , and Yu-Feng Huang   
Research Article (10 pages), Article ID 3371091, Volume 2021 (2021)

### **The Antioxidant Resveratrol Protects against Chondrocyte Apoptosis by Regulating the COX-2/NF- $\kappa$ B Pathway in Created Temporomandibular Osteoarthritis**

Wen Li , Shiyu Hu , Xuepeng Chen , and Jiejun Shi   
Research Article (7 pages), Article ID 9978651, Volume 2021 (2021)

### **miR-125a-5p Regulates Osteogenic Differentiation of Human Adipose-Derived Mesenchymal Stem Cells under Oxidative Stress**

Yongheng Ye , Quan Liu, Changzhao Li , and Peiheng He   
Research Article (9 pages), Article ID 6684709, Volume 2021 (2021)

### **Identification of Critical Genes and lncRNAs in Osteolysis after Total Hip Arthroplasty and Osteoarthritis by RNA Sequencing**

Guang Yang , Kai Tang, Li Qiao, Yixin Li, and Shui Sun   
Research Article (13 pages), Article ID 6681925, Volume 2021 (2021)

### **Icariin Promotes the Osteogenesis of Bone Marrow Mesenchymal Stem Cells through Regulating Sclerostin and Activating the Wnt/ $\beta$ -Catenin Signaling Pathway**

Jianliang Gao, Shouyu Xiang, Xiao Wei, Ram Ishwar Yadav, Menghu Han, Weihao Zheng, Lili Zhao, Yichuan Shi, and Yanming Cao   
Research Article (10 pages), Article ID 6666836, Volume 2021 (2021)

## Editorial

# Redox Imbalance in Chronic Inflammatory Diseases

Ziqing Li <sup>1,2</sup>, Dongliang Xu,<sup>3</sup> Xinhua Li,<sup>4</sup> Yilun Deng,<sup>5</sup> and Chaohong Li<sup>6</sup>

<sup>1</sup>Department of Joint Surgery, Shandong Provincial Hospital Affiliated to Shandong First Medical University, Jinan, China

<sup>2</sup>Orthopaedic Research Laboratory, Medical Science and Technology Innovation Center, Shandong First Medical University & Shandong Academy of Medical Sciences, Jinan, China

<sup>3</sup>Department of Joint Surgery, The First Affiliated Hospital of Sun Yat-Sen University, Sun Yat-Sen University, Guangzhou, China

<sup>4</sup>Department of Orthopedics, Shanghai General Hospital, Shanghai Jiao Tong University School of Medicine, Shanghai, China

<sup>5</sup>Department of Medicine, Hematology & Oncology Division, University of Texas Health San Antonio, San Antonio, USA

<sup>6</sup>Department of Histology and Embryology, Zhongshan School of Medicine, Sun Yat-Sen University, Guangzhou, China

Correspondence should be addressed to Ziqing Li; [liziqing@sdfmu.edu.cn](mailto:liziqing@sdfmu.edu.cn)

Received 19 March 2022; Accepted 19 March 2022; Published 8 April 2022

Copyright © 2022 Ziqing Li et al. This is an open access article distributed under the Creative Commons Attribution License, which permits unrestricted use, distribution, and reproduction in any medium, provided the original work is properly cited.

Redox homeostasis, a crucial determinant of physiological processes that maintain the health of cellular function, is intimately relying on the balance between prooxidative productions and concomitant antioxidant defense system [1, 2]. Often caused by an aggressive accumulation of reactive oxygen species (ROS) or weakened antioxidant defenses in multiple organs, stubborn redox imbalance is one of the notorious features in patients suffering from chronic inflammatory diseases [2]. ROS are produced in all cell types as byproducts of the mitochondrial electron transport chain (ETC) during ATP synthesis or formed by NADPH oxidase (NOX) in a controlled manner for targeted purposes such as the respiratory burst in macrophages and neutrophils against microbial invasion [3]. In turn, organisms have evolved several defense mechanisms to detoxify ROS, ranging from transcription factors to enzymes that elevated intracellular antioxidative defenses [4, 5]. Also, many natural products and organic compounds demonstrate a prominent protective effect of antioxidants on targeted tissues, contributing to the relief of chronic inflammatory symptoms in patients [6]. Therefore, understanding the complicated relationship between redox regulation and concomitant inflammatory consequences, from a molecular basis to tissue levels, represents a significant challenge for developing efficient therapeutics for chronic inflammatory diseases. This special issue is aimed at presenting recent research efforts in both molecular and macro mechanisms of redox regulation

during the chronic inflammatory process and the novel role of antioxidant factors in protecting organs from chronic inflammatory damage.

Bone marrow mesenchymal stem cell- (BMSC-) based therapy is a promising strategy for osteoporosis (OP) treatment. The study by J. Gao et al. reports Icaria (ICA), a traditional Chinese medicine that is used for tonifying the kidneys, could also promote the proliferation and osteogenic differentiation of BMSCs through the sclerostin/Wnt/ $\beta$ -catenin signaling pathway. By overexpressing or knocking down sclerostin gene in rat BMSCs, the authors found that sclerostin significantly inhibited BMSC proliferation and downregulated osteogenic genes (Runx2,  $\beta$ -catenin, and c-myc) and antioxidant factors (Prdx1, Cata, and Nqo1), whereas the presence of ICA could restore these inhibitory effects via the activation of Wnt/ $\beta$ -catenin pathway and the upregulation of antioxidant factors. Therefore, ICA may promote the therapeutic efficiency of BMSC-based regenerative therapy for OP.

Osteoarthritis (OA) is a debilitating disease and leads to chronic disability in old people, whereas total hip arthroplasty (THA) is an effective way for late-stage treatment. However, as a severe complication of THA, osteolysis leads to prosthesis loosening and additional revision surgery for OA patients. By using RNA sequencing, the study by G. Yang et al. explores the relevant molecular biomarkers for osteolysis after THA and identifies expressed mRNAs and

lncRNAs during OA and osteolysis. The authors highlighted four identical interaction pairs, including two shared lncRNA-mRNA interaction pairs during OA and osteolysis (AC111000.4-CD8A and AC016831.6-CD8B) and other two osteolysis-specific interaction pairs (AC090607.4-FOXO3 and TAL1-BALON), contributing to the understanding of osteolysis pathophysiology.

Oxidative stress and microRNAs (miRNAs/miRs) affect the osteogenic induction of adipose-derived mesenchymal stem cells (ADSCs). The study by Y. Ye et al. investigates the mechanism of miR-125a-5p in regulating the osteogenesis of human ADSCs (hADSCs) under oxidative stress and finds that the expression of miR-125a-5p was negatively correlated with the osteogenic differentiation of hADSCs. The authors further demonstrated that miR-125a-5p was induced under oxidative stress and inhibited the expression of VEGF, leading to the reduction of osteogenic differentiation of hADSCs and proving to be a potential clinical target for bone repairing.

Temporomandibular joint osteoarthritis (TMJOA) is a typical chronic inflammatory disease characterized by the degradation of mandibular condylar cartilage (MCC). NF- $\kappa$ B plays a crucial role in the inflammatory and immune responses during the development of TMJOA. The study by W. Li et al. investigates the protective effects of resveratrol (RES) against MCC degradation via antioxidant characteristics and regulation of COX-2/NF- $\kappa$ B expression. The authors showed that RES could reverse the MCC degradation caused by inflammation. For the mechanism study, RES exerted the antioxidant effects by downregulating COX-2/NF- $\kappa$ B/MMP expression and increasing cartilage markers, suggesting the therapeutic effects of RES against chondrocyte apoptosis of MCC during TMJOA.

Intervertebral disc degeneration (IVDD) is bound up with oxidative stress that caused intervertebral disc senescence. A clear diagnosis of IVDD at the early stage is pretty challenging. To assess the application value of serum cartilage oligomeric matrix protein (COMP) and extracellular matrix degradation products of C-telopeptide of type II collagen (CTX-II) as molecular markers for IVDD diagnosis, a comprehensive analysis based on protein expression, histological, and MRI changes in adult male rats during IVDD was carried out by D.-D. Qi et al. The authors reported that the expressions of COMP and CTX-II increased with the process of IVDD. Moreover, oxidative stress markers were found to correlate with CTX-II and COMP, wherein MDA (malondialdehyde) was positively correlated and SOD (superoxide dismutase) was negatively correlated with CTX-II and COMP, indicating reliable diagnostic markers for IVDD.

Promoting rehabilitation training in postoperative patients reduces overall oxidative stress caused by OA and surgical trauma. Compared with traditional oral education, video-assisted health education is believed to be an effective way in accelerating rehabilitation. By assessing clinical outcomes, inflammatory biomarkers, and monitoring rehabilitation progress of postoperative patients, P. Li et al. evaluate the effectiveness of video-assisted health education in promoting the postoperative rehabilitation of OA patients, as well as

in reducing the job stress and burnout of participated nurses. The authors suggested that video-assisted health education could significantly promote patients' recovery after receiving total knee arthroplasty and reduce job stress in nurses when compared with traditional oral education.

Due to excellent characteristics (high efficiency, sustained stability, and low costs) compared to natural enzymes, nanozymes have been widely studied and applied in various fields such as clinical medicine, basic science, chemical engineering, food industry, and even agriculture. The review by H. Wang et al. summarizes the utilization development of nanozymes in the medicine field and discusses the therapeutic applications of antioxidant-like properties of nanozymes in treating chronic inflammatory diseases. In addition, multiple materials and different types of nanozymes that are used for the treatment of chronic inflammatory diseases were also summarized in this review.

In conclusion, a comprehensive understanding of ongoing efforts would help researchers to identify efficient approaches in the field and eventually lead to the successful discovery of therapeutics. The guest editorial team wishes that this special issue will help in evidencing research from multiple disciplines in this area and encourage future collaborations from multidisciplinary aspects.

## Conflicts of Interest

The editors declare that there are no conflicts of interest regarding the publication of this special issue.

## Acknowledgments

We would like to express our great gratitude to all authors and reviewers who contributed to this special issue. Special thanks to Dr. Guangpu Yang (The Chinese University of Hong Kong), who served as an academic specialist to our special issue. *Ziqing Li, Dongliang Xu, Xinhua Li, Yilun Deng, Chaohong Li.*

*Ziqing Li  
Dongliang Xu  
Xinhua Li  
Yilun Deng  
Chaohong Li*

## References

- [1] A. V. Snezhkina, A. V. Kudryavtseva, O. L. Kardymon et al., "ROS generation and antioxidant defense systems in normal and malignant cells," *Oxidative Medicine and Cellular Longevity*, vol. 2019, Article ID 6175804, 17 pages, 2019.
- [2] H. Sies and D. P. Jones, "Reactive oxygen species (ROS) as pleiotropic physiological signalling agents," *Nature Reviews. Molecular Cell Biology*, vol. 21, no. 7, pp. 363–383, 2020.
- [3] K. Schroder, "NADPH oxidases in bone homeostasis and osteoporosis," *Free Radical Biology & Medicine*, vol. 132, pp. 67–72, 2019.
- [4] J. Zhang, X. Wang, V. Vikash et al., "ROS and ROS-mediated cellular signaling," *Oxidative Medicine and Cellular Longevity*, vol. 2016, Article ID 4350965, 67 pages, 2016.

- [5] J. Jezek, K. F. Cooper, and R. Strich, "Reactive oxygen species and mitochondrial dynamics: the yin and yang of mitochondrial dysfunction and cancer progression," *Antioxidants*, vol. 7, no. 1, article 13, 2018.
- [6] S. F. Hosseini, M. Rezaei, and D. J. McClements, "Bioactive functional ingredients from aquatic origin: a review of recent progress in marine-derived nutraceuticals," *Critical Reviews in Food Science and Nutrition*, vol. 62, no. 5, pp. 1242–1269, 2022.

## Research Article

# Video-Assisted Health Education Promotes Rehabilitation Training of Total Knee Arthroplasty Patients and Reduces Stress and Burnout in Nurses Compared to Oral Education

Ping Li <sup>1</sup>, Xing Li <sup>2</sup>, Hua Meng <sup>3</sup>, Ling Huang <sup>1</sup>, Li Zhang <sup>1</sup>, Shuang Wang <sup>1</sup>,  
and Shaohua Chen <sup>2</sup>

<sup>1</sup>Department of Joint Surgery, Shandong Provincial Hospital Affiliated to Shandong First Medical University, Jinan 250000, China

<sup>2</sup>Department of Orthopedic Surgery, The Second Affiliated Hospital of Guangzhou University of Chinese Medicine, Guangzhou 510120, China

<sup>3</sup>Department of Joint Surgery/Sports Medicine, The Second Hospital, Cheeloo College of Medicine, Shandong University, Jinan 250033, China

Correspondence should be addressed to Shuang Wang; wangshuang200803@163.com and Shaohua Chen; shi-8232@163.com

Received 6 April 2021; Revised 16 July 2021; Accepted 20 September 2021; Published 22 October 2021

Academic Editor: Chaohong Li

Copyright © 2021 Ping Li et al. This is an open access article distributed under the Creative Commons Attribution License, which permits unrestricted use, distribution, and reproduction in any medium, provided the original work is properly cited.

Emerging evidence suggests video-assisted health education being an effective way in promoting rehabilitation. The present study was aimed at evaluating the effectiveness of video-assisted health education in promoting rehabilitation training in postoperative OA patients and at comparing it with oral education. This study was a noncontemporaneous control study involving 179 patients who underwent TKA. For the intervention group, a bedside interactive system that recorded a series of educational videos showing a rehabilitation training program was established. For the control group, oral education having the same content as that in the videos for the intervention group was provided. After education, clinical outcomes such as occurrence of complications, circulating biomarkers of inflammation, and rehabilitation progress of the patients were obtained. Furthermore, job stress and burnout in nurses who participated in the present study were assessed. Results showed that C-reactive protein levels of patients were significantly lower in the intervention group than in the control group ( $84.54 \pm 36.09$  vs.  $99.45 \pm 31.73$  mg/L,  $P = 0.004$ ). Faster achievement of postoperative knee flexion to 90 degrees ( $21.31 \pm 5.83$  vs.  $35.72 \pm 9.93$  h,  $P < 0.001$ ) and first ambulation ( $19.91 \pm 4.57$  vs.  $50.15 \pm 7.00$  h,  $P < 0.001$ ), reduced number of postoperative complications such as postoperative orthostatic intolerance (7 vs. 19,  $P = 0.008$ ) and constipation (10 vs. 23,  $P = 0.009$ ), and reduced length of hospital stay ( $7.51 \pm 1.79$  vs.  $8.21 \pm 2.15$  days,  $P = 0.019$ ) in the intervention group in comparison to the control group were noted. Emotional exhaustion and burnout of nurses were reduced significantly in the intervention group than in the control group ( $21.00 \pm 8.04$  vs.  $36.50 \pm 11.22$ ,  $P = 0.002$ ;  $55.90 \pm 11.57$  vs.  $85.50 \pm 6.80$ ,  $P < 0.001$ , respectively). Reduced personal accomplishments in nurses were improved significantly in the intervention group when compared with the control group ( $41.90 \pm 4.91$  vs.  $32.80 \pm 7.07$ ,  $P = 0.004$ ). We concluded that video-assisted health education may promote TKA patient recovery and reduce burnout and stress in nurses when compared with oral education. Video-assisted health education could be helpful in situation where manpower of nurse is in shortage.

## 1. Introduction

Knee osteoarthritis (KOA) is a chronic, progressive, and recurrent joint disorder that leads to joint instability and physical disability [1]. KOA is multifactorial in origin, and both inflammatory and biomechanical whole-organ disease

processes play an important role in disease progression [2–4] that is affected by several factors, including family history, age, obesity, diabetes, and synovitis [5]. KOA has a prevalence rate of up to 8.1% with a higher frequency among women than among men at any given age more than 50 years old [5]. For patients who are at the end stage of

KOA, total knee arthroplasty (TKA) has been demonstrated to be an effective treatment [6] and postoperative training after TKA is receiving growing attention from clinicians globally.

Elevated immune response was observed following TKA procedures. Increased immune response, systematic or localized, to acute oxidative stress and levels of cytokines after surgery was reported [7, 8]. Postoperative complications such as postoperative orthostatic intolerance [9] and deep vein thrombosis [10] could contribute to the stress and thus lead to a slow recovery of patients. As an antioxidant stress strategy, postoperative rehabilitation training could reduce circulating markers of neutrophil activation and the concentration of cytokines [11, 12]. In several areas around the world, such as China, the most common way of implementing postoperative rehabilitation training health education is through oral education provided by nurses, while the nurses in these areas are experiencing high workloads nowadays [13].

Recently, video-assisted health education, a fast and intuitive educational method, has been reported to be helpful for patients to understand health information and thus improve their acceptance and promote their rehabilitation [14]. Studies showed that video-assisted health education can significantly improve the quality of life in patients with bronchiectasis and reduce the complications [15]. Furthermore, video-assisted health education was suggested to be able to reduce burnout in nurses that was caused by heavy workload and could improve work efficiency and job satisfaction in nurses [16]. However, to the best of our knowledge, the current evidence is insufficient to determine the effects of video-assisted health education on rehabilitation in patients who have undergone TKA and on work stress of nurses. We hypothesized that video-assisted health education could promote postoperative recovery and reduce burnout and job stress in nurses when compared with oral education.

## 2. Materials and Methods

**2.1. Ethics.** The present study was conducted after approval by the Research Ethics Committee of Shandong Provincial Hospital affiliated to Shandong First Medical University (no. 2017-055) and was reported in accordance with the CONSORT 2010 statement. Written consent was obtained from each patient who participated in the study.

**2.2. Participants and Baseline Information.** The present study was a noncontemporaneous control study. A convenience sampling method was used for the recruitment of subjects from January 2018 to October 2019. Subjects who met the following inclusion criteria were included: (1) 18 years of age or older and (2) subjects who were diagnosed as having degenerative osteoarthritis and underwent primary TKA. The exclusion criteria were as follows: (1) having any diagnosed hip or ankle disorders, (2) having any balance disorders or ligament instability, (3) severe osteoporosis or severe cardiopulmonary diseases, or (4) ankylosing spondylitis, hemophilic arthritis, and severe deformities of the knee joint due to diseases other than KOA that could affect the

results. Subjects who underwent TKA from January 2018 to December 2018 were assigned to the control group, and the patients from January 2019 to October 2019 who underwent TKA were assigned to the intervention group.

Baseline information including age, gender, marital status, and education level, comorbidities, and osteoarthritis history were obtained on the day of admission. The Numerical Rating Scale (NRS) was used to evaluate pain, and the Barthel index (BI) was used to evaluate the ability of daily living.

**2.3. Intervention.** A standardized exercise plan for TKA patients was developed by the rehabilitation team in our hospital. The content of the exercise plan included ankle pump, isometric contraction, straight leg raising, and flexion knee exercises (Table 1). A 3-minute video that showed the exercise plan was made, and a bedside interactive system was established for playing the video.

The patients in the control group were provided with oral education by the trained nurses about the exercise plan shown in Table 1. The patients in the intervention group were provided with a demonstration of the exercises (Table 1) and then were shown with the video by the bedside interactive system. The patients were quizzed to test their level of comprehension regarding the exercise plan, and tutorial was provided as needed.

**2.4. Postoperative Recovery.** The time to achieve first ambulation, straight leg elevation, and knee flexion to 90 degrees was evaluated at 8:00 am, 12:00 pm, 16:00 pm, and 22:00 pm every day. Occurrence of the following postoperative complications was recorded if they were diagnosed following the criteria reported elsewhere [17–19]: (1) deep venous thrombosis (DVT), (2) postoperative orthostatic intolerance, and (3) constipation. Venous blood samples were collected by trained nurses. Red blood cell count, white blood cell count, absolute number of lymphocytes, and absolute number of neutrophils were measured using Sysmex XN9000 (Sysmex, Japan). C-reactive protein level was evaluated by the nephelometry immunoassay using the BN ProSpec System (Siemens, Germany).

**2.5. Job Burnout and Job Stress.** Job burnout in nurses was assessed using the Maslach Burnout Inventory (MBI) before and after the intervention. MBI was compiled by Maslach and Jackson in 1986 [20, 21] and translated in 2000 by Li. MBI has been shown to have good reliability and validity in the Chinese population [22]. Briefly, the MBI consists of 22 items in three dimensions: emotional exhaustion (nine items), depersonalization (five items), and reduced personal accomplishment (eight items). The nurses responded to each item using a 7-point Likert scale. The higher the score, the higher the degree of emotional exhaustion and depersonalization and the lower the degree of reduced personal accomplishments.

Job stress in nurses was evaluated using the China Nurses' Job Stressors Scale (CNSS) before and after intervention, which was compiled by Li in 1999 [22]. Briefly, the CNSS consists of 35 items in five dimensions: nursing

TABLE 1: Training after total knee arthroplasty.

Content	Method	Time
Ankle pump exercise	(i) Take supine position (ii) Actively flex and extend the ankle joint (iii) Relax the thigh (iv) Slowly and forcefully extend the ankle joint back as far as possible within the limit of no pain or only slight pain for 10 seconds (v) Plantar flexion for 10 seconds	5-10 minutes per hour
Intramuscular quadriceps isometric contraction exercise	(i) Take supine position with the knees straight (ii) Strain the thigh muscles for 5-10 seconds (iii) Relax and repeat	3-5 times per set, 10-20 sets per day
Hamstrings isometric contraction exercise	(i) Take supine position (ii) Press muscles in the posterior upper leg by extending the upper leg against pillows (iii) Relax and repeat	
Straight leg raising exercise	(i) Take supine position (ii) Hook up the toe of the affected limb (iii) Straighten and raise the leg to an angle of 30-40 degrees from the bed (iv) Maintain the position as long as possible (v) Relax and repeat	5-10 times per set, 3-5 sets per day
Flexion knee exercise in the supine position	(i) Take supine position (ii) The lower leg is relaxed and sagging naturally	5 minutes per set, 2-3 sets a day
Flexion knee exercise in the prone position	(i) Take prone position (ii) Flex the affected knee joint	

specialty and work (seven items), workload and time allocation (five items), working environment and resources (three items), patient care (11 items), management, and interpersonal relationship (nine items). The nurses responded to each item using a 4-point Likert scale. The total score was between 35 and 140 with higher scores indicating higher levels of job stressors.

**2.6. Statistical Analyses.** G\*Power 3.1 software was used for sample size estimation. Based on our pilot results, a minimal sample size of 82 was suggested to reach a power of 0.80% and a significance of 0.05. Statistical analysis was performed using IBM SPSS Statistics software (version 22.0, IBM Corporation, USA). Numerical variables are expressed as the means and standard deviations (SDs) if data were normally distributed. Discrete data were expressed as frequencies or percentages. Differences between two groups were tested using the independent *t*-test and chi-squared test for continuous data and discrete data, respectively. Fisher's exact test was used in the analysis of contingency tables. A *P* value less than 0.05 was considered statistically significant.

### 3. Results

**3.1. Baseline Information.** A total of 185 patients participated in the study. Six patients were transferred to the intensive care unit due to severe postoperative cardiopulmonary disease and thus were excluded. The mean age of the participants was 63.6 years (SD = 7.3 years, range = 45–82 years). The ratio for female and for married was 76.5% and 96.6%, respectively. Demographic and disease-related data of the participants are summarized in Table 2. Difference in

these demographic and disease-related variables between two groups was not statistically significant (Table 2).

**3.2. Postoperative Recovery and Complications.** The hospitalization time and time to first ambulation, straight leg raising, and knee flexion to 90 degrees after the intervention in the video-assisted health education group were significantly shortened compared to those in the oral education group with data summarized in Table 3.

After the intervention, constipation and postoperative orthostatic intolerance were significantly reduced. Comparisons of postoperative complications are summarized in Table 4. The difference in the DVT rate between two groups was not statistically significant ( $P = 0.243$ ).

**3.3. Biomarkers.** Levels of biomarkers are summarized in Table 5. CRP levels were significantly lower, and red blood cell counts were significantly higher in the intervention group when compared with the control group ( $P = 0.004$  and  $P = 0.016$ , respectively).

**3.4. Job Burnout and Job Stress in Nurses.** Job burnout and job stress in nurses are summarized in Table 6. There were significant differences in emotional exhaustion, reduced personal accomplishments, and job stress between the two groups ( $P = 0.002$ ,  $P = 0.004$ , and  $P < 0.001$ , respectively).

### 4. Discussion

In this study, video-assisted health education was shown to be more useful than oral education in promoting postoperative recovery on TKA patients and reducing job burnout and job stress in nurses.

TABLE 2: Baseline information of the participants.

Variables	Intervention group (n = 91) (Mean ± SD)	Control group (n = 88) (Mean ± SD)	<i>t</i> / $\chi^2$	<i>P</i> value
Age	62.87 ± 7.46	64.27 ± 7.20	-1.28	0.202
Gender				
Male	16	26	3.57	0.059
Female	75	62		
Marital status				
Single	3	3	0.002	0.967
Married	88	85		
Education				
Primary school and below	47	35	2.58	0.275
Junior middle school	25	29		
Senior high school and above	19	24		
Comorbidity				
Yes	58	57	0.021	0.885
No	33	31		
Pain score	2.34 ± 0.87	2.36 ± 0.94	-0.17	0.865
Barthel index score	89.67 ± 5.47	90.17 ± 5.59	-0.61	0.546

TABLE 3: Postoperative recovery of participants in the two groups.

Variables	Intervention group (n = 91) (Mean ± SD)	Control group (n = 88) (Mean ± SD)	<i>t</i>	<i>P</i> value
Hospitalization time (days)	7.51 ± 1.79	8.21 ± 2.15	-2.37	0.019
First ambulation (h)	19.91 ± 4.57	50.15 ± 7.00	-34.34	< 0.001
Straight leg raising (h)	26.55 ± 12.19	40.38 ± 11.64	-7.76	< 0.001
90 degrees flexion (h)	21.31 ± 5.83	35.72 ± 9.93	-11.88	< 0.001

TABLE 4: Complications in intervention and control groups.

Complications	Intervention group (n = 91)	Control group (n = 88)	$\chi^2$	<i>P</i> value
DVT	10	15	1.37	0.243
Postoperative orthostatic intolerance	7	19	6.96	0.008
Constipation	10	23	6.83	0.009

TABLE 5: Count of blood cells in intervention and control groups.

Items	Intervention group (n = 91)		Control group (n = 88)		<i>t</i>	<i>P</i> value
	Mean ± SD	Coefficient of variation (%)	Mean ± SD	Coefficient of variation (%)		
CRP (mg/L)	84.54 ± 36.09	42.68	99.45 ± 31.73	31.90	-2.93	0.004
WBC (10 <sup>9</sup> /L)	6.89 ± 1.60	23.16	7.38 ± 1.82	24.72	-1.90	0.060
RBC (10 <sup>12</sup> /L)	3.73 ± 0.40	10.73	3.57 ± 0.46	12.77	2.44	0.016
LYMPH (10 <sup>9</sup> /L)	1.33 ± 0.63	47.24	1.25 ± 0.42	33.76	1.04	0.300
NEUT (10 <sup>9</sup> /L)	4.99 ± 2.98	59.69	5.40 ± 1.59	29.53	-1.15	0.254

CRP, C-reactive protein; WBC, white blood cell; RBC, red blood cell; LYMPH, absolute lymphocyte count; NEUT, absolute neutrophil count.

TABLE 6: Job burnout and job stress in nurses for intervention and control groups.

Items	Intervention group (n = 10) (Mean +/- SD)	Control group (n = 10) (Mean +/- SD)	<i>t</i>	<i>P</i> value
Emotional exhaustion	21.00 ± 8.04	36.50 ± 11.22	3.55	0.002
Depersonalization	9.10 ± 4.77	12.30 ± 7.53	1.14	0.271
Reduced personal accomplishments	41.90 ± 4.91	32.80 ± 7.07	-3.34	0.004
Job stress	55.90 ± 11.57	85.50 ± 6.80	6.97	<0.001

Manpower shortage of nurse in the public healthcare system remains challenging, and thus, the registered nurses are under a heavy workload, which probably affects the quality of healthcare service. For example, in one survey, 51.6% of nurses believed that the main factor affecting nurses' performance of health education duties was time tension [23]. Furthermore, the heavy workload and differences in interpersonal communication skills, work efficiency, and personality of nurses were suggested to be the difficulties to achieve consistency, continuity, and standardization in patient education [24]. Therefore, an effective method by which nurses can maintain the quality of patient education in the situation of heavy workload is urgently warranted. Some clinicians suggested that using video health education has the potential to help patients memorize the information and reduce the workload of nurses at the same time [25]. The present study provided evidence for advantages of video-assisted health education over oral education in providing comprehensive, standardized, and easy-to-assimilate information, which accelerated postoperative recovery.

The condition of heavy workload increases the pressure of nurses. The application of video-assisted health education in the rehabilitation training on patients after TKA reduces repetitive explanation for questions that were commonly raised and for the inconsistent oral expressions. In this way, video-assisted health education can improve work efficiency of nurses and thus reduce their work pressure and job burnout. Besides, application of video-assisted health education can be extended to community care services, home care services, and other fields to promote rehabilitation training [26]. Health education assisted by a video could be at least a supplement to traditional teaching modes and standardize health education at relatively low cost in community.

Oxidative stress can cause oxidative damage to various macromolecules, and it has been considered to be one of the causative factors in the pathogenesis of KOA [2, 3]. TKA was demonstrated to be effective in reducing local chronic oxidative damage in OA patients [27]. Nevertheless, a level of oxidative stress continues during postoperative recovery until the peripheral tissues of the knee joint are repaired [28]. Video-assisted health education on rehabilitation training was found to be a macroscopic antistress strategy that modulated low-grade chronic inflammation and active antioxidant enzymes and stimulated the secretion of anti-inflammatory cytokines [12, 29]. Ihalainen and colleagues [30] reported a decrease in proinflammatory biomarkers, such as CRP and inhibited systemic or wound local inflammatory reactions after rehabilitation training. Chen

and colleagues [31] suggested that active functional exercise after TKA improved the levels of TNF- $\alpha$ , IL-1 $\beta$ , and IL-6 and promoted the recovery of joint function. The present study enhanced the evidence for the benefits of rehabilitation training and further suggested an advantage of video-assisted health education over oral education in the training provided by nurses who had heavy workload.

This study has some limitations. First, confounding information about KOA classification and evaluation of knee function was not obtained, which may have led to bias in the results. Second, compliance of patients was not assessed, and it probably caused response bias, which may limit the generalizability of the study results. Therefore, further studies with confounding factors better controlled and with larger sample size are warranted.

## 5. Conclusion

Video-assisted health education may promote the recovery after total knee arthroplasty and reduce job burnout and job stress in nurses when compared with classical oral education. Video-assisted health education could be helpful in situation where manpower of nurse is in shortage.

## Data Availability

Data are available from Shuang Wang (wangshuang200803@163.com) for researchers who meet the criteria for access to confidential data.

## Conflicts of Interest

Each author of this study declares that there is still no relationship with the companies or manufacturers that will benefit from the results of this study. There are no conflicts of interest involved.

## Acknowledgments

The authors acknowledge the Shandong Provincial Hospital affiliated to Shandong First Medical University and the Second Affiliated Hospital of Guangzhou University of Chinese Medicine for their support and all the participating patients for their permission to conduct this study. The authors would like to thank nurses at the Department of Osteoarthritis for their contribution and support of the project. This study was supported by the Chinese Medicine Science and Technology Research Project of Guangdong

Provincial Hospital of Chinese Medicine (No. YN2019HL07), the Guangdong Natural Science Foundation (No. 2020A1515011349), and the China Postdoctoral Science Foundation (No. 2019M662876).

## Supplementary Materials

CONSORT 2010 checklist of information to include when reporting a randomised trial. (*Supplementary Materials*)

## References

- [1] L. Sharma, "Osteoarthritis of the knee," *The New England Journal of Medicine*, vol. 384, no. 1, pp. 51–59, 2021.
- [2] J. A. Bolduc, J. A. Collins, and R. F. Loeser, "Reactive oxygen species, aging and articular cartilage homeostasis," *Free Radical Biology & Medicine*, vol. 132, pp. 73–82, 2019.
- [3] P. Lepetsos, K. A. Papavassiliou, and A. G. Papavassiliou, "Redox and NF- $\kappa$ B signaling in osteoarthritis," *Free Radical Biology & Medicine*, vol. 132, pp. 90–100, 2019.
- [4] Y. Yang, P. Shen, T. Yao et al., "Novel role of circRSU1 in the progression of osteoarthritis by adjusting oxidative stress," *Theranostics*, vol. 11, no. 4, pp. 1877–1900, 2021.
- [5] X. Tang, S. Wang, S. Zhan et al., "The prevalence of symptomatic knee osteoarthritis in China: results from the China Health and Retirement Longitudinal Study," *Arthritis & Rheumatology*, vol. 68, no. 3, pp. 648–653, 2016.
- [6] H. Kamaruzaman, P. Kinghorn, and R. Oppong, "Cost-effectiveness of surgical interventions for the management of osteoarthritis: a systematic review of the literature," *BMC Musculoskeletal Disorders*, vol. 18, no. 1, p. 183, 2017.
- [7] N. Prince, J. A. Penatzer, M. J. Dietz, and J. W. Boyd, "Localized cytokine responses to total knee arthroplasty and total knee revision complications," *Journal of Translational Medicine*, vol. 18, no. 1, p. 330, 2020.
- [8] H. B. Si, T. M. Yang, Y. Zeng et al., "Correlations between inflammatory cytokines, muscle damage markers and acute postoperative pain following primary total knee arthroplasty," *BMC Musculoskeletal Disorders*, vol. 18, no. 1, p. 265, 2017.
- [9] Ø. Jans and H. Kehlet, "Postoperative orthostatic intolerance: a common perioperative problem with few available solutions," *Canadian Journal of Anaesthesia*, vol. 64, no. 1, pp. 10–15, 2017.
- [10] S. M. Heo, I. Harris, J. Naylor, and A. M. Lewin, "Complications to 6 months following total hip or knee arthroplasty: observations from an Australian clinical outcomes registry," *BMC Musculoskeletal Disorders*, vol. 21, no. 1, p. 602, 2020.
- [11] R. Cerqueira, D. A. Marinho, H. P. Neiva, and O. Lourenço, "Inflammatory effects of high and moderate intensity exercise—a systematic review," *Frontiers in Physiology*, vol. 10, p. 1550, 2020.
- [12] K. Suzuki, "Chronic inflammation as an immunological abnormality and effectiveness of exercise," *Biomolecules*, vol. 9, no. 6, p. 223, 2019.
- [13] P. Zhang, H.-M. Wang, J. Zhang, W.-W. Zhao, and Y. Zhao, "The effect of color page education on health education of patients with hyperlipidemia high blood viscosity purify treatment," *Nursing Journal of Chinese People's Liberation Army*, vol. 33, no. 10, pp. 72–74, 2016.
- [14] Y. Kang, L. Xing, and Y. Zhang, "Effects of video teaching combined with empowerment theory on rehabilitation training in elderly patients undergoing total knee arthroplasty," *Chinese Journal of Practical Nursing*, vol. 36, no. 7, pp. 481–485, 2020.
- [15] Y. Zhou, S.-T. Xu, and X.-Y. Wan, "Application effect of video-assisted health education based on PowerPoint in patients with bronchiectasis," *Chinese Nursing Research*, vol. 33, no. 9, pp. 1620–1622, 2019.
- [16] M.-L. Xu, W.-W. Shen, L.-L. Shen, and C.-X. Shen, "Application of video education in the excellent nursing of emergency transfusion room," *Systems Medicine*, vol. 198, no. 14, pp. 173–175, 2018.
- [17] Y.-L. Xiao, S.-L. Pan, X.-R. Li, D. Tian, and D.-M. Hu, "Efficacy analysis of low molecular weight heparin for preventing the formation of deep vein thrombosis in high-risk gravida and parturient," *Medical Journal of Chinese People's Liberation Army*, vol. 46, no. 3, pp. 263–266, 2021.
- [18] B. P. Grubb, "Neurocardiogenic syncope and related disorders of orthostatic intolerance," *Circulation*, vol. 111, no. 22, pp. 2997–3006, 2005.
- [19] Chinese Medical Doctor Association of Coloproctology, "Guidelines for the diagnosis and treatment of constipation," *Chinese Journal of Gastrointestinal Surgery*, vol. 20, no. 3, pp. 241–243, 2017.
- [20] H. Wheeler and R. Riding, "Occupational stress in general nurses and midwives," *The British Journal of Nursing*, vol. 3, no. 10, pp. 527–534, 1994.
- [21] J. Maslach, *Maslach Burnout Inventory California*, Consulting Psychologists Press, 1986.
- [22] X.-M. Li and Y.-J. Liu, "Job stressors and burnout among staff nurses," *Chinese Journal of Nursing*, vol. 35, no. 11, pp. 645–649, 2000.
- [23] M.-P. Cao, "The path of improving hospital nursing health education," *Technology Innovation Herald*, vol. 14, p. 244, 2009.
- [24] C. Yang, J. Yan, T. Shen, and S.-M. Yi, "Application effect of visualized health education in the nursing of patients after spinal surgery," *Journal of Nursing Science*, vol. 31, no. 8, pp. 10–12, 2016.
- [25] Y. Chen, "Application of mobile video playback in functional exercise of patients with knee and hip replacement," *Journal of Clinic Nursing's Practicality*, vol. 2, no. 46, p. 60, 2017.
- [26] M. Saidinejad and J. Zorc, "Mobile and web-based education: delivering emergency department discharge and aftercare instructions," *Pediatric Emergency Care*, vol. 30, no. 3, pp. 211–216, 2014.
- [27] B. Zhang, S.-X. Ren, X.-X. Zhao, and Y. Lin, "A preliminary study on the ischemia-reperfusion injury induced by tourniquet during knee arthroplasty," *Journal of Medical Postgraduates*, vol. 34, no. 3, pp. 273–277, 2021.
- [28] G. P. Dobson, "Trauma of major surgery: a global problem that is not going away," *International Journal of Surgery*, vol. 81, pp. 47–54, 2020.
- [29] J. C. Mcleod, T. Stokes, and S. M. Phillips, "Resistance exercise training as a primary countermeasure to age-related chronic disease," *Frontiers in Physiology*, vol. 10, p. 645, 2019.
- [30] J. K. Ihalainen, M. Schumann, D. Eklund et al., "Combined aerobic and resistance training decreases inflammation markers in healthy men," *Scandinavian Journal of Medicine & Science in Sports*, vol. 28, no. 1, pp. 40–47, 2018.
- [31] D.-X. Chen, J.-M. Zhu, Y.-H. Chen, H. Lu, H. Lu, and R.-P. Zhao, "Influence of active functional exercise on the degree of inflammation after total knee arthroplasty," *China Modern Medicine*, vol. 28, no. 15, pp. 91–94, 2021.

## Review Article

# Therapeutic Applications of Nanozymes in Chronic Inflammatory Diseases

Haojue Wang,<sup>1</sup> Zichen Cui,<sup>2,3</sup> Xuan Wang,<sup>4,5,6</sup> Shui Sun,<sup>2,3</sup> Dongsheng Zhang,<sup>4,5,6</sup>  
and Chuanyun Fu <sup>4,5,6</sup>

<sup>1</sup>School of Queen Mary, Nanchang University, Xuefu Avenue, Nanchang, Jiangxi 330031, China

<sup>2</sup>Department of Joint Surgery, Shandong Provincial Hospital Affiliated to Shandong First Medical University, Jinan, Shandong 250021, China

<sup>3</sup>Orthopaedic Research Laboratory, Medical Science and Technology Innovation Center, Shandong First Medical University & Shandong Academy of Medical Sciences, Jinan, Shandong 250117, China

<sup>4</sup>Department of Stomatology, Shandong Provincial Hospital, Cheeloo College of Medicine, Shandong University, Jinan, Shandong 250021, China

<sup>5</sup>Department of Stomatology, Shandong Provincial Hospital Affiliated to Shandong First Medical University, Jinan, Shandong 250021, China

<sup>6</sup>School of Stomatology, Shandong First Medical University, Jinan, Shandong 250021, China

Correspondence should be addressed to Chuanyun Fu; [fuchuanyun@sdfmu.edu.cn](mailto:fuchuanyun@sdfmu.edu.cn)

Received 1 April 2021; Revised 12 June 2021; Accepted 31 July 2021; Published 11 August 2021

Academic Editor: Dongliang Xu

Copyright © 2021 Haojue Wang et al. This is an open access article distributed under the Creative Commons Attribution License, which permits unrestricted use, distribution, and reproduction in any medium, provided the original work is properly cited.

Since the discovery of horseradish peroxidase-like activity of magnetite nanoparticles in 2007, many researchers have investigated different types of nanoparticles that show enzyme-like activities, namely, nanozymes. Nanozymes possess high efficiency, stability, and low production costs compared to natural enzymes. Thus, nanozymes have already been widely studied in various domains including medical science, food industry, chemical engineering, and agriculture. This review presents the utilization of nanozymes in medicine and focuses particularly on their therapeutic applications in chronic inflammatory diseases because of their antioxidant-like activity. Furthermore, the treatment of chronic inflammatory diseases with nanozymes of different materials was introduced emphatically.

## 1. Introduction

Enzymes are biocatalysts with high efficiency that are highly selective to their specific substrates, but they also have some inherent defects such as low stability and high production cost, which limit their application [1]. Therefore, identifying enzyme mimics is an important study.

In 2007, it was discovered that magnetite nanoparticles possessed an activity similar to the enzyme-like property of horseradish peroxidases [2]. Further studies showed that these metallic nanoparticles exhibited an enzyme-like activity and were defined as nanozymes. These include nanoparticles that exhibit enzyme-like activities of peroxidase [3], catalase

(CAT) [4], superoxide dismutase (SOD) [5], and hydro-lase [6]. The most prominent characteristic of nanozymes is that the size of the nanoparticles is less than 100 nm in at least one dimension, which means they can be regarded as two-dimensional sheets with a high specific surface area and thus have excellent catalytic activities [7]. Moreover, the metallic nature of the nanozymes helps them in sustaining in hostile environments, such as high temperature, acidic environment, or alkaline environment; thus, nanozymes are more stable than natural enzymes [8]. Moreover, some nanozymes show unique characteristics and have low production costs compared to natural enzymes [9].

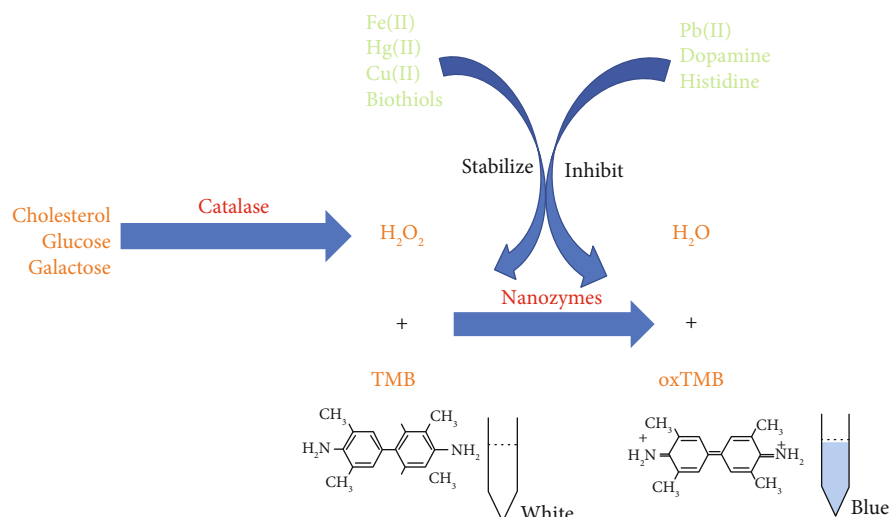


FIGURE 1: Brief diagram of the nanozyme-based  $H_2O_2$  sensor and its application in the detection of cholesterol, glucose, and galactose.

## 2. Application of Nanozyme in Medicine

### 2.1. Nanozyme-Based Sensors

**2.1.1.  $H_2O_2$  Sensors.** Hydrogen peroxide is the most popular and detectable reactive oxygen species (ROS), which is formed by the reduction of oxygen. When the formation of ROS abnormally increases,  $H_2O_2$  causes oxidative damage *in vivo* by targeting the DNA, proteins, and biofilms [10]. The sensing of  $H_2O_2$  utilizes the nanozyme with peroxidase-like activity, such as iron-based nanoparticles (NPs) (with the detection limit of  $50 \mu M$ ) [11], vanadium-based NPs (with the detection limit of  $0.5 \mu M$ ) [12], and metal-organic framework-based nanocomposites (NCs) (with the detection limit of  $0.24 \mu M$ ) [13] to catalyze the oxidation of 3,3',5,5'-tetramethylbenzidine (TMB) by  $H_2O_2$  to generate a blue-colored product, 3,3',5,5'-tetramethylbenzidine (oxTMB) (Figure 1). Apart from this colorimetric reaction, scientists have also developed other methods for sensing  $H_2O_2$  using an electrochemical process [14], fluorometric sensor [15], and Raman scattering sensor [16].

The sensing of  $H_2O_2$  is quite important in the research of nanozyme, not only for the physiological effects of  $H_2O_2$  but also due to the fact that detection of  $H_2O_2$  is usually coupled with the sensing of other biomolecules or chemical particles such as biothiols [17], dopamine [18], metal ions [19–21], histidine, and  $Cu^{2+}$  [22], which can inhibit or stabilize the peroxidase-like activity of nanozymes and indirectly mediate the oxidative generation of TMB (Figure 1). Furthermore, some biomolecules like cholesterol [23], glucose [24], and galactose [25] can be oxidized by their oxidases to generate  $H_2O_2$ ; so, combining these two reactions can help quantify the molecules easily (Figure 1). Due to the sensitivity of nanozymes to detect  $H_2O_2$ , it can also sense these molecules.

**2.1.2. Nanozyme-Based Enzyme-Linked Immunosorbent Assay (ELISA).** ELISA is a labelled immunoassay which is widely used in clinical laboratory to quantitatively detect antigens like cancer markers, proteins, viruses, and hormones.

Traditional ELISA is based on the activity of natural enzymes and the unique interaction between the antigen and the antibody [26], but preparation and purification, as well as preservation of these enzymes, are expensive and laborious [27]. The development of nanozyme offers an alternative solution.

Oh et al. developed an ultrasensitive ELISA to detect the influenza A virus [28]. This method utilizes magnetic nanobead capture probes and Au nanozyme probes to detect the influenza A virus. The Au nanozyme probes were made of Au NPs, which have higher stability and activity than traditional horseradish peroxidase, and anti-influenza virus antibodies (Ab2 or Ab3). The magnetic nanobead capture probes were made of magnetic nanobeads and anti-influenza virus antibodies (Ab1 or Ab3) (Figure 2(a)). Then, both of these were mixed, and they formed a sandwich structure with the influenza A virus; this structure was selected by a magnet. Then, the Au nanozyme probe with peroxidase-like activity catalyzed  $H_2O_2$  to oxidize TMB into oxTMB (Figure 2(b)) [28].

Similar methods that use nanozymes with peroxidase-like activity (usually Au or Au alloy NPs) as the enzyme complex and TMB as the chromogenic substance are very useful for detecting different antigens. It has been employed for the detection of *Escherichia coli* [29], coronavirus [30], norovirus [31], and measles virus [32].

### 2.2. Nanozyme-Based Therapy

**2.2.1. Cancer Therapy.** The application of nanozyme in cancer therapy can be classified into two categories. The first is a direct method, the basic principle of which is to generate ROS in tumor tissues utilizing the peroxidase-like activity and oxidase-like activity of nanozymes. Gao et al. designed a nanoplatform by integrating Au NPs and iron oxide NPs into dendritic mesoporous silica nanoparticles which served as the glucose oxidase to catalyze the oxidation of glucose to generate  $H_2O_2$ . Then, iron oxide converts  $H_2O_2$  into high cytotoxic hydroxyl radicals by means of a Fenton-like

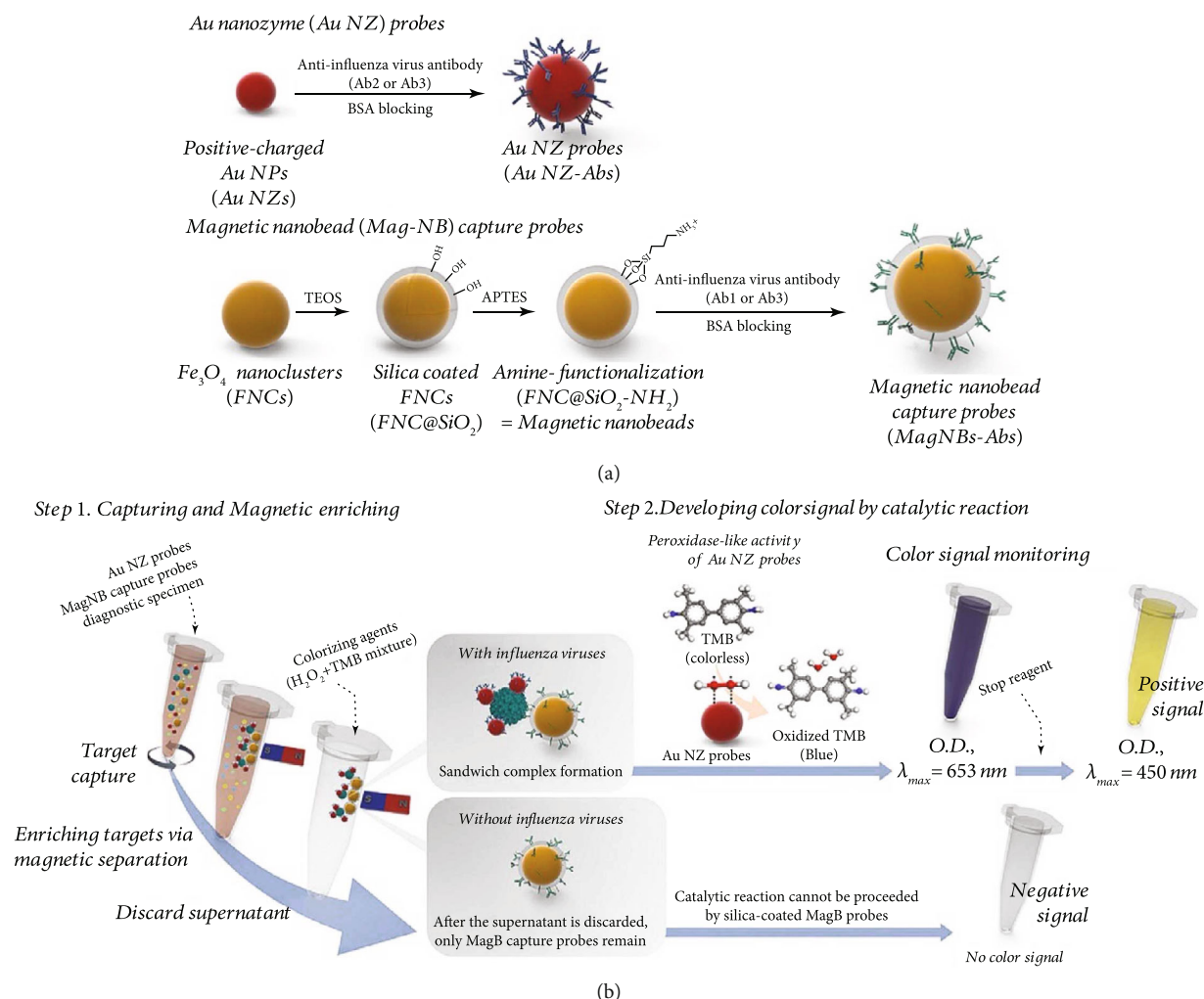


FIGURE 2: The preparation of the Au nanozyme probes and the magnetic capture nanobead probes and the procedure of this ELISA (cited from Scheme 1 of Oh et al. [28]).

reaction, which finally leads to the apoptosis of the cancer cells [33].

Radiotherapy and photodynamic therapy (PDT) are common therapeutics for cancer which are facilitated by the production of ROS [34]. But the generation of ROS needs oxygen, which is always deficient in cancer tissues [34]. So, the other method is to use catalase-mimic nanozymes to increase local oxygen concentration and indirectly improve the efficiency of radiotherapy and PDT to cancer tissues. Li et al. successfully synthesized porous platinum NPs which are catalase-mimic nanozymes that react with H<sub>2</sub>O<sub>2</sub> and produce oxygen, which then effectively enhance the radiation dose in the targeted tumor tissues [35]. Similar effects were also reported by Hao et al. in PDT [36].

**2.2.2. Neuroprotection.** Generation of ROS can be used in cancer therapy, but the overproduction of ROS is the pathological marker of many diseases, especially those that affect the neuro system. Prussian blue (PB) can effectively remove ROS due to its catalase-, superoxide dismutase-,

and peroxidase-mimic activities. Based on these characteristics, Zhang et al. developed a hollow PB nanozyme which protects the neuro system against ischemic shock by scavenging ROS, relieving inflammation, and controlling cellular apoptosis [37].

**2.2.3. Anti-Inflammation.** Because of the multienzyme-mimic activities, nanozymes display excellent ability in regulating oxidation-regulation reaction [37]. Inflammation is a pathological response that is intended to eliminate inflammatory stimuli and initiate tissue repair. Overproduction of ROS is an important characteristic of chronic inflammation, which leads to redox imbalance. Thus, restoring redox homeostasis is an important method to relieve inflammation reaction. Besides Alzheimer’s disease and ischemic shock, nanozymes can also reduce the ROS level and resist inflammation in chronic inflammatory diseases.

Thus, we can summarize that nanozymes have been extensively studied in biomedical domains because of their unique characteristics. Herein, we will categorize nanozymes

systematically and introduce their therapeutic applications in chronic inflammatory diseases.

### 3. Chronic Inflammatory Diseases

Chronic inflammation is a response to long-term inflammation, tissue injury, and attempted repair, which are usually caused by persisting infections, hypersensitivity diseases, and prolonged exposure to potentially toxic agents [38]. Typical chronic inflammatory diseases include Alzheimer's disease, Crohn's diseases, ulcerative colitis, rheumatoid arthritis, and periodontitis [39]. Inflammatory reaction is the collective characteristic of these diseases which includes vasodilation, increased vascular permeability, and leukocyte infiltration and activation [38]. The main method by which activated leukocytes recognize and eliminate the microbes or necrotic tissues is through phagocytosis, which mainly relies on ROS.  $H_2O_2$ , an ROS, then forms the  $H_2O_2$ -MPO-halide system, which is the most efficient sterilization system [38].

Although ROS as a physiological substance helps maintain hemostasis in normal condition, but the overproduction of ROS in chronic inflammatory reaction is highly toxic to normal tissue, its activity must be controlled *in vivo* by antioxidant mechanisms which involves enzymes like catalase, superoxide dismutase, and glutathione peroxidase [38]. The cause of most of the chronic inflammatory diseases is unclear, and so, the therapy for these diseases usually targets its inflammatory reaction [40]. Thus, the mimics of these enzymes may be potential drugs to relieve the inflammatory reaction and treat chronic inflammatory diseases.

An increasing number of researches have been performed toward the treatment of chronic inflammatory diseases. Using glucocorticoids to inhibit immune reaction and using nonsteroidal anti-inflammatory drugs (NSAID) to inhibit the biosynthesis of cyclooxygenase are the two major means used in clinical application to attenuate inflammation, which have extensive side effects of gastrointestinal complications, cardiovascular complications, and inducing or aggravating infection, among others [41–45]. Hence, identifying other anti-inflammatory agents is of utmost importance. Among these, antioxidants are widely sought after, and quite a few of antioxidants such as curcumin [46], polyphenol [47], chlorogenic acid [48], and ascorbic acid [49] have been reported for their anti-inflammatory potential. Some of these have already been used in clinical therapy. Thus, nanozyme, as the high-efficiency mimic of antioxidant enzyme, is no doubt a considerable option for chronic inflammatory disease therapy.

### 4. Therapeutic Applications of Nanozymes in Chronic Inflammatory Diseases

**4.1. Cerium Oxide-Based Nanomaterial.** Cerium oxide-based nanozymes are widely used in many fields, such as medicine, because of their unique characteristics. Cerium oxide NPs have superoxide dismutase-, catalase-, and oxidase-like activities [50, 51]. Furthermore, cerium oxide-based nanozymes are stable in both acidic and basic conditions. At physiologi-

cal pH values (pH 7.4), cerium oxide-based nanozymes perform great SOD- and CAT-like activities; thus, the nanozymes can protect cells from oxidants, but under acidic conditions (pH 4.5), the oxidase-like activity of cerium oxide-based nanozymes can effectively kill cancer cells by producing ROS [52].

Some studies showed that the  $Ce^{3+}/Ce^{4+}$  ratio depends on the CAT- and SOD-like activities, and cerium oxide nanoparticles can simulate the chemical reaction and antioxidant activity of CAT and SOD [53]; thus, it can protect cells by regulating the level of ROS in cells.

One of the important functions of cerium oxide nanoparticles is inhibiting inflammatory mediators and protecting the cell structure from inflammatory diseases. Inflammation *in vivo* and *in vitro* can be effectively treated by scavenging free radicals or ROS [54]. Arya et al. [55] synthesized spherical cerium oxide nanozymes as an anti-inflammatory drug to evaluate the protective effect of hypoxia on the lung. After repeated intraperitoneal injection,  $CeO_2$  was deposited in the lung, which reduced the oxidation of active oxygen and lipid, thus protecting the lung from oxidative stress and tissue damage caused by the endotoxin.

Studies have shown that the ceria nanozyme is very effective in neuroprotection. Alzheimer's disease is an insidious disease characterized by progressive neurodegenerative changes including amyloid-beta peptide aggregates, overproduction of ROS, and inflammatory reactions. Based on these pathological markers, Guan et al. [56] designed a ceria/polyoxometalate hybrid with SOD and proteolytic activities (Figure 3). This nanozyme could cross the blood-brain barrier, degrade amyloid-beta peptide aggregates, reduce the ROS levels, boost the proliferation of PC12 cells, and inhibit the activation of BV2 microglia cells induced by the amyloid-beta peptides. Thus, it provides an evidence for the therapeutic application of nanozymes in Alzheimer's disease.

Scientists have also developed an effective anti-ischemic treatment agent based on monodispersed ceria nanoparticles, which are loaded with edaravone and modified with angiopep-2 and poly (ethylene glycol) on their exterior [57]. This material can effectively treat stroke by eliminating ROS, as it can greatly enhance the brain uptake; simultaneously, it can effectively protect the blood-brain barrier and thus has great potential in stroke treatment.

Parkinson's disease is a hypokinetic disorder disease, which is characterized by the failure of the disinhibition that is normally mediated by the basal ganglia. The direct cause of Parkinson's disease is the loss of the substantia nigra pars compacta due to cell death. Kwon et al. [58] used  $CeO_2$  to enhance the activities of SOD and CAT enzymes and remove ROS inside and outside the cells to prevent the initiation of microglia and peroxidation of lipid and to protect tyrosine hydroxylase to treat Parkinson's disease.

As mentioned above, these experiments present the excellent ROS-reducing ability of ceria NPs inside and outside the cells, which greatly alleviates the oxidative stress in the brain and lung [55–58]. Curative effects of ceria NPs are shown in animal models with Parkinson's, stroke, and lung inflammation. Thus, the broad potentials of ceria NPs are shown in anti-inflammation therapy. But what needs

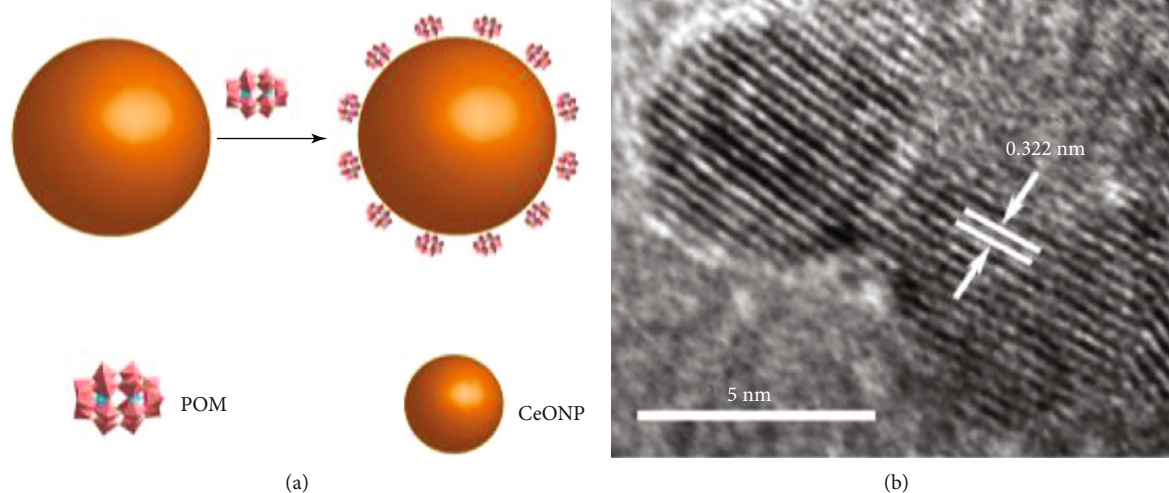


FIGURE 3: (a) Schematic structure of ceria/polyoxometalate hybrid molecule. (b) Electron microscope image of ceria/polyoxometalate hybrid molecule (cited from Figure 1 of Guan et al. [56]).

consideration is how the ceria NPs are eliminated from the body, if the ceria NPs possessed biological toxicity, and also the stability and activity of this nanozyme. Hence, deeper research on ceria NPs is still needed.

**4.2. Iron Oxide-Based Nanomaterial.** Iron oxide-based nanozymes are great peroxidase mimics with excellent stability. Even when placed in high temperatures of 90°C and pH value from 1.5 to 12.0 for 2 hours, iron oxide-based nanozymes can still retain its catalytical activity, which is much better than the natural enzyme, which rapidly loses its activity at 40°C and pH value of 5.0 [59].

At present, iron oxide-based nanozymes have certain value in the treatment of chronic inflammatory diseases, but their usage as antioxidants has therapeutic effects in nervous system diseases [60]. *In vivo*, researchers demonstrated that iron oxide NPs protect cells from oxidative stress and apoptosis induced by H<sub>2</sub>O<sub>2</sub>. Also, iron oxide NPs can relieve intracellular oxidative stress, postpone animal aging, and prevent neurodegeneration because of their catalase-like activity. *In vitro*, the level of ROS of PC12 cells, which were exposed to MPP<sup>+</sup>, declined greatly due to the treatment of iron oxide NPs, and the death of the PC12 cells was alleviated. Therefore, the function of iron oxide NPs in the therapy of Parkinson's disease has been evaluated [60].

In addition, researchers used the *Drosophila* Alzheimer's disease model to examine the effects of iron oxide NPs on neuronal dysfunction. They found that dietary iron oxide NPs can improve neurodegeneration, due to the decomposition of ROS by iron oxide NPs. Another study developed a ferritin nanozyme (Fenozyme) formed by recombinant human ferritin (HFn) protein shells [61]. This nanozyme can not only specifically target blood-brain barrier endothelial cells (the effect of HFn) but also exhibits catalase-like activity to scavenge ROS. An *in vivo* experiment showed that

Fenozyme significantly improved the destruction of the blood-brain barrier caused by parasites and significantly promoted the survival of infected mice.

In addition, it has been verified that iron oxide NPs have a protective effect on cardiomyocytes, because they have catalase- and peroxidase-like activities and are used in antioxidant therapy. Xiong et al. [62] reported that Fe<sub>2</sub>O<sub>3</sub>-DMSA NPs can preserve the heart from ischemic injury by inhibiting intracellular ROS in several ways and relieve the peroxidation injury of the membrane lipid.

The above experiments preliminarily demonstrate the peroxidase- and catalase-like activities of iron oxide NPs, which can effectively eliminate superfluous H<sub>2</sub>O<sub>2</sub> generated under oxidative stress or produced through SOD and also successfully protect myocardial and neural cells [60–62]. An even better curative effect was observed in mice with myocardial ischemia and reperfusion, which were treated with iron oxide NPs compared to when the same model was treated with verapamil. No apparent cytotoxicity was observed in iron oxide NPs with the dosage between 0.01 and 0.5 mg ml<sup>-1</sup>.

**4.3. Manganese-Based Nanomaterial.** MnO<sub>2</sub> NPs have been proven to have a variety of enzyme-like activities such as peroxidase-, oxidase-, catalase-, SOD-, and glutathione peroxidase-like activities, and they are more stable than natural enzymes. Therefore, MnO<sub>2</sub> NPs have broad applications in different aspects, such as biotechnology, bioassays, and biomedicine [63]. Due to the abnormal increase in ROS level, the balance of redox *in vivo* will be destroyed, which will cause oxidative stress, and ultimately leads to the destruction of the structure and function of cellular macromolecules. The peroxidase- and SOD-like activities of nanozymes are generally utilized to control the level of ROS in cells, and this function plays an important role in protecting the cells.

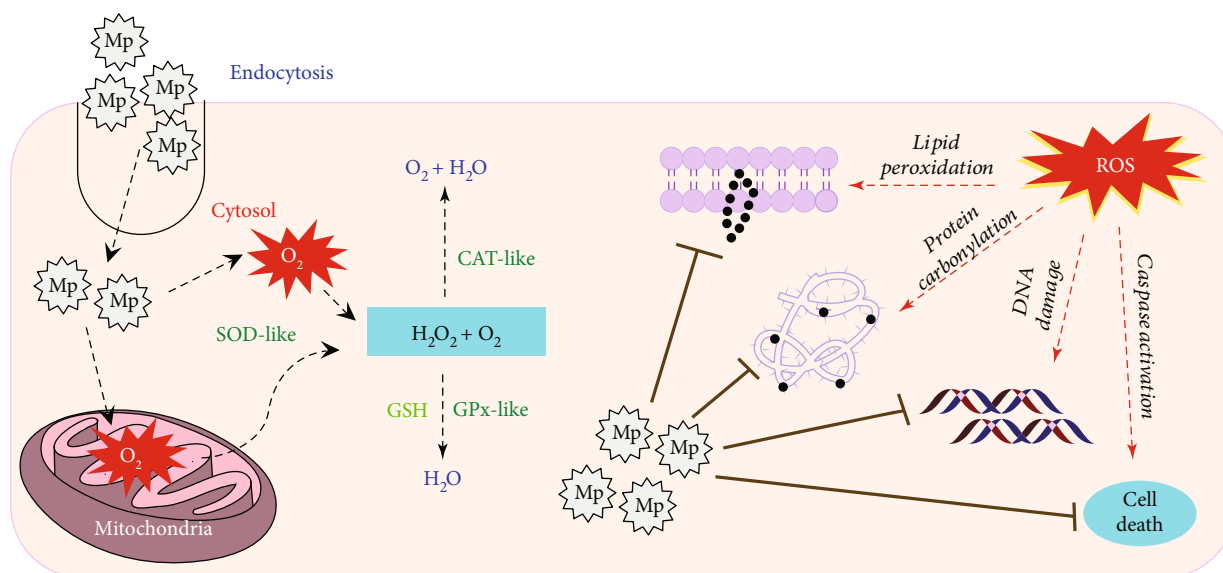


FIGURE 4: The basic mechanisms of the working of SOD-, CAT-, and GPx-mimic nanozymes in ROS-imbalanced cells (cited from the graphical abstract of Singh et al. [65]).

Singh et al. [64] found that  $Mn_3O_4$  NPs with flower-like morphology performed the activities of several antioxidant enzymes such as SOD, CAT, and glutathione peroxidase. These activities are related to the mixed oxidation states of manganese, unusually large-sized pore, high stability against irreversible oxidation, and large surface area. They have proven that the multienzyme mimic,  $Mn_3O_4$  nanoflowers, could modulate the redox status of the cells caused by oxidative stress by protecting biomolecules from protein oxidation, lipid peroxidation, and DNA damage mediated by ROS (Figure 4). Furthermore, these nanozymes, with the ability to mimic the cellular antioxidant enzymes to protect cell from oxidative damage, will not alter the response of Nrf2 protein under oxidative stress, so the nanozymes can regulate the redox homeostasis of cells without interfering with the antioxidant proteins/enzymes in the cells [65]. Also, the  $Mn_3O_4$  nanoflowers showed great ability to save the cells from ROS-mediated inflammatory injury and prevent neurological diseases, such as Parkinson's, caused by the imbalance of ROS.

Besides the multienzyme-mimic activity, the high catalytic capacity of  $Mn_3O_4$  NPs, compared to not only the natural enzyme but also other NPs, is an amazing finding.  $Mn_3O_4$  NPs showed better ability in the scavenging of oxygen radical and hydroxyl radical when compared to  $Fe^{2+}$  and  $CeO_2$  NPs; thus,  $Mn_3O_4$  NPs exhibited greater anti-inflammatory ability. Based on this, Yao et al. designed a strategy to cure ear inflammation in mice [66].

The multiple enzyme-mimic activities and the comparative high catalytic activities are the major characteristics of manganese-based nanomaterial, which are rarely found in other nanozymes [63]. This implies that manganese-based nanomaterials can protect cells from ROS-induced cell injury and inflammatory reaction without disturbing the inherent antioxidation system of the cells. Thus, manganese-based

nanozymes can be a good choice for the treatment of chronic inflammation with broad prospect.

**4.4. Gold- and Platinum-Based Nanomaterials.** Gold nanomaterials have entered public sight as a nanozyme material because of the function of mimicking oxidase. In order to play a better role in simulating enzyme activity, some studies have used gold nanoparticles along with other materials to synthesize nanostructures, such as Au-Pt.

In the field of cell protection, gold nanozyme showed great antioxidant properties and highly catalytic activity. Keratinocytes are most affected by ultraviolet (UV) light irradiation, because these cells are located in the outermost layer of skin. UV-induced cell damage is caused by superfluous ROS. Xiong et al. [67] prepared enzyme-mimic Au-Pt NCs to catalyze the clearance of ROS. They have demonstrated that the active and biocompatible Au-Pt NCs can eliminate ROS induced by UV rays and prevent subsequent oxidative damage to cells *in vivo*.

**4.5. Platinum-Based Nanomaterial.** The major utilization of platinum in medicine is in anticancer therapy such as cisplatin, carboplatin, and oxaliplatin. With increased research in metal NPs, researchers have identified its excellent ability in anti-inflammation. Similar to other nanozymes, platinum NPs (PtNPs) performing as SOD and CAT mimics can eliminate ROS and reduce oxidative stress. Furthermore, PtNPs are different from other enzymes as they can directly inhibit the overproduction of nitric oxide, tumor necrosis factor- $\alpha$ , interleukin-6, and other inflammatory mediators; they can also inhibit the activity of macrophages through inhibition of the NF- $\kappa$ B signaling pathway. Based on this comprehensive anti-inflammation ability, oral PtNPs produced a marked effect in mouse colitis which greatly alleviated local and systemic inflammatory reaction [68]. Similar effects were

also observed in the prevention of pneumonia in mice exposed to smoke [69].

Although PtNPs are great antioxidants, they can be easily oxidized in air, but combining them with PdNPs can solve this problem and broaden the application of PtNPs. Shibuya et al. [70] used a mixture of PdNPs and PtNPs, namely, PAPTAL, to treat chronic diseases. Besides, due to the SOD- and catalase-like activities of PAPTAL, it can inhibit the intrinsic superoxide *in vivo* and treat aging-related skin diseases caused by oxidative stress.

**4.6. Carbon-Based Nanomaterial.** Carbon-based nanomaterials have been widely used in biomedicine. Compared to natural enzymes, carbon nanomaterials have higher stability and lower cost.

Fullerene is the first carbon-based nanozyme that has been found to possess SOD-like activity. C3 is a first-in-class functionalized water-soluble fullerene, and it has been confirmed that C3 can reduce ROS, which has been shown to be related to neurodegenerative diseases *in vitro*. Dugan et al. [71] found that after the treatment of the potent antioxidant C3, Parkinsonian motor ratings significantly improved in monkeys and the striatal dopamine levels increased. Even though the damage process had begun, C3 could reduce striatal injury. Furthermore, C3 has anti-inflammatory properties which can reduce MPTP- and 6-hydroxydopamine-induced neuronal cell death by reducing oxidative damage. These studies found little evidence of toxicity for C3.

**4.7. Summary.** Natural enzymes require strict physiological conditions for performing catalytic functions. Their limited stability in harsh environmental conditions and other significant drawbacks such as the high cost of synthesis, isolation, and purification greatly limit their practical applications [72]. Therefore, to address the limitations of natural enzymes, nanozymes have attracted considerable interest over the past decade owing to their obvious advantages. Nanozymes are nanomaterials with intrinsic enzyme-like characteristics which can offer unflinching biocatalytic activity even in the extreme conditions of pH, temperatures, and resistance to the digestion from proteases. Their advantages also include low cost, easy large-scale production, high stability, and smooth surface modification of nanomaterials [2, 72]. Moreover, the unique physicochemical properties of nanomaterials not only endow nanozymes with multiple functionalities but also provide more possibilities for rational design and future applications. As an alternative to natural enzymes, the antioxidant effects of nanozymes have been extensively explored for antiaging, anti-inflammatory, antioxidative, and neuroprotective functions and in the treatment of Alzheimer's and Parkinson's disease [73].

Although it is well established that nanozymes possess several distinct advantages over natural enzymes, they still face several limitations. Biological enzymes are highly selective to their targets; however, nanozymes show limited selectivity toward their substrates. So far, most studies focused on the activity regulation and only a few on their selectivity [74].

## Conflicts of Interest

All authors declare there is no conflict of interest.

## Authors' Contributions

Haojue Wang and Zichen Cui contributed equally to this work.

## Acknowledgments

Research reported in this publication was supported by the Natural Science Foundation of Shandong Province, China (Grant No. ZR2020QH157).

## References

- [1] A. Sun, L. Mu, and X. Hu, "Graphene oxide quantum dots as novel nanozymes for alcohol intoxication," *ACS Applied Materials & Interfaces*, vol. 9, no. 14, pp. 12241–12252, 2017.
- [2] L. Gao, J. Zhuang, L. Nie et al., "Intrinsic peroxidase-like activity of ferromagnetic nanoparticles," *Nature Nanotechnology*, vol. 2, no. 9, pp. 577–583, 2007.
- [3] Z. Zhang, Y. Tian, P. Huang, and F. Y. Wu, "Using target-specific aptamers to enhance the peroxidase-like activity of gold nanoclusters for colorimetric detection of tetracycline antibiotics," *Talanta*, vol. 208, p. 120342, 2020.
- [4] X. E. Zhao, Y. N. Zuo, X. Qu, J. Sun, L. Liu, and S. Zhu, "Colorimetric determination of the activities of tyrosinase and catalase via substrate-triggered decomposition of MnO<sub>2</sub> nanosheets," *Mikrochimica Acta*, vol. 186, no. 12, p. 848, 2019.
- [5] J. Xi, G. Wei, L. An et al., "Copper/carbon hybrid nanozyme: tuning catalytic activity by the copper state for antibacterial therapy," *Nano Letters*, vol. 19, no. 11, pp. 7645–7654, 2019.
- [6] L. Uribe, G. Diezemann, J. Gauss, J. P. Morth, and M. Cascella, "Structural origin of metal specificity in isatin hydrolase from *Labrenzia aggregata* Investigated by computer simulations," *Chemistry*, vol. 24, no. 20, pp. 5074–5077, 2018.
- [7] E. A. Bleeker, W. H. de Jong, R. E. Geertsma et al., "Considerations on the EU definition of a nanomaterial: science to support policy making," *Regulatory Toxicology and Pharmacology*, vol. 65, no. 1, pp. 119–125, 2013.
- [8] S. Sabale, P. Kandesar, V. Jadhav, R. Komorek, R. K. Motkuri, and X. Y. Yu, "Recent developments in the synthesis, properties, and biomedical applications of core/shell superparamagnetic iron oxide nanoparticles with gold," *Biomaterials Science*, vol. 5, no. 11, pp. 2212–2225, 2017.
- [9] S. Maddela, A. Makula, and N. Jayarambabu, "Fe<sub>3</sub>O<sub>4</sub> nanoparticles mediated synthesis of novel isatin-dihydropyrimidinone hybrid molecules as antioxidant and cytotoxic agents," *Anti-Cancer Agents in Medicinal Chemistry*, vol. 17, no. 3, pp. 456–463, 2017.
- [10] V. Cecarini, J. Gee, E. Fioretti et al., "Protein oxidation and cellular homeostasis: emphasis on metabolism," *Biochimica et Biophysica Acta*, vol. 1773, no. 2, pp. 93–104, 2007.
- [11] N. V. S. Vallabani, A. S. Karakoti, and S. Singh, "ATP-mediated intrinsic peroxidase-like activity of Fe<sub>3</sub>O<sub>4</sub>-based nanozyme: one step detection of blood glucose at physiological pH," *Colloids and Surfaces. B, Biointerfaces*, vol. 153, pp. 52–60, 2017.

- [12] F. Honarasa, F. H. Kamshoori, S. Fathi, and Z. Motamedifar, "Carbon dots on  $V_2O_5$  nanowires are a viable peroxidase mimic for colorimetric determination of hydrogen peroxide and glucose," *Mikrochimica Acta*, vol. 186, no. 4, p. 234, 2019.
- [13] Y. Zhang, J. Song, Q. Pan et al., "An Au@NH<sub>2</sub>-MIL-125(Ti)-based multifunctional platform for colorimetric detections of biomolecules and Hg<sup>2+</sup>," *Journal of Materials Chemistry B*, vol. 8, no. 1, pp. 114–124, 2020.
- [14] Y. Xie, M. Xu, L. Wang, H. Liang, L. Wang, and Y. Song, "Iron-porphyrin-based covalent-organic frameworks for electrochemical sensing H<sub>2</sub>O<sub>2</sub> and pH," *Materials Science & Engineering. C, Materials for Biological Applications*, vol. 112, p. 110864, 2020.
- [15] X. Huang, H. Zhou, Y. Huang et al., "Silver nanoparticles decorated and tetraphenylethene probe doped silica nanoparticles: a colorimetric and fluorometric sensor for sensitive and selective detection and intracellular imaging of hydrogen peroxide," *Biosensors & Bioelectronics*, vol. 121, pp. 236–242, 2018.
- [16] Y. Li, Y. Wang, C. Fu et al., "A simple enzyme-free SERS sensor for the rapid and sensitive detection of hydrogen peroxide in food," *Analyst*, vol. 145, no. 2, pp. 607–612, 2020.
- [17] Y. Sun, J. Wang, W. Li, J. Zhang, Y. Zhang, and Y. Fu, "DNA-stabilized bimetallic nanozyme and its application on colorimetric assay of biothiols," *Biosensors & Bioelectronics*, vol. 74, pp. 1038–1046, 2015.
- [18] M. X. Guo and Y. F. Li, "Cu (II)-based metal-organic xerogels as a novel nanozyme for colorimetric detection of dopamine," *Spectrochimica Acta. Part A, Molecular and Biomolecular Spectroscopy*, vol. 207, pp. 236–241, 2019.
- [19] Y. Tang, Y. Hu, Y. Yang, B. Liu, and Y. Wu, "A facile colorimetric sensor for ultrasensitive and selective detection of lead(II) in environmental and biological samples based on intrinsic peroxidase-mimic activity of WS<sub>2</sub> nanosheets," *Analytica Chimica Acta*, vol. 1106, pp. 115–125, 2020.
- [20] Y. Wang, J. Hu, Q. Zhuang, and Y. Ni, "Enhancing sensitivity and selectivity in a label-free colorimetric sensor for detection of iron(II) ions with luminescent molybdenum disulfide nanosheet-based peroxidase mimetics," *Biosensors & Bioelectronics*, vol. 80, pp. 111–117, 2016.
- [21] C. Ma, Y. Ma, Y. Sun et al., "Colorimetric determination of Hg<sup>2+</sup> in environmental water based on the Hg<sup>2+</sup>-stimulated peroxidase mimetic activity of MoS<sub>2</sub>-Au composites," *Journal of Colloid and Interface Science*, vol. 537, pp. 554–561, 2019.
- [22] Y. Liu, D. Ding, Y. Zhen, and R. Guo, "Amino acid-mediated 'turn-off/turn-on' nanozyme activity of gold nanoclusters for sensitive and selective detection of copper ions and histidine," *Biosensors & Bioelectronics*, vol. 92, pp. 140–146, 2017.
- [23] C. Hong, X. Zhang, C. Wu et al., "On-site colorimetric detection of cholesterol based on polypyrrole nanoparticles," *ACS Applied Materials & Interfaces*, vol. 12, no. 49, pp. 54426–54432, 2020.
- [24] Y. M. Wang, J. W. Liu, J. H. Jiang, and W. Zhong, "Cobalt oxyhydroxide nanoflakes with intrinsic peroxidase catalytic activity and their application to serum glucose detection," *Analytical and Bioanalytical Chemistry*, vol. 409, no. 17, pp. 4225–4232, 2017.
- [25] X. Zhou, M. Wang, J. Chen, X. Xie, and X. Su, "Peroxidase-like activity of Fe-N-C single-atom nanozyme based colorimetric detection of galactose," *Analytica Chimica Acta*, vol. 1128, pp. 72–79, 2020.
- [26] M. Alhaji and A. Farhana, *Enzyme linked immunosorbent assay*, StatPearls, Treasure Island, FL, USA, 2020.
- [27] Y. Ju and J. Kim, "Dendrimer-encapsulated Pt nanoparticles with peroxidase-mimetic activity as biocatalytic labels for sensitive colorimetric analyses," *Chemical Communications*, vol. 51, no. 72, pp. 13752–13755, 2015.
- [28] S. Oh, J. Kim, V. T. Tran et al., "Magnetic nanozyme-linked immunosorbent assay for ultrasensitive influenza A virus detection," *ACS Applied Materials & Interfaces*, vol. 10, no. 15, pp. 12534–12543, 2018.
- [29] J. Han, L. Zhang, L. Hu et al., "Nanozyme-based lateral flow assay for the sensitive detection of *Escherichia coli* O157:H7 in milk," *Journal of Dairy Science*, vol. 101, no. 7, pp. 5770–5779, 2018.
- [30] G. Nikaen, S. Abbaszadeh, and S. Yousefinejad, "Application of nanomaterials in treatment, anti-infection and detection of coronaviruses," *Nanomedicine*, vol. 15, no. 15, pp. 1501–1512, 2020.
- [31] I. M. Khoris, K. Takemura, J. Lee et al., "Enhanced colorimetric detection of norovirus using in-situ growth of Ag shell on Au NPs," *Biosensors & Bioelectronics*, vol. 126, pp. 425–432, 2019.
- [32] L. Long, J. Liu, K. Lu et al., "Highly sensitive and robust peroxidase-like activity of Au-Pt core/shell nanorod-antigen conjugates for measles virus diagnosis," *Journal of Nanobiotechnology*, vol. 16, no. 1, p. 46, 2018.
- [33] S. Gao, H. Lin, H. Zhang, H. Yao, Y. Chen, and J. Shi, "Nanocatalytic tumor therapy by biomimetic dual inorganic nanozyme-catalyzed cascade reaction," *Advanced Science*, vol. 6, no. 3, article 1801733, 2019.
- [34] R. C. Bast Jr. and J. F. Holland, *Holland-Frei Cancer Medicine* 8, PMPH-USA, 2010.
- [35] Y. Li, K. H. Yun, H. Lee, S. H. Goh, Y. G. Suh, and Y. Choi, "Porous platinum nanoparticles as a high-Z and oxygen generating nanozyme for enhanced radiotherapy in vivo," *Biomaterials*, vol. 197, pp. 12–19, 2019.
- [36] Y. Hao, Y. Chen, X. He et al., "Polymeric nanoparticles with ROS-responsive prodrug and platinum nanozyme for enhanced chemophotodynamic therapy of colon cancer," *Advanced Science*, vol. 7, no. 20, article 2001853, 2020.
- [37] K. Zhang, M. Tu, W. Gao et al., "Hollow Prussian blue nanozymes drive neuroprotection against ischemic stroke via attenuating oxidative stress, counteracting inflammation, and suppressing cell apoptosis," *Nano Letters*, vol. 19, no. 5, pp. 2812–2823, 2019.
- [38] V. Kumar, A. K. Abbas, and J. C. Aster, *Robbins Basic Pathology*, Elsevier, Philadelphia, Pennsylvania, 2018.
- [39] D. A.-O. Placha and J. A.-O. Jampilek, "Chronic inflammatory diseases, anti-inflammatory agents and their delivery nanosystems," *Pharmaceutics*, vol. 13, 2021.
- [40] J. Zhao, W. Gao, X. Cai et al., "Nanozyme-mediated catalytic nanotherapy for inflammatory bowel disease," *Theranostics*, vol. 9, no. 10, pp. 2843–2855, 2019.
- [41] G. Garcia-Rayado, M. Navarro, and A. Lanás, "NSAID induced gastrointestinal damage and designing GI-sparing NSAIDs," *Expert Review of Clinical Pharmacology*, vol. 11, no. 10, pp. 1031–1043, 2018.
- [42] T. Grosser, E. Ricciotti, and G. A. FitzGerald, "The cardiovascular pharmacology of nonsteroidal anti-inflammatory drugs," *Trends in Pharmacological Sciences*, vol. 38, no. 8, pp. 733–748, 2017.

- [43] S. Bacchi, P. Palumbo, A. Sponta, and M. F. Coppolino, "Clinical pharmacology of non-steroidal anti-inflammatory drugs: a review," *Anti-Inflammatory & Anti-Allergy Agents in Medicinal Chemistry*, vol. 11, 2012.
- [44] M. Oray, K. Abu Samra, N. Ebrahimiadib, H. Meese, and C. S. Foster, "Long-term side effects of glucocorticoids," *Expert Opinion on Drug Safety*, vol. 15, no. 4, pp. 457–465, 2016.
- [45] J. Vandewalle, A. Luybaert, K. De Bosscher, and C. Libert, "Therapeutic mechanisms of glucocorticoids," *Trends in Endocrinology & Metabolism*, vol. 29, no. 1, pp. 42–54, 2018.
- [46] Y. He, Y. Yue, X. Zheng, K. Zhang, S. Chen, and Z. Du, "Curcumin, inflammation, and chronic diseases: how are they linked?," *Molecules*, vol. 20, no. 5, pp. 9183–9213, 2015.
- [47] T. Hussain, B. Tan, Y. Yin, F. Blachier, M. C. B. Tossou, and N. Rahu, "Oxidative stress and inflammation: what polyphenols can do for us?," *Oxidative Medicine and Cellular Longevity*, vol. 2016, Article ID 7432797, 9 pages, 2016.
- [48] N. Liang and D. D. Kitts, "Role of chlorogenic acids in controlling oxidative and inflammatory stress conditions," *Nutrients*, vol. 8, no. 1, 2016.
- [49] K. A. Ahmad, D. Yuan Yuan, W. Nawaz et al., "Antioxidant therapy for management of oxidative stress induced hypertension," *Free Radical Research*, vol. 51, no. 4, pp. 428–438, 2017.
- [50] I. Celardo, J. Z. Pedersen, E. Traversa, and L. Ghibelli, "Pharmacological potential of cerium oxide nanoparticles," *Nanoscale*, vol. 3, no. 4, pp. 1411–1420, 2011.
- [51] A. Karakoti, S. Singh, J. M. Dowding, S. Seal, and W. T. Self, "Redox-active radical scavenging nanomaterials," *Chemical Society Reviews*, vol. 39, no. 11, pp. 4422–4432, 2010.
- [52] C. Xu, Y. Lin, J. Wang et al., "Nanoceria-triggered synergetic drug release based on CeO<sub>2</sub>-capped mesoporous silica host-guest interactions and switchable enzymatic activity and cellular effects of CeO<sub>2</sub>," *Advanced Healthcare Materials*, vol. 2, no. 12, pp. 1591–1599, 2013.
- [53] A. Y. Estevez, S. Pritchard, K. Harper et al., "Neuroprotective mechanisms of cerium oxide nanoparticles in a mouse hippocampal brain slice model of ischemia," *Free Radical Biology & Medicine*, vol. 51, no. 6, pp. 1155–1163, 2011.
- [54] R. Pautler, E. Y. Kelly, P. J. J. Huang, J. Cao, B. Liu, and J. Liu, "Attaching DNA to nanoceria: regulating oxidase activity and fluorescence quenching," *ACS Applied Materials & Interfaces*, vol. 5, no. 15, pp. 6820–6825, 2013.
- [55] Bhargava, A. Arya, N. Sethy, S. Singh, and M. Das, "Cerium oxide nanoparticles protect rodent lungs from hypobaric hypoxia-induced oxidative stress and inflammation," *International Journal of Nanomedicine*, vol. 8, pp. 4507–4520, 2013.
- [56] Y. Guan, M. Li, K. Dong et al., "Ceria/POMs hybrid nanoparticles as a mimicking metalloproteinase for treatment of neurotoxicity of amyloid- $\beta$  peptide," *Biomaterials*, vol. 98, pp. 92–102, 2016.
- [57] Q. Bao, P. Hu, Y. Xu et al., "Simultaneous blood-brain barrier crossing and protection for stroke treatment based on edaravone-loaded ceria nanoparticles," *ACS Nano*, vol. 12, no. 7, pp. 6794–6805, 2018.
- [58] H. J. Kwon, D. Kim, K. Seo et al., "Ceria nanoparticle systems for selective scavenging of mitochondrial, intracellular, and extracellular reactive oxygen species in Parkinson's disease," *Angewandte Chemie (International Ed. in English)*, vol. 57, no. 30, pp. 9408–9412, 2018.
- [59] Y. Liu, M. Yuan, L. Qiao, and R. Guo, "An efficient colorimetric biosensor for glucose based on peroxidase-like protein-Fe<sub>3</sub>O<sub>4</sub> and glucose oxidase nanocomposites," *Biosensors & Bioelectronics*, vol. 52, pp. 391–396, 2014.
- [60] Y. Zhang, Z. Wang, X. Li et al., "Dietary iron oxide nanoparticles delay aging and ameliorate neurodegeneration in *Drosophila*," *Advanced Materials*, vol. 28, no. 7, pp. 1387–1393, 2016.
- [61] S. Zhao, H. Duan, Y. Yang, X. Yan, and K. Fan, "Fenozyme protects the integrity of the blood-brain barrier against experimental cerebral malaria," *Nano Letters*, vol. 19, no. 12, pp. 8887–8895, 2019.
- [62] F. Xiong, H. Wang, Y. Feng et al., "Cardioprotective activity of iron oxide nanoparticles," *Scientific Reports*, vol. 5, no. 1, p. 8579, 2015.
- [63] X. Liu, Q. Wang, H. Zhao, L. Zhang, Y. Su, and Y. Lv, "BSA-templated MnO<sub>2</sub> nanoparticles as both peroxidase and oxidase mimics," *Analyst*, vol. 137, no. 19, pp. 4552–4558, 2012.
- [64] N. Singh, M. A. Savanur, S. Srivastava, P. D'Silva, and G. Muges, "A redox modulatory Mn<sub>3</sub>O<sub>4</sub>Nanozyme with multi-enzyme activity provides efficient cytoprotection to human cells in a Parkinson's disease model," *Angewandte Chemie*, vol. 56, no. 45, pp. 14267–14271, 2017.
- [65] N. Singh, M. A. Savanur, S. Srivastava, P. D'Silva, and G. Muges, "A manganese oxide nanozyme prevents the oxidative damage of biomolecules without affecting the endogenous antioxidant system," *Nanoscale*, vol. 11, no. 9, pp. 3855–3863, 2019.
- [66] J. Yao, Y. Cheng, M. Zhou et al., "ROS scavenging Mn<sub>3</sub>O<sub>4</sub>nanozymes for in vivo anti-inflammation," *Chemical Science*, vol. 9, no. 11, pp. 2927–2933, 2018.
- [67] B. Xiong, R. Xu, R. Zhou, Y. He, and E. S. Yeung, "Preventing UV induced cell damage by scavenging reactive oxygen species with enzyme-mimic Au-Pt nanocomposites," *Talanta*, vol. 120, pp. 262–267, 2014.
- [68] S. Zhu, M. Zeng, G. Feng, and H. Wu, "Platinum nanoparticles as a therapeutic agent against dextran sodium sulfate-induced colitis in mice," *International Journal of Nanomedicine*, vol. 14, pp. 8361–8378, 2019.
- [69] S. Onizawa, K. Aoshiba, M. Kajita, Y. Miyamoto, and A. Nagai, "Platinum nanoparticle antioxidants inhibit pulmonary inflammation in mice exposed to cigarette smoke," *Pulmonary Pharmacology & Therapeutics*, vol. 22, no. 4, pp. 340–349, 2009.
- [70] S. Shibuya, Y. Ozawa, K. Watanabe et al., "Palladium and platinum nanoparticles attenuate aging-like skin atrophy via antioxidant activity in mice," *PLoS One*, vol. 9, no. 10, article e109288, 2014.
- [71] L. L. Dugan, L. L. Tian, K. L. Quick et al., "Carboxyfullerene neuroprotection postinjury in Parkinsonian nonhuman primates," *Annals of Neurology*, vol. 76, no. 3, pp. 393–402, 2014.
- [72] S. Singh, "Nanomaterials exhibiting enzyme-like properties (nanozymes): current advances and future perspectives," *Frontiers in Chemistry*, vol. 7, p. 46, 2019.
- [73] M. Liang and X. Yan, "Nanozymes: from new concepts, mechanisms, and standards to applications," *Accounts of Chemical Research*, vol. 52, no. 8, pp. 2190–2200, 2019.
- [74] J. Wu, X. Wang, Q. Wang et al., "Nanomaterials with enzyme-like characteristics (nanozymes): next-generation artificial enzymes (II)," *Chemical Society Reviews*, vol. 48, no. 4, pp. 1004–1076, 2019.

## Research Article

# A Study on COMP and CTX-II as Molecular Markers for the Diagnosis of Intervertebral Disc Degeneration

Dong-Duo Qi , Zhong-Han Liu , De-Sheng Wu , and Yu-Feng Huang 

Department of Spine Surgery, Shanghai East Hospital, School of Medicine, Tongji University, Shanghai 200092, China

Correspondence should be addressed to De-Sheng Wu; eastspine@163.com and Yu-Feng Huang; surgeonhng@163.com

Received 8 April 2021; Revised 7 June 2021; Accepted 24 July 2021; Published 4 August 2021

Academic Editor: Ziqing Li

Copyright © 2021 Dong-Duo Qi et al. This is an open access article distributed under the Creative Commons Attribution License, which permits unrestricted use, distribution, and reproduction in any medium, provided the original work is properly cited.

**Background.** Diagnosis of intervertebral disc degeneration (IVDD) is challenging at the early stage. The cartilage oligomeric matrix protein (COMP) and extracellular matrix degradation products of C-telopeptide of type II collagen (CTX-II) serve as markers for the serological diagnosis of IVDD. Oxidative stress might cause IVDD and matrix degeneration. **Methods.** A total of 128 male adult Sprague-Dawley (SD) rats were randomly and equally assigned to the experimental and control groups. The experimental group was used to construct IVDD models by acupuncture, while the control group underwent sham operation. The animals were executed every week for 8 weeks after intervertebral disc acupuncture, and serum samples were collected for the estimation of CTX-II and COMP concentrations by enzyme-linked immunosorbent assay (ELISA). Also, the histological changes and caudal magnetic resonance imaging (MRI) changes were examined in the intervertebral disc. **Results.** IVDD in rats worsened with prolonged follow-up after acupuncture. At all the time points, the experimental group showed altered histological and caudal vertebra MRI signals, and serum CTX-II and COMP concentrations were significantly greater than those of the control group. These levels increase with the process of IVDD. **Conclusion.** Serum CTX-II and COMP estimation is a reliable method to diagnose IVDD, and their concentrations show a positive correlation with the process of IVDD.

## 1. Background

Neck and lower back pain is the most common reason for patients to seek medical advice. The pain in about 39% of the patients is the result of intervertebral disc disorders [1]. Neck and lower back pain significantly lowers the work efficiency and prolongs the working hours [2], posing heavy medical burdens to the patients. Statistically, the lifetime prevalence of neck and lower back pain is 84%, resulting in disability in 11-12% of patients. The impact of this disability on the medical industry is increasing, with a sharp increase in treatment costs every year. The medical expense on neck and lower back pain exceeds USD 200 billion every year [3, 4].

The treatment strategy for intervertebral disc degeneration- (IVDD-) induced protrusion of the intervertebral disc focuses on alleviating clinical symptoms. Spinal fusion is the gold standard for the treatment of protrusion of the intervertebral disc but causes degeneration at adjacent segments and requires repeated surgeries in some patients. The recent advances in biological therapies, including gene therapy,

stem cell-based tissue engineering, IVDD-regulating biological factors, and microRNA therapy, prevent IVDD by promoting extracellular matrix repair and regeneration. With continuous breakthroughs in studies, these new therapies could replace surgery as an early intervention of IVDD but impose high requirements for the early diagnosis of IVDD.

The current diagnosis of protrusion of the intervertebral disc at the neck and lower back is based on the consistent findings in medical history, clinical physical examination, and imaging examination; magnetic resonance imaging (MRI) is an optimal noninvasive imaging method for a definite diagnosis [2, 5]. Furthermore, in clinical practice, IVDD is graded according to different intervertebral disc signals and heights in MRI findings but does not reflect the staging of IVDD [6], and no diagnosis could be made at the early stage of the pathological changes because histopathological changes precede the imaging modifications. Further studies on IVDD showed that IVDD patients had increased expression of extracellular matrix degradation products and some inflammatory mediators in serum or urine. This increase

was observed concurrently or before the pathological changes of IVDD, which might serve as the potential molecular markers than MRI findings in the early diagnosis of IVDD. With the development of diagnostic technology, the detection of molecular markers in blood or urine enables the prevention, prognosis, and precise (grading and staging) diagnosis of IVDD.

IVDD is closely related to intervertebral disc senescence. Oxidative stress is the main factor that causes cell senescence. ECM (extracellular matrix) destruction results in the loss of normal biomechanical correlation between intervertebral discs and accelerates disc degeneration. The levels of ECM, type II collagen, and proteoglycan are critical for normal disc function, especially in the nucleus pulposus [7].

C-telopeptide of type II collagen (CTX-II) is one of the leading products of type II collagen degradation during IVDD and is the degradation product of C-telopeptide, the 1/4 segment of type II collagen. The cartilage oligomeric matrix protein (COMP) is a vital member of the platelet cadherin family discovered recently. It consists of five independent subunits and is a pentameric protein linked by disulfide bonds. Prof. Dick Heinegård [8] from Lund University, Sweden, first discovered and reported COMP in the cartilage tissues in 1992. COMP binds to type I collagen, type II collagen, type IX collagen, fibromuscular fibroin, and proteoglycan and plays a key role in the composition, stability, and water molecule transport of cartilage extracellular matrix. Some studies [9, 10] have shown that CTX-II and COMP are potential molecular markers for joint degenerative diseases as detected by serology; however, the correlation between CTX-II and COMP concentrations and IVDD is yet unknown. To evaluate the value of serum COMP and CTX-II as molecular markers for IVDD diagnosis, a longitudinal analysis of the proteins in adult male rats during IVDD was carried out, and the correlation between the concentrations and histological and MRI changes in IVDD was analyzed.

In addition, the concentration of MDA (malondialdehyde) and SOD (superoxide dismutase), oxidative stress markers, was positively correlated with CTX-II and COMP. The level of MDA was correlated positively with that of CTX-II [11] and COMP [12], while the level of SOD [13] was negatively correlated with that of CTX-II and COMP.

## 2. Methods and Materials

**2.1. Animals.** A total of 128 healthy adult Sprague–Dawley (SD) male rats ( $200 \pm 20$  g, 2–3 weeks old) were obtained from the Animal Experiment Center of Tongji University (Shanghai, China), because they have thick tails that are convenient for experimental operations and reducing operational error. Aged rats were excluded because they already have spontaneous IVDD. None of the rats were administered any drugs before the experiment. The rats were given at least one week to acclimatize to the surrounding environment. The rats were randomly grouped into the control and experimental groups ( $n = 64/\text{group}$ ). The control group was further divided equally into 8 subgroups and fed normally. The experimental group was also randomly and equally

grouped into 8 subgroups and subjected to caudal intervertebral disc acupuncture for modeling after one week of adaptive feeding. Following acupuncture surgery, both groups were free to move in the cages; their health status was observed twice every day. This study was approved by the Animal Ethics Committee of Shanghai East Hospital of Tongji University.

**2.2. Caudal Vertebra Acupuncture.** The experimental group (2–3 weeks old) rats were anesthetized by inhaled anesthesia: induced anesthesia with 3–4% isoflurane and maintained anesthesia with 1–2% isoflurane (flow rate 0.6–0.8 L/h). When the anesthesia took effect, relevant sites were located anatomically by X-ray, and the seventh and eighth in caudal vertebra (Co7/8) segment of the intervertebral disc were marked in the rats for subsequent experiments (Figure 1). In the caudal vertebra acupuncture operation, the marked site was disinfected, the SD rat was placed in the prone position, and the intervertebral disc was punctured with a no. 26 needle until the needle reached the contralateral annulus fibrosus. Then, the internal structure of the intervertebral disc was broken by rotating the annulus fibrosus  $360^\circ$  clockwise, and the needle was left in the intervertebral disc for 30 min. Subsequently, the needle was taken out, the skin was disinfected, and the rat was placed in the awakening room, as described previously [14]. To evaluate the disc degeneration, one rat was randomly selected from each of the eight experimental groups postoperatively. These rats were euthanized for further histological evaluation.

**2.3. Hematoxylin-Eosin (H&E) Staining and Safranin O-Fast Green FCF Staining.** A total of 8 rats from the experimental and control groups were sacrificed, respectively, every week for 8 weeks after modeling by intervertebral disc acupuncture. The caudal vertebra was cut open in each rat; the intervertebral disc layer was removed, fixed in 10% buffer formalin for 72 h, decalcified by EDTA (ethylenediaminetetraacetic acid) for 4 weeks, and stained with HE and safranin O-fast green FCF. One pathologist not aware of the grouping was engaged to evaluate the histopathological changes of the intervertebral disc, as described previously [14].

**2.4. CTX-II and COMP Concentration Measurement.** A total of eight rats with fasting overnight from the experimental and control groups were sacrificed, respectively, every week for 8 weeks after modeling by intervertebral disc acupuncture. A blood sample of 5 mL was withdrawn from the eyeball of each rat in the control or experimental group, and the serum was collected by centrifugation at  $2000 \times g$  at room temperature for 15 min and stored at  $-80^\circ\text{C}$  until further use (CTX-II and COMP did not depend on the measurement time). The serum COMP and CTX-II levels were estimated by enzyme-linked immunosorbent assay (ELISA; rat serum COMP detection kit and rat serum CTX-II detection kit, Cosmo Bio, Carlsbad, CA, USA).

**2.5. MRI Analysis.** Eight animals from each group were sacrificed, respectively, at every week for 8 weeks. All the animals were subjected to caudal vertebra MRI on a Philips 1.5T superconducting MRI scanner to elucidate the



FIGURE 1: The model of caudal vertebrae was completed by acupuncture. Caudal vertebra acupuncture: the experimental group (2–3 weeks old) rats were anesthetized by inhaled anesthesia: induced anesthesia with 3–4% isoflurane and maintained anesthesia with 1–2% isoflurane (flow rate 0.6–0.8 L/h). When the anesthesia took effect, relevant sites were located anatomically, and the caudal vertebra Co7/8 segment of the intervertebral disc was marked in the rats for the experiment. The arrow indicated the segment for the acupuncture. All male rats were selected to avoid the effect of estrogen on intervertebral disc degeneration ( $n = 8$  in each group).

morphological changes of the vertebral and coccygeal tissues and the signal changes in the intervertebral disc reflected in MRI. The MRI findings were read randomly and presented by different imaging physicians in a single-blind manner and analyzed using the computer image reading analysis system (IMPAX 6.5.3.3009 Radiologist with QC). The high signal areas of the entire intervertebral disc were extracted. The images were selected randomly, and each selected image was measured three times.

**2.6. Immunohistochemical Staining.** A total of 8 rats in the experimental and control groups were sacrificed, respectively, every week for 8 weeks after modeling by intervertebral disc acupuncture. The caudal vertebra was cut open in

each rat, and the intervertebral disc layer was removed, fixed in 10% buffer formalin for 72 h, and decalcified by EDTA for 4 weeks. The sections were deparaffinized and rehydrated, and then, antigen was retrieved in the microwave for 15 min each. Then, endogenous peroxidase activity was blocked for 10 min by 3% hydrogen peroxide, and nonspecific binding sites were blocked for 30 min at room temperature by 5% BSA. Then, the sections were incubated with primary antibodies: MMP3 (ab268084, Abcam, Cambridge, UK), aggrecan (ab216965, Abcam, Cambridge, UK), and Col2a1 (ab188570, Abcam, Cambridge, UK) at 4°C overnight, followed by secondary antibodies. Finally, the slides were sealed and photographed under a microscope.

**2.7. Statistical Analysis.** Prism 5.0 (GraphPad Software Inc., San Diego, CA, USA) and SPSS 20.0 (SPSS Inc., Chicago, IL, USA) software were used for statistical analysis. The measurement data were expressed as mean  $\pm$  standard deviation, and the enumeration data were evaluated by nonparametric statistics. Chi-square and exact probability tests were used to perform row-column ( $R \times C$ ) cross-tabulation.  $P < 0.05$  indicated a statistical significance.

### 3. Results

**3.1. MRI Findings Showed Increasingly Significant Degeneration of the Acupunctured Segment in Rats over Time.** After modeling by acupuncture at the same site in the caudal vertebra 7–8 (Co7–8), the rats were sacrificed every week for 8 weeks and examined by MRI scan. The findings showed that the degeneration of the acupunctured segment in the rat worsened over time; the severity of IVDD increased; the nucleus pulposus (NP) structure changed from a uniform and bright white to uneven and black; the boundary between NPC and annulus fiber disappeared; the MRI T2 phase changed from high signal to low signal, and the height of the intervertebral disc decreased progressively (Figure 2).

**3.2. H&E Staining and Safranin O-Fast Green Staining Showed Severe IVDD in the Rats of the Experimental Group.** According to safranin O-fast green staining results, no significant difference was detected among different time points in the control group. Moreover, the control group showed intact NPCs in the intervertebral disc: a quasicircular central NPC, a large number of notochord cells, a small number of chondroid cells, and the peripheral annulus fibrosus arranged in an annular manner with a distinct boundary with the NPCs. Conversely, the experimental group showed varied degeneration in the NPCs of the intervertebral disc: the annulus fibrosus worsened over time, the inner fiber of the annulus fibrosus twisted and protruded into the intervertebral disc with an unclear boundary with the NPCs and the cracks inside NPCs, and the chondroid cells were replaced by fibrocartilage cell and inflammatory cell infiltration. Consistently, examination by H&E staining revealed that the experimental group showed degeneration of the NPCs, and the annulus fibrosus was manifested by annular disruption, NPC herniation, endplate calcification and thickening,

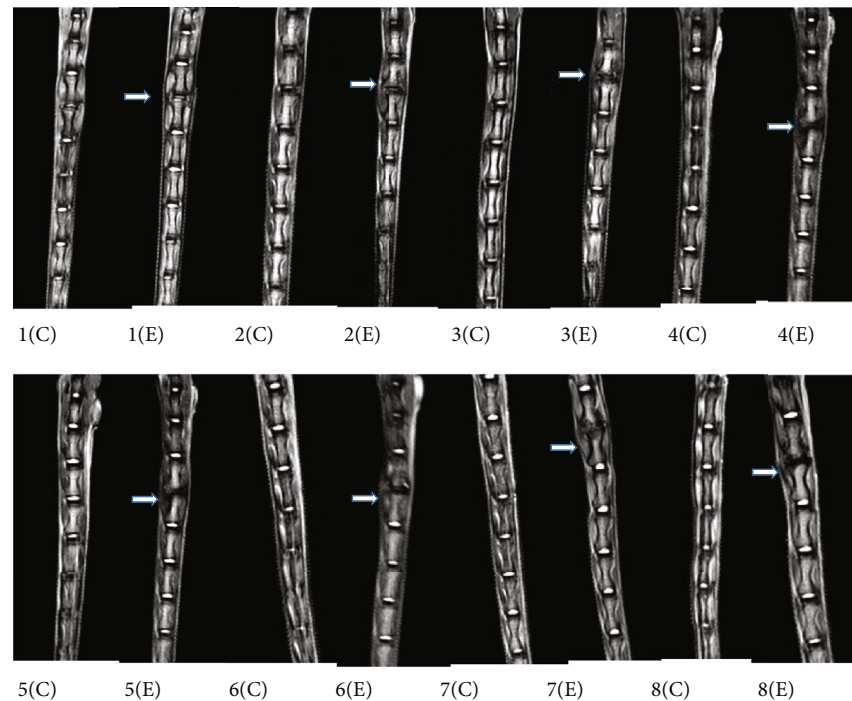


FIGURE 2: MRI findings showed increasingly significant degeneration of the acupuncture segment in rats over time ( $n = 8$  in each group). 1(C) and 1(E): 1-week flowing acupuncture in the control and experimental groups. 2(C) and 2(E): 2-week flowing acupuncture in the control and experimental groups. 3(C) and 3(E): 3-week flowing acupuncture in the control and experimental groups. 4(C) and 4(E): 4-week flowing acupuncture in the control and experimental groups. 5(C) and 5(E): 5-week flowing acupuncture in the control and experimental groups. 6(C) and 6(E): 6-week flowing acupuncture in the control and experimental groups. 7(C) and 7(E): 7-week flowing acupuncture in the control and experimental groups. 8(C) and 8(E): 8-week flowing acupuncture in the control and experimental groups. The rats were sacrificed in each week until week 8, and all the injured segments were examined by MRI. The MRI findings showed that the severity of IVDD (the nucleus pulposus (NPC) structure changed from a uniform and bright white to uneven and black, the boundary between NPC and annulus fiber disappeared, the MRI T2 phase changed from high signal to low signal, and the height of the intervertebral disc decreased progressively) increased over time from week 1 to week 8.

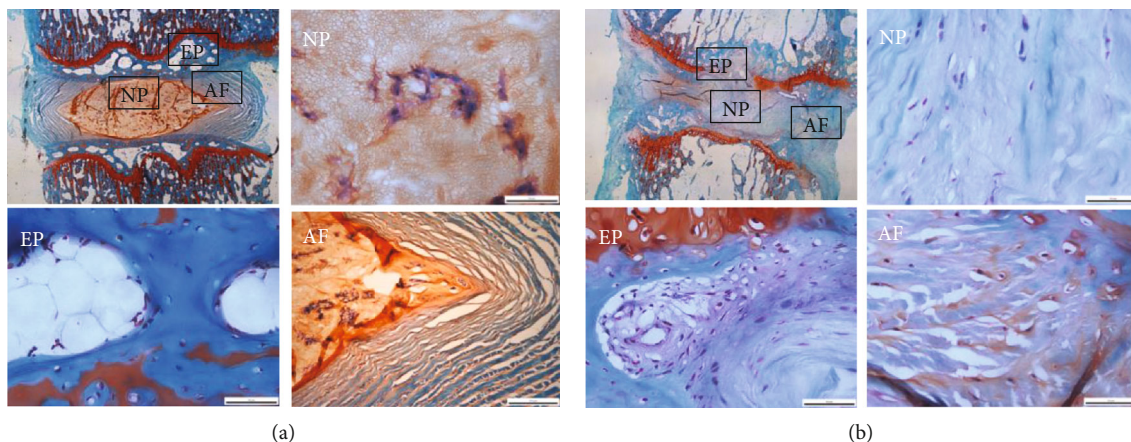


FIGURE 3: Safranin O-fast green staining showed severe IVDD in the rats of the experimental group. (a) The control group showed complete NPCs in the intervertebral disc, a quasicircular central NPC, a large number of notochord cells, a small number of chondroid cells, and the peripheral annulus fibrosus arranged in an annular manner with a clear boundary with the NPCs. (b) The experimental group (acupuncture group) showed the annulus fibrosus disrupted and disorganized over time (the inner fiber of the annulus fibrosus twisted and protruded into the intervertebral disc with an unclear boundary with the NPCs and the cracks inside NPCs) and the chondroid cells were replaced by fibrocartilage cells and inflammatory cell infiltration. AF: annulus fibrosus; NP: nucleus pulposus; EP: endplate cartilage.

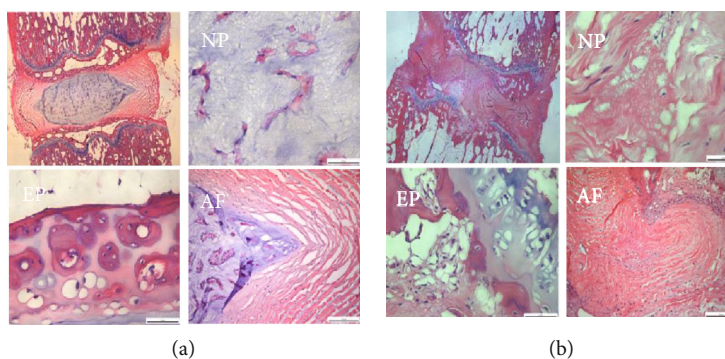


FIGURE 4: H&E staining showed severe IVDD in the rats of the experimental group. (a) The control group showed no significant difference was detected between different time points. (b) The experimental group showed the annulus fibrosus was manifested by annular disruption, NPC loss, endplate calcification, and cell necrosis. AF: annulus fibrosus; NP: nucleus pulposus; EP: endplate cartilage.  $n = 8$  in each group.

hyaline membrane thinning, and cartilage cell necrosis (Figures 3 and 4).

**3.3. Expressions of Aggrecan and Type II Collagen Decreased, and the Expression of Matrix Metalloproteinase-3 (MMP3) Increased with the Progress of IVDD.** Immunohistochemical staining results of aggrecan and type II collagen in the caudal intervertebral disc of rats showed that NPC tissues were absent or partially missing in the degenerative rats, and the annulus fibrosus and endplate structure were damaged. Aggrecan and type II collagen were clearly expressed in the cytoplasm of the cartilage endplate, NPC, and annulus fibrosus, and the expression levels were higher in the normal intervertebral disc than those in the degenerative groups. The immunohistochemical staining results of MMP3 in the caudal intervertebral disc of rats showed that NPC tissues were absent or partially missing in the degenerative rats and the annulus fibrosus and the endplate structure were damaged. The expression of MMP3 was mainly expressed in the cytoplasm, and the experimental group had a significantly higher MMP3 expression than the control group. These findings may indicate that type II collagen in the NPC and annulus fibrosus was degraded and gradually replaced by type I collagen with the progress of degeneration. Moreover, the increased expression of matrix metalloproteinase (MMP) in the degenerated group suggested the degenerated pathology during IVDD (Figure 5).

**3.4. Serum CTX-II Concentration Increased with the Process of IVDD.** The experimental group showed an increase in CTX-II concentration (pg/mL), which was  $73.95 \pm 5.53$ ,  $90.71 \pm 13.5$ ,  $74.48 \pm 10.38$ ,  $87.35 \pm 20.256$ ,  $86.16 \pm 15.95$ ,  $108.59 \pm 17.45$ ,  $111.27 \pm 15.08$ , and  $119.16 \pm 6.95$  at weeks 1–8, respectively. A statistically significant difference was detected in the increase in CTX-II concentration between the experimental and control groups ( $P < 0.05$ ,  $n = 128$ ) (Figure 6, Table 1).

**3.5. Serum COMP Concentration Increased with the Development of IVDD.** The experimental group showed an increase in the COMP concentration (pg/mL), which was  $41.71 \pm 2.86$ ,  $51.94 \pm 7.64$ ,  $53.37 \pm 6.3$ ,  $59.37 \pm 6.3$ ,  $61.94 \pm$

$1.23$ ,  $62.63 \pm 8.24$ ,  $63.71 \pm 3.52$ , and  $65.95 \pm 2.86$  at weeks 1–8, respectively. A statistically significant difference was detected in the increase in COMP concentration between the experimental and control groups ( $P < 0.05$ ,  $n = 128$ ) (Figure 7, Table 2).

**3.6. Serum MDA Concentration Increased and SOD Concentration Decreased with the Development of IVDD.** Reactive oxygen species (ROS) production is inevitable due to the oxygen-utilizing metabolism of disc cells despite the hypoxic microenvironment in IVDD. Reportedly, CTX-II and COMP are closely related to oxidative stress, which was further verified in IVDD based on the correlation study between MDA and SOD and IVDD. We found a correlation between the level of MDA and SOD and oxidative stress markers with the development of IVDD. The serum MDA concentration at 8 w after modeling was significantly higher than that at 4 w ( $n = 3$ ,  $*P < 0.05$ ) (Figure 8(a)), while the serum SOD concentration at 8 w after modeling was significantly lower than that at 4 w ( $n = 3$ ,  $*P < 0.05$ ) (Figure 8(b)).

## 4. Discussion

The spine is one of the load-bearing structures in the human body, and the intervertebral disc is vital in maintaining mechanical transmission and spinal movement in humans. In this process, the extracellular matrix in the intervertebral disc maintains the smoothness of the intervertebral disc cartilage structure and buffering forces. The intervertebral disc is composed of the endplate cartilage, NPC, and annulus fibrosus. The extracellular matrix in the intervertebral disc is mainly composed of proteoglycan and type II and type I collagen, with proteoglycan as one of the critical components.

The serum CTX-II and COMP concentrations increase in the experimental group with the development of IVDD. Subsequently, the degeneration of the acupunctured segment in the rat worsened, and CTX-II and COMP concentrations were positively correlated with IVDD. Type II collagen is a triple-helix protein composed of three identical polypeptide chain- $\alpha$  chains and a significant macromolecule in the extracellular matrix in the intervertebral disc. The initial form of the  $\alpha$ -chain is the  $\alpha$ -chain precursor composed of the

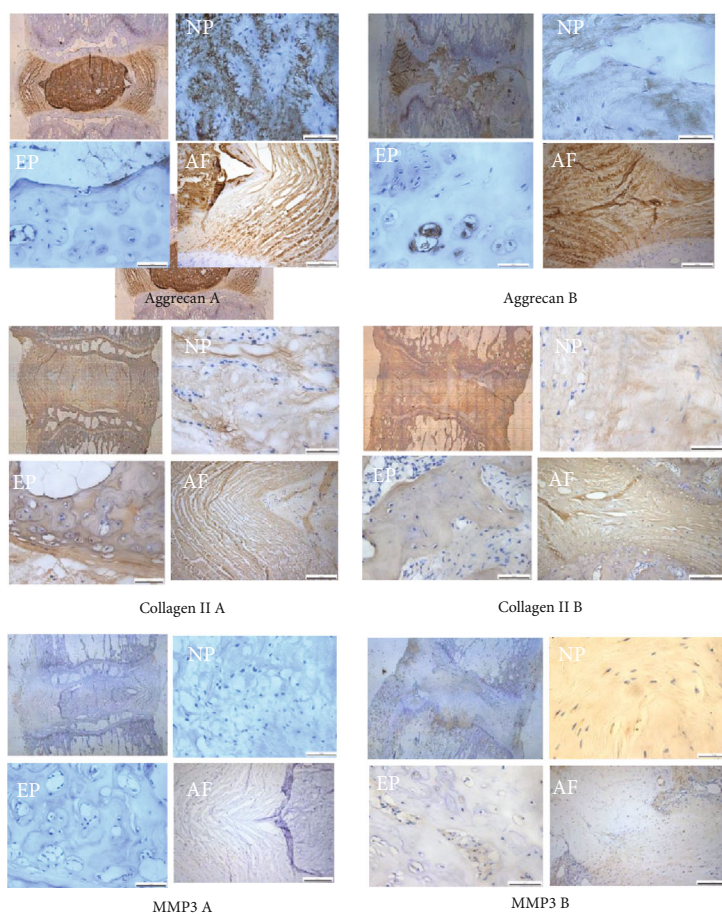


FIGURE 5: The expressions level of aggrecan and type II collagen decreased, and the expression of MMP3 increased with the progress of IVDD. Immunohistochemistry showed that the expression levels of aggrecan and type II collagen are significantly decreased. Immunohistochemistry showed that the level of MMP3 in the caudal intervertebral disc of (b) experimental rats is significantly increased than that of the (a) control group.  $n = 8$  in each group.

propeptides at the amino terminal and carboxy terminal, the triple helix in the middle, and the telopeptide between the propeptides and the triple-helix structure [15]. During modification, the propeptides at both terminals are hydrolyzed by enzymes, leaving only the triple-helix structure and the telopeptide, which turn into collagen precursors that crosslinks to form the collagen fiber network.

Type II collagen plays a critical role in maintaining structural stability and functional integrity of the intervertebral disc [16]. The degradation of the extracellular matrix is one of the major pathological changes during IVDD, while the degradation of type II collagen in NPC and the annulus fibrosus and its replacement by type I collagen are the leading pathological manifestations of IVDD [16, 17]. Furthermore, during IVDD, various MMPs, including MMP1, MMP3, and MMP13, occur predominantly during the degradation and change in type II collagen [18]. Under the effect of MMPs, type II collagen is hydrolyzed and forms a type II 3/4 segment of 794-amino acid length and a type II 1/4 fragment of 266 amino acids. Subsequently, the triple-helix structures of these two segments are uncoiled and further degraded by other MMPs. The end products of type II collagen mainly include CTX-II, type II neopeptide (TIINE), and

nitroated type II collagen-1 (Coll2-1NO2), among which CTX-II is one of the main products of type II collagen in the intervertebral disc degraded via MMPs and the degradation product of the telopeptide of type II collagen 1/4 segment at the carboxyl terminal [19]. Therefore, with the development of IVDD, the external blood vessels expand continually, releasing serum CTX-II into blood, which serves as the theoretical basis for using serum or urinary molecular markers to diagnose IVDD.

Current studies have shown that serum and urinary CTX-II are potential molecular markers for osteoarthritis and rheumatoid arthritis. Another study showed that the expression of serum CTX-II was significantly increased and positively correlated with MMP3 in rheumatoid arthritis, deeming it as a vital indicator to judge the severity and prognosis of rheumatoid arthritis [20–22]. Furthermore, serum and urinary CTX-II concentrations were positively correlated with the degree of surface cartilage destruction, K-L score, and the degree of joint space narrowing in osteoarthritis, indicating that CTX-II is an optimal molecular marker to judge the prognosis of osteoarthritis [23]. In addition, serum and urinary CTX-II concentrations have been shown to gradually decrease, suggesting that these could be the

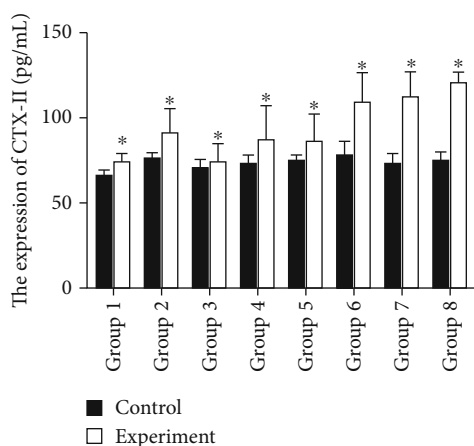


FIGURE 6: Serum CTX-II concentration increased with the process of IVDD. Group 1: 1-week flowing acupuncture in the control and experimental groups. Group 2: 2-week flowing acupuncture in the control and experimental groups. Group 3: 3-week flowing acupuncture in the control and experimental groups. Group 4: 4-week flowing acupuncture in the control and experimental groups. Group 5: 5-week flowing acupuncture in the control and experimental groups. Group 6: 6-week flowing acupuncture in the control and experimental groups. Group 7: 7-week flowing acupuncture in the control and experimental groups. Group 8: 8-week flowing acupuncture in the control and experimental groups. The level of CTX-II concentration is significantly increased with time following injury. The concentration of CTX-II in groups 1-8 is listed in Table 1. A statistically significant difference was detected in the increase in CTX-II concentration between the experimental and control groups ( $P < 0.05$ ) ( $n = 8$  in each group).

TABLE 1: The expression level of serum CTX-II in the control group and the experimental group in each week following acupuncture.

Time CTX-II	Control group (pg/mL)	Experimental group (pg/mL)	<i>P</i>
1 w	65.59 ± 3.25	73.95 ± 5.53	<0.05
2 w	75.66 ± 3.80	90.71 ± 13.5	<0.05
3 w	70.18 ± 4.35	74.48 ± 10.38	<0.05
4 w	72.94 ± 5.39	87.35 ± 20.256	<0.05
5 w	74.73 ± 4.18	86.16 ± 15.95	<0.05
6 w	77.32 ± 8.47	108.59 ± 17.45	<0.05
7 w	72.4 ± 6.54	111.27 ± 15.08	<0.05
8 w	73.95 ± 5.5	119.16 ± 6.95	<0.05

$N = 8$  in each group. CI: 95% confidence interval.

potential markers for the treatment efficacy on osteoarthritis [24] and rheumatoid arthritis [22, 25], as well as reliable markers for recovery and healing. Similar conclusions have been drawn on serum and urinary CTX-II concentrations in IVDD. Garnero et al. [26] studied the urine of 324 postmenopausal females and found that the urinary CTX-II concentration was between 166 and 299 ng/mmol and closely related to the intervertebral space narrowing, knee osteoarthritis with clinical symptoms, and hand osteoarthritis. A

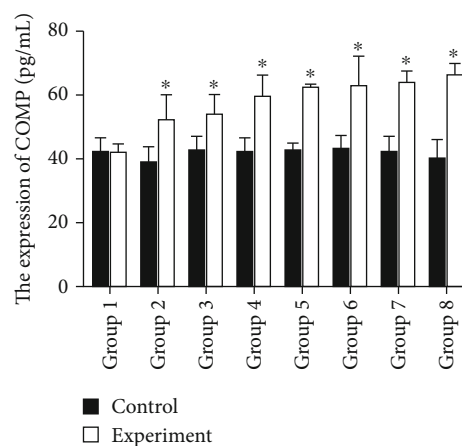


FIGURE 7: Serum COMP concentration increased with the development of IVDD. Group 1: 1-week flowing acupuncture in the control and experimental groups. Group 2: 2-week flowing acupuncture in the control and experimental groups. Group 3: 3-week flowing acupuncture in the control and experimental groups. Group 4: 4-week flowing acupuncture in the control and experimental groups. Group 5: 5-week flowing acupuncture in the control and experimental groups. Group 6: 6-week flowing acupuncture in the control and experimental groups. Group 7: 7-week flowing acupuncture in the control and experimental groups. Group 8: 8-week flowing acupuncture in the control and experimental groups. The level of COMP concentration is significantly increased with time following injury. The concentration of CTX-II in groups 1-8 is listed in Table 2. A statistically significant difference was detected in the increase in COMP concentration between the experimental and control groups ( $P < 0.05$ ) ( $n = 8$  in each group).

TABLE 2: The expression level of serum COMP in the control group and the experimental group in each week following acupuncture.

Time COMP	Control group (pg/mL)	Experimental group (pg/mL)	<i>P</i>
1 w	41.41 ± 4.39	41.71 ± 2.86	>0.05
2 w	38.22 ± 5.34	51.94 ± 7.64	<0.05
3 w	40.32 ± 4.3	53.37 ± 6.3	<0.05
4 w	41.83 ± 4.5	59.37 ± 6.3	<0.05
5 w	41.85 ± 2.68	61.94 ± 1.23	<0.05
6 w	42.93 ± 4.4	62.63 ± 8.24	<0.05
7 w	41.52 ± 4.82	63.71 ± 3.52	<0.05
8 w	39.52 ± 5.59	65.95 ± 2.86	<0.05

$N = 8$  in each group. CI: 95% confidence interval.

recent study by Brayda-Bruno et al. [27] compared serum vitamin D, CTX-I, and CTX-II concentrations in 79 males with and without IVDD and found that active serum vitamin D and serum CTX-II concentrations were rhythmically distributed over a year. Also, the serum CTX-I concentration was positively correlated with the active serum vitamin D concentration and negatively with serum CTX-II concentration, and the IVDD patients with osteochondrosis showed that serum CTX-II concentration was significantly higher

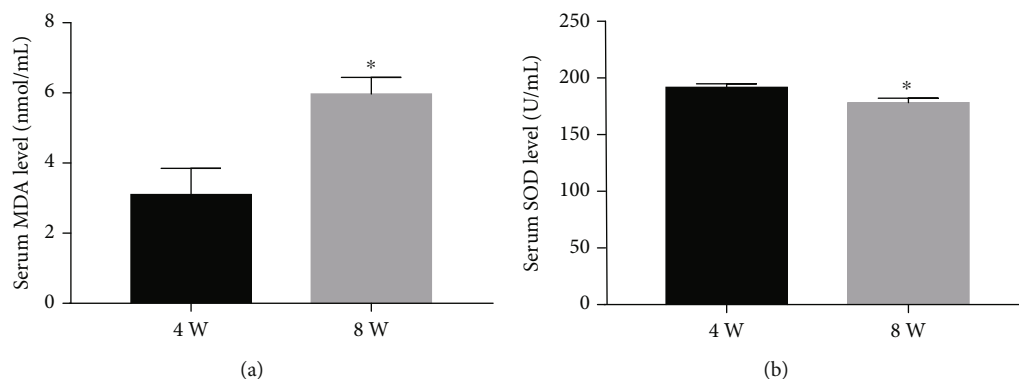


FIGURE 8: The serum concentration of MDA and SOD is increased with the extent of IVDD. (a) The serum MDA level in the control and experimental groups at 4 weeks and 8 weeks following acupuncture. (b) The serum SOD level in the control and experimental groups at 4 weeks and 8 weeks following acupuncture ( $n = 3$ ,  $*P < 0.05$ ).

than in those without IVDD and osteochondrosis. Meulenbelt et al. [28] analyzed the urinary CTX-II concentration in 302 patients and found that it was closely correlated with knee osteoarthritis, hip osteoarthritis, and IVDD.

Recent studies have shown that COMP is correlated with articular cartilage destruction and extracellular matrix degradation. Some studies have shown that COMP is a bone marker for knee osteoarthritis, hip osteoarthritis, and rheumatoid arthritis due to its correlation with cartilage destruction and matrix degradation. It can also be a critical molecular marker to judge the prognosis and treatment efficacy on knee and hip osteoarthritis. In the extracellular matrix of the intervertebral disc, COMP binds to type II collagen and proteoglycan to stabilize the cartilage collagen network to maintain the integrity of the intervertebral disc [29]. Taken together, it could be deduced that COMP is a macromolecule released into the blood during cartilage matrix destruction and degradation similar to CTX-II. Goode et al. [30] analyzed the serum COMP, hyaluronic acid, and urinary CTX-II concentrations in 547 patients and found that the serum hyaluronic acid concentration is correlated to the intervertebral space narrowing in females, the urinary CTX-II concentration is correlated with the intervertebral space narrowing, and the serum COMP concentration is closely correlated to the lower back pain induced by intervertebral space narrowing.

Similar to osteoarthritis and rheumatoid arthritis, IVDD is a degenerative disease of the cartilage manifested as extracellular matrix degradation [31]. Therefore, CTX-II and COMP, the molecules released into the blood after extracellular matrix degradation, are potential molecular biomarkers for IVDD. Several studies have focused on CTX-II and COMP in osteoarthritis and rheumatoid arthritis [32], and only a few have reported the specific correlation between CTX-II and COMP. The liability of these molecules as the clinical markers for IVDD needs further exploration in animal and clinical studies.

Oxidative stress is speculated as one of the causes of IVDD. Reactive oxygen species (ROS) production is inevitable due to oxygen-utilizing metabolism of disc cells despite the hypoxic microenvironment in IVDD [33]. IVDD is mainly caused by the changes in nucleus pulposus cells and

extracellular matrix. The destruction of ECM leads to the loss of normal biomechanical correlations between intervertebral discs and accelerates the degeneration of intervertebral discs [34]. The degradation of proteoglycan decreases the osmotic pressure of the ECM and the decrease in the NP water content in the nucleus pulposus. In NP, type II collagen is converted to type I collagen [7]. Therefore, it can be concluded that oxidative stress is closely related to the expression levels of CTX-II and COMP during intervertebral disc degenerative changes. Recent studies have shown that oxidative stress promotes the production of apoptotic bodies (Abs) in endplate chondrocytes in rats to increase the expressions of relevant ossification genes, such as *Runx2*, in endplate chondrocytes [35], and the expressions of type X collagen (ColX), *Runx2*, osteoprotegerin, and alkaline phosphatase (ALP) were significantly higher in degenerative intervertebral discs than in normal intervertebral discs, suggesting that IVDD involves proliferative differentiation similar to that in advanced osteoarthritis [36]. The current study showed that the concentration of MDA and SOD, oxidative stress markers, was correlated to the development of IVDD. The activity of serum and intervertebral disc SOD decreased and MDA increased gradually with disc degeneration [37]. Therefore, the oxidative stress could be a reason for elevated CTX-II and COMP. Watari et al. [11] demonstrated that the serum MDA concentration was correlated to that of CTX-II concentration, but not to CPII concentration and significantly correlated to the serum lipid (total cholesterol and triglyceride) level and body weight. These findings indicated that oxidative stress might be involved in the degradation of type II collagen in the articular cartilage. Coustry et al. [38] utilized MT-COMP pseudoachondroplasia (PSACH) mouse models and found that the accumulation of misfolded COMP in the endoplasmic reticulum of growth plate chondrocytes resulted in premature death and loss of linear growth of chondrocytes. Intriguingly, the premature death of chondrocytes was the result of activated oxidative stress and inflammation via the CHOP-er pathway, which disrupted the adipogenesis-osteogenesis balance. These phenomena suggested that the increase in CTX-II and COMP concentrations might be correlated with enhanced oxidative stress in the intervertebral disc.

Therefore, the detection of serum and urinary molecular markers is a reliable method to diagnose IVDD. However, IVDD is similar to degenerative diseases of the cartilage, such as osteoarthritis, arising from extracellular matrix degradation and inflammatory responses. Thus, serum and urinary molecular markers may not be specific for IVDD diagnosis, thereby necessitating continuous anatomical and physiological analyses of the intervertebral disc in osteoarthritis in several clinical and animal experiments. Substances specific to intervertebral disc tissues may be identified in future studies based on the anatomy and physiology of the disc and emphasize the significance of the diagnosis of intervertebral disc-related diseases according to serum and urine detection results.

## 5. Conclusion

CTX-II and COMP are potential indicators for IVDD in rats, and their expression is a positive correlation with the degeneration extent of IVD.

## Data Availability

The data used to support the findings of this study are available from the corresponding authors (Yu-Feng Huang and De-Sheng Wu) upon request.

## Disclosure

The funding agencies have no role in the design of the study; collection, analysis, and interpretation of data; and writing of the manuscript. The authors are solely responsible for the design of the study; collection, analysis, interpretation, and reporting of data; and writing of the manuscript.

## Conflicts of Interest

The authors declare that they have no conflicts of interest.

## Acknowledgments

This study was funded by the Shanghai Nature Science Fund projects (Grant no. 19ZR1441700; Shanghai, China) and the Discipline Leader Training Project of Pudong New Area Municipal Health Commission (Grant no. PWRd2020-03; Shanghai, China).

## References

- [1] M. J. DePalma, J. M. Ketchum, and T. R. Saullo, "Etiology of chronic low back pain in patients having undergone lumbar fusion," *Pain Medicine*, vol. 12, no. 5, pp. 732–739, 2011.
- [2] D. S. Kreiner, S. W. Hwang, J. E. Easa et al., "An evidence-based clinical guideline for the diagnosis and treatment of lumbar disc herniation with radiculopathy," *The Spine Journal*, vol. 14, no. 1, pp. 180–191, 2014.
- [3] W. C. Jacobs, S. M. Rubinstein, P. C. Willems et al., "The evidence on surgical interventions for low back disorders, an overview of systematic reviews," *European Spine Journal*, vol. 22, no. 9, pp. 1936–1949, 2013.
- [4] D. E. Martins, N. Astur, M. Kanas, M. Ferretti, M. Lenza, and M. Wajchenberg, "Quality assessment of systematic reviews for surgical treatment of low back pain: an overview," *The Spine Journal*, vol. 16, no. 5, pp. 667–675, 2016.
- [5] S. E. Hamilton-Bennett and S. Behr, "Clinical presentation, magnetic resonance imaging features, and outcome in 6 cats with lumbar degenerative intervertebral disc extrusion treated with hemilaminectomy," *Veterinary Surgery*, vol. 48, no. 4, pp. 556–562, 2019.
- [6] J. Zeckser, M. Wolff, J. Tucker, and J. Goodwin, "Multipotent mesenchymal stem cell treatment for discogenic low back pain and disc degeneration," *Stem Cells International*, vol. 2016, Article ID 3908389, 13 pages, 2016.
- [7] J. Dowdell, M. Erwin, T. Choma, A. Vaccaro, J. Iatridis, and S. K. Cho, "Intervertebral disk degeneration and repair," *Neurosurgery*, vol. 80, no. 3S, pp. S46–S54, 2017.
- [8] T. Saxne and D. Heinegård, "Cartilage oligomeric matrix protein: a novel marker of cartilage turnover detectable in synovial fluid and blood," *British journal of rheumatology*, vol. 31, no. 9, pp. 583–591, 1992.
- [9] T. Toda, Y. Sugioka, and T. Koike, "Soybean isoflavone can protect against osteoarthritis in ovariectomized rats," *Journal of food science and technology*, vol. 57, no. 9, pp. 3409–3414, 2020.
- [10] L. M. Vos, R. Kuijjer, J. J. Huddleston Slater, and B. Stegenga, "Alteration of cartilage degeneration and inflammation markers in temporomandibular joint osteoarthritis occurs proportionally," *Journal of oral and maxillofacial surgery: official journal of the American Association of Oral and Maxillofacial Surgeons*, vol. 71, no. 10, pp. 1659–1664, 2013.
- [11] T. Watari, K. Naito, K. Sakamoto, H. Kurosawa, I. Nagaoka, and K. Kaneko, "Evaluation of the effect of oxidative stress on articular cartilage in spontaneously osteoarthritic STR/OrtCrli mice by measuring the biomarkers for oxidative stress and type II collagen degradation/synthesis," *Experimental and Therapeutic Medicine*, vol. 2, no. 2, pp. 245–250, 2011.
- [12] S. I. Shafiey, W. R. Mohamed, and A. A. Abo-Saif, "Paroxetine and rivastigmine mitigates adjuvant-induced rheumatoid arthritis in rats: impact on oxidative stress, apoptosis and RANKL/OPG signals," *Life sciences*, vol. 212, pp. 109–118, 2018.
- [13] Y. Sun, C. Wang, and C. Gong, "Repairing effects of glucosamine sulfate in combination with etoricoxib on articular cartilages of patients with knee osteoarthritis," *Journal of orthopaedic surgery and research*, vol. 15, no. 1, p. 150, 2020.
- [14] X. Li, S. Yang, L. Han, K. Mao, and S. Yang, "Ciliary IFT80 is essential for intervertebral disc development and maintenance," *The FASEB Journal*, vol. 34, no. 5, pp. 6741–6756, 2020.
- [15] N. Willems, A. R. Tellegen, N. Bergknut et al., "Inflammatory profiles in canine intervertebral disc degeneration," *BMC veterinary research*, vol. 12, no. 1, 2016.
- [16] Q. Wu, C. Mathers, E. W. Wang, D. Wenkert, J. H. Huang, and S. Sheng, "TGF- $\beta$  initiates  $\beta$ -catenin-mediated CTGF secretory pathway in old bovine nucleus pulposus cells: a potential mechanism for intervertebral disc degeneration," *JBMR Plus*, vol. 3, no. 2, article e10069, 2019.
- [17] M. Molinos, C. R. Almeida, J. Caldeira, R. M. Gonçalves, M. A. Barbosa, and C. Cunha, "Inflammation in intervertebral disc degeneration and regeneration," *Journal of the Royal Society Interface*, vol. 12, no. 108, 2015.

- [18] J. E. Mayer, J. C. Iatridis, D. Chan, O. Gottesman, A. C. Hecht, and S. A. Qureshi, "Genetic polymorphisms associated with intervertebral disc degeneration," *The Spine Journal*, vol. 13, no. 3, pp. 299–317, 2013.
- [19] Y. M. Park, S. J. Kim, K. J. Lee, S. S. Yang, B. H. Min, and H. C. Yoon, "Detection of CTX-II in serum and urine to diagnose osteoarthritis by using a fluoro-microbeads guiding chip," *Biosensors & Bioelectronics*, vol. 67, pp. 192–199, 2015.
- [20] J. R. Wang, W. N. Gao, R. Grimm et al., "A method to identify trace sulfated IgG N-glycans as biomarkers for rheumatoid arthritis," *Nature Communications*, vol. 8, no. 1, p. 631, 2017.
- [21] D. Vosse, R. Landewe, P. Garnero, D. van der Heijde, S. van der Linden, and P. Geusens, "Association of markers of bone and cartilage-degradation with radiological changes at baseline and after 2 years follow-up in patients with ankylosing spondylitis," *Rheumatology (Oxford)*, vol. 47, no. 8, pp. 1219–1222, 2008.
- [22] R. Landewé, P. Geusens, M. Boers et al., "Markers for type II collagen breakdown predict the effect of disease-modifying treatment on long-term radiographic progression in patients with rheumatoid arthritis," *Arthritis and Rheumatism*, vol. 50, no. 5, pp. 1390–1399, 2004.
- [23] M. Attur, S. Krasnokutsky-Samuels, J. Samuels, and S. B. Abramson, "Prognostic biomarkers in osteoarthritis," *Current Opinion in Rheumatology*, vol. 25, no. 1, pp. 136–144, 2013.
- [24] P. Wang, J. Song, and D. Qian, "CTX-II and YKL-40 in early diagnosis and treatment evaluation of osteoarthritis," *Experimental and Therapeutic Medicine*, vol. 17, no. 1, pp. 423–431, 2019.
- [25] H. Q. Hao, J. F. Zhang, Q. Q. He, and Z. Wang, "Cartilage oligomeric matrix protein, C-terminal cross-linking telopeptide of type II collagen, and matrix metalloproteinase-3 as biomarkers for knee and hip osteoarthritis (OA) diagnosis: a systematic review and meta-analysis," *Osteoarthritis and Cartilage*, vol. 27, no. 5, pp. 726–736, 2019.
- [26] P. Garnero, E. Sornay-Rendu, M. Arlot, C. Christiansen, and P. D. Delmas, "Association between spine disc degeneration and type II collagen degradation in postmenopausal women: the OFELY study," *Arthritis and Rheumatism*, vol. 50, no. 10, pp. 3137–3144, 2004.
- [27] M. Brayda-Bruno, M. Viganò, S. Cauci et al., "Plasma vitamin D and osteo-cartilaginous markers in Italian males affected by intervertebral disc degeneration: focus on seasonal and pathological trend of type II collagen degradation," *Clinica Chimica Acta*, vol. 471, pp. 87–93, 2017.
- [28] I. Meulenbelt, M. Kloppenburg, H. M. Kroon et al., "Urinary CTX-II levels are associated with radiographic subtypes of osteoarthritis in hip, knee, hand, and facet joints in subject with familial osteoarthritis at multiple sites: the GARP study," *Annals of the Rheumatic Diseases*, vol. 65, no. 3, pp. 360–365, 2006.
- [29] A. N. Khan, H. E. Jacobsen, J. Khan et al., "Inflammatory biomarkers of low back pain and disc degeneration: a review," *Annals of the New York Academy of Sciences*, vol. 1410, no. 1, pp. 68–84, 2017.
- [30] A. P. Goode, S. W. Marshall, V. B. Kraus et al., "Association between serum and urine biomarkers and lumbar spine individual radiographic features: the Johnston County Osteoarthritis Project," *Osteoarthritis and Cartilage*, vol. 20, no. 11, pp. 1286–1293, 2012.
- [31] W. Guo, B. Zhang, Y. Li et al., "Gene expression profile identifies potential biomarkers for human intervertebral disc degeneration," *Molecular Medicine Reports*, vol. 16, no. 6, pp. 8665–8672, 2017.
- [32] H. A. Benabdoun, M. Kulbay, E. P. Rondon et al., "In vitro and in vivo assessment of the proresolutive and antiresorptive actions of resolvin D1: relevance to arthritis," *Arthritis Research & Therapy*, vol. 21, no. 1, p. 72, 2019.
- [33] D. C. Lee, C. S. Adams, T. J. Albert, I. M. Shapiro, S. M. Evans, and C. J. Koch, "In situ oxygen utilization in the rat intervertebral disc," *Journal of Anatomy*, vol. 210, no. 3, pp. 294–303, 2007.
- [34] C. L. Le Maitre, A. J. Freemont, and J. A. Hoyland, "Accelerated cellular senescence in degenerate intervertebral discs: a possible role in the pathogenesis of intervertebral disc degeneration," *Arthritis Research & Therapy*, vol. 9, no. 3, p. R45, 2007.
- [35] F. L. Yuan, R. S. Xu, J. X. Ye, M. D. Zhao, X. Li, and L. J. Ren, "Apoptotic bodies from endplate chondrocytes enhance the oxidative stress-induced mineralization by regulating PPI metabolism," *Journal of Cellular and Molecular Medicine*, vol. 23, no. 5, pp. 3665–3675, 2019.
- [36] J. P. Rutges, R. A. Duit, J. A. Kummer et al., "Hypertrophic differentiation and calcification during intervertebral disc degeneration," *Osteoarthritis and Cartilage*, vol. 18, no. 11, pp. 1487–1495, 2010.
- [37] G. Hou, H. Lu, M. Chen, H. Yao, and H. Zhao, "Oxidative stress participates in age-related changes in rat lumbar intervertebral discs," *Archives of gerontology and geriatrics*, vol. 59, no. 3, pp. 665–669, 2014.
- [38] F. Coustry, K. L. Posey, T. Maerz et al., "Mutant cartilage oligomeric matrix protein (COMP) compromises bone integrity, joint function and the balance between adipogenesis and osteogenesis," *Matrix Biology*, vol. 67, pp. 75–89, 2018.

## Research Article

# The Antioxidant Resveratrol Protects against Chondrocyte Apoptosis by Regulating the COX-2/NF- $\kappa$ B Pathway in Created Temporomandibular Osteoarthritis

Wen Li , Shiyu Hu , Xuepeng Chen , and Jiejun Shi 

Stomatology Hospital, School of Stomatology, Zhejiang University School of Medicine, Clinical Research Center for Oral Diseases of Zhejiang Province, Key Laboratory of Oral Biomedical Research of Zhejiang Province, Cancer Center of Zhejiang University, Hangzhou 310006, China

Correspondence should be addressed to Jiejun Shi; [sjiejun@zju.edu.cn](mailto:sjiejun@zju.edu.cn)

Received 23 March 2021; Revised 30 May 2021; Accepted 27 June 2021; Published 9 July 2021

Academic Editor: Dongliang Xu

Copyright © 2021 Wen Li et al. This is an open access article distributed under the Creative Commons Attribution License, which permits unrestricted use, distribution, and reproduction in any medium, provided the original work is properly cited.

Temporomandibular joint osteoarthritis (TMJOA) is characterized by chronic inflammatory degradation of mandibular condylar cartilage (MCC). Studies have found a positive correlation between inflammation and cyclooxygenase- (COX-) 2 in OA pathology. NF- $\kappa$ B is a crucial transcription factor of inflammatory and immune responses in the cause of TMJOA pathology. Resveratrol (RES) plays a critical role in antioxidation and anti-inflammation. But, studies on the effects of RES on TMJOA are very limited. So, the purpose of this study is to investigate the antioxidant and protective effects of RES against MCC degradation through downregulating COX-2/NF- $\kappa$ B expression. In vitro studies, the MCC cells were divided into three groups: the NC group, OA group, and RES group. The optimum dose of RES (10  $\mu$ M) was determined. The TMJOA model of mice was created by injection of collagenase. And mice were injected with RES (100  $\mu$ g/10  $\mu$ l) 3 times one week for 4 weeks in the RES group. The expressions of COX-2, P65, MMP1, MMP13, COL2, and ACAN were measured by RT-PCR. Morphological changes of MCC were studied with HE staining. The results showed that inflammation could induce MCC degradation in vitro and vivo, while RES could reverse the degradation. Meanwhile, RES could downregulate COX-2/NF- $\kappa$ B/MMP expression and increase cartilage markers in vitro and vivo studies. The results indicated that RES treatment had antioxidant effects against chondrocyte apoptosis by downregulating the COX-2/NF- $\kappa$ B pathway in created TMJOA.

## 1. Introduction

Temporomandibular joint osteoarthritis (TMJOA) is characterized by chronic inflammatory degradation of mandibular condylar cartilage (MCC) [1, 2]. The exact etiology of TMJOA is still unknown, but several risk factors have been reported, such as oxidative stress and inflammation [3–5]. Many studies reported that inflammatory pathway as a “triggering factor” is closely related to TMJOA [6]. Our previous study showed that interleukin-1 $\beta$  (IL-1 $\beta$ ) contributed to the pathogenesis of TMJOA and induced the inflammation and destruction of the MCC [4]. The nuclear factor kappa B (NF- $\kappa$ B) family of transcription factors is a key regulator of immune development, immune responses, and inflammation [7, 8]. The association between NF- $\kappa$ B and the pathogenesis

of TMJOA has been confirmed in animal experiments [4]. IL-1 $\beta$ -activated NF- $\kappa$ B promotes OA development via its action on MCC. Therefore, in order to alleviate or even cure TMJOA, it is of great significance to understand the molecular mechanism of the effect of inflammation on TMJOA.

Cyclooxygenase (COX) is the rate-limiting enzyme for arachidonic acid to synthesize prostaglandin E2 (PGE2)—one of the major mediators involved in the degradation of articular cartilage in OA [9]. There are two isoforms of COX in human that have been described, COX-1 and COX-2. COX-1 is expressed constitutively in various tissues for homeostasis maintenance, while COX-2 is induced by numerous stimuli including excessive mechanical stress, chemical stimuli, and inflammation, being regarded as a pathological enzyme [10, 11]. Studies have found a positive

TABLE 1: The primer sequences for RT-PCR.

Gene	Sequences 5'-3'	PrimerBank ID
GAPDH	Forward: AGGTCGGTGTGAACGGATTG Reverse: GGGGTCGTTGATGGCAACA	126012538c1
COX-2	Forward: TTCCAATCCATGTCAAAACCGT Reverse: AGTCCGGGTACAGTCACACTT	118130137c1
P65	Forward: GGGCTTGGAAATAGAGACATTGA Reverse: GTTCACGGATGACCTCTTTGTTT	20379991a1
MMP1	Forward: CCTTGATGAGACGTGGACCAA Reverse: ATGTGGTGTGTTGCACCTGT	133778986c1
MMP13	Forward: TGTTTGCAGAGCACTACTTGAA Reverse: CAGTCACCTCTAAGCCAAAGAAA	291463259c1
ACAN	Forward: GTGGAGCCGTGTTTCCAAG Reverse: AGATGCTGTTGACTCGAACCT	116875857c1
COL2a	Forward: GGGTCACAGAGGTTACCCAG Reverse: ACCAGGGGAACCACTCTCAC	166064039c1

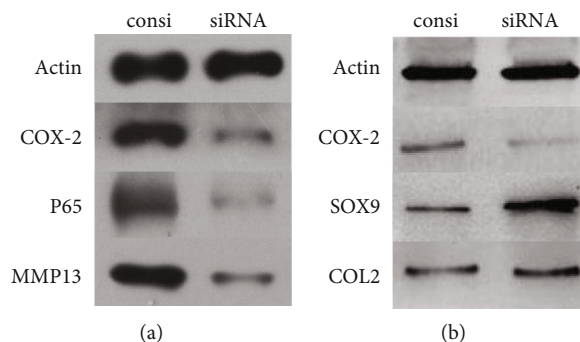


FIGURE 1: Effect of COX-2 on IL-1 $\beta$ -induced chondrocyte degradation. Chondrocytes treated with COX-2 siRNA or control vehicle siRNA were subjected to IL-1 $\beta$ . Whole-cell lysis was subjected to western blot analysis. (a) The effects of COX-2 on inflammation pathway. Inhibition of COX-2 could decrease the expression of P65 and MMP13. (b) The effects of COX-2 on MCC degradation. Inhibition of COX-2 could increase the expression of SOX9 and COL2.

correlation between inflammation, oxidative stress reaction, and the expression of COX-2. Induced COX-2 expression leads to the secretion of proinflammatory cytokines such as PGE<sub>2</sub>, PGH<sub>2</sub>, and VEGF, inducing the generation of oxidative stress-associated products like oxygen radicals and ROS, and resulting in the cellular injury [12, 13]. And in TMJ, COX-2 plays an important part in condylar cartilage degeneration [14]. Therefore, targeting COX-2 may be a promising method to suppress TMJOA.

Resveratrol (RES) is a kind of multifunctional biological polyphenol and plays a critical role in the cell viability, proliferation, anti-inflammation, and antioxidant [15] properties, moreover, in the prevention and progression of chronic diseases related to inflammation [16]. Some studies have demonstrated that RES alleviates rheumatoid arthritis by reducing inflammation, inhibiting MAPK signaling pathways, and suppressing angiogenesis [17]. Although some studies revealed that the intra-articular RES treatment could exert a curative effect by preventing the inflammation and cartilage destruction of TMJOA [18], the mechanism remained unknown.

In this study, we investigated the therapeutic effect and the possible mechanism of RES on MCC in vitro and in OA mice, then presumed that RES has restorative effects on

cartilage destruction by inhibition of COX-2/NF- $\kappa$ B signaling pathways.

## 2. Materials and Methods

**2.1. Cell Culture and RES Treatment.** The procedures for cell culture were referred to Izawa's study [4]. Briefly, cells were isolated from condylar cartilage of 6-week-old female C57BL/6J mice by mechanical dissection and digestion with trypsin and collagenase II. All cells were cultured in CO<sub>2</sub> incubator (DMEM, 37°C, 5% CO<sub>2</sub>). Third cultures were treated with 5, 10, 20, 50, and 100  $\mu$ M RES (Sigma, USA) for 12 h and then tested by MTT to observe the optimum dose of RES on cell viability.

**2.2. IL-1 $\beta$ -Induced Apoptosis.** The third-generation cells were divided into three groups: the normal control group (NC), osteoarthritis group (OA), and RES treatment group (RES). The OA group cells were induced by IL-1 $\beta$  (10 ng/ml, Pepro-Tech Inc., USA) [19]. The RES group cells were treated with IL-1 $\beta$  (10 ng/ml) and RES (10  $\mu$ M). Cell apoptosis was measured by flow cytometry using AnnexinV Apoptosis Detection Kit I (BD Bioscience).

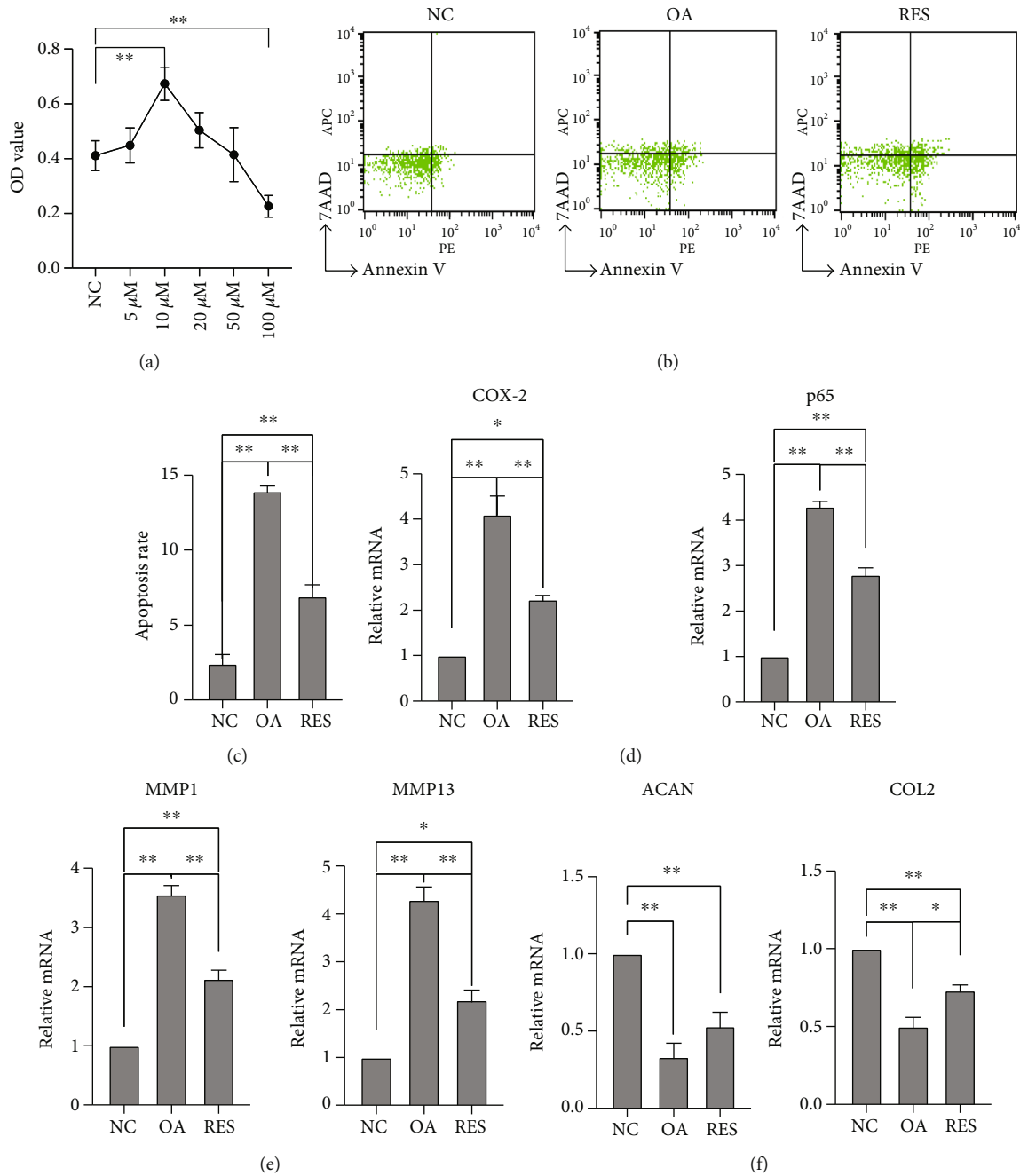


FIGURE 2: Effect of RES on IL-1 $\beta$ -induced apoptosis in the chondrocytes. (a) The optimum dose of RES was determined by MTT after cotreatment for 12 h. (b, c) Flow cytometric analysis for chondrocyte apoptosis. RES treatment could decrease cell apoptosis. (d) The mRNA expression of COX-2 and P65 in each group; RES treatment could suppress COX-2 and P65 expression in vitro. (e) The mRNA expression of MMP1 and MMP13 in each group. (f) The levels of cartilage markers' (ACAN, COL2) gene expressions in chondrocytes were determined by RT-PCR. RES treatment could increase cartilage markers' expression ( $n = 3$ ; \* $P < 0.05$ , \*\* $P < 0.01$ ).

2.3. *siRNA Treatment for COX-2.* The cells ( $2.0 \times 10^5$ /well) were seeded and cultured in a 6-well culture plate until 70% confluence, the culture medium was changed to reduced serum medium (Opti-MEM, Gibco) for overnight, and then, the cells were treated with COX-2 siRNA (GenePharma, China), or control vehicle siRNA with lipofectamine reagent (Invitrogen) for 24h, according to the manufacturer's instructions. Then, treated cells were cultured with IL-1 $\beta$

(10 ng/ml). 24h later, the cells were harvested and used for western blot analysis.

2.4. *Setup TMJOA Model.* 12 female mice (8 week old,  $17.3 \pm 1.5$  g) were purchased from the Animal Center of Zhejiang Academy of Medical Sciences. The mice were divided into the normal control group (NC), OA group (OA), and RES group (RES). The TMJOA model was set up by injection of

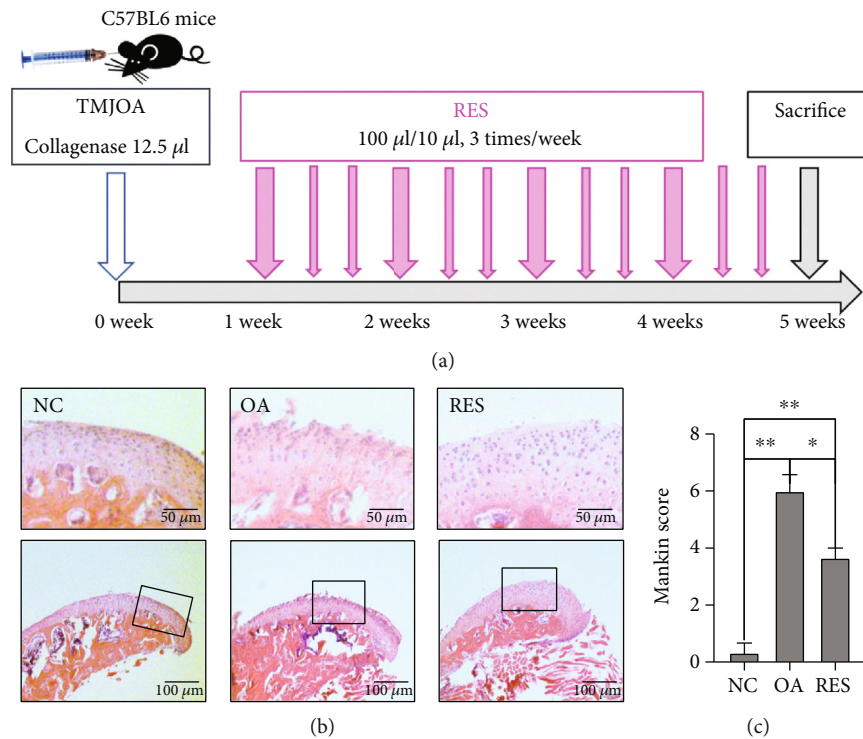


FIGURE 3: RES alleviated structure changes in mouse TMJOA model. (a) Procedure for setting up the TMJOA model and injecting RES. (b) Histological analysis of condylar cartilage by H&E staining. RES treatment could partly reverse cartilage degradation. (c) Mankin score of the condylar articular cartilage of three groups ( $n = 3$ ; \* $P < 0.05$ , \*\* $P < 0.01$ ).

collagenase (12.5 μl, Sigma Biochemical, St. Louis) in the upper cavity of TMJ according to previous studies and made some modifications [2, 18]. 1 week later, the OA mice were injected by RES (100 μg/10 μl) [18] 3 times one week. 4 weeks later, the mice were sacrificed and the condyle was harvested. Animals were treated according to the Guidelines for Animal Care at Zhejiang University School of Medicine at Hangzhou.

**2.5. Histopathology.** The condylar tissues were fixed in 4% PFA, then decalcified in 10% EDTA for 4 weeks. After dehydration, the samples were embedded in paraffin. For histological analysis, sections were deparaffinized and stained with hematoxylin and eosin (H&E). Mankin score was used to evaluate the structure changes of condylar articular cartilage.

**2.6. Measurement of COX-2/P65/MMPs and Cartilage Markers.** Total RNA was extracted with TRIzol (Invitrogen), and the cDNA was synthesized according to the GeneAmp PCR kit (ABI, USA). RT-PCR was performed according to the SYBR green RT-qPCR kit (TOYOBO Corporation). All PCR reactions were performed using iCycleriQTM (Bio-Rad, Hercules, CA, USA). The cycling conditions were 10 min at 95°C, followed by 40 cycles: denaturation at 94°C for 15 s, annealing for 30 s at 57°C, and extension at 72°C for 30 s. The primers of GAPDH, COX-2, P65, MMPs, and cartilage markers were shown in Table 1.

**2.7. Statistical Analysis.** SPSS 22.0 was used for the statistical analysis, and  $P$  value less than 0.05 was considered signifi-

cantly different. Student's  $t$ -test was used for comparisons between two groups.

### 3. Results

**3.1. Mechanism of COX-2 on MCC Degradation.** To examine the effect and mechanism of COX-2 on cartilage degradation, chondrocytes were treated with COX-2 siRNA or control vehicle siRNA before being treated with IL-1β. P65, MMP13, and the cartilage markers (SOX9 and COL2) were measured by western blot. The present study found that COX-2 siRNA treatment could significantly decrease the expression of P65 and MMP13 and reverse the decrease of the expression of SOX9 and COL2 induced by IL-1β (Figure 1).

**3.2. Effects of RES on IL-1β-Induced Apoptosis.** The optimum dose of RES (10 μM) was determined by MTT (Figure 2(a)). IL-1β induced the upregulation of apoptosis compared with the NC group. Meanwhile, RES could decrease the apoptosis induced by IL-1β (Figures 2(b) and 2(c)). The mRNA expression of COX-2, P65, and MMPs in the OA group increased significantly, and RES treatment reversed this increase (Figures 2(d) and 2(e)). The mRNA level of cartilage markers (COL2 and ACAN) decreased obviously in the OA group, and RES could increase the markers expression (Figure 2(f)).

**3.3. Structure Changes of Condylar Articular Cartilage.** HE staining showed normal morphology of joints in the normal control group, whereas the joints in the OA groups exhibited irregular surface. With intra-articular injection of RES, the

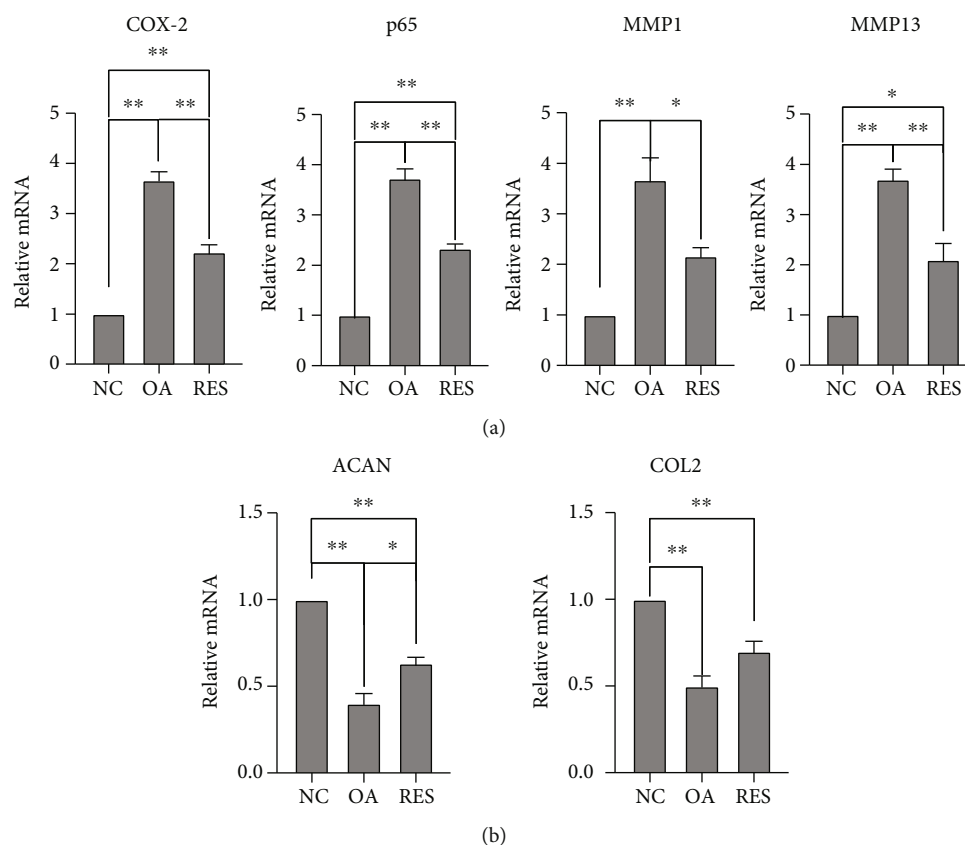


FIGURE 4: RES influenced the expression of COX-2/P65/MMPs and cartilage markers in mouse TMJOA model. (a) The mRNA expression of COX-2, P65, and MMP1 and MMP13 in MCC was detected by RT-PCR. RES treatment could suppress COX-2 expression and related inflammation pathway. (b) The levels of ACAN and COL2 gene expressions in the mouse condylar cartilage were determined by RT-PCR. RES treatment had therapeutic effects against MCC degradation ( $n = 3$ ; \* $P < 0.05$ , \*\* $P < 0.01$ ).

surface of the articular cartilage was a little bit smoother than the OA group, and cartilage thickness was increased (Figure 3(b)). Mankin score revealed that RES could reverse the damage of MCC of OA mice to some extent (Figure 3(c)).

**3.4. The Expression of COX-2/P65/MMPs and Cartilage Markers in MCC.** Compared with the NC group, the mRNA expression of COX-2, P65, and MMP1 and MMP13 increased significantly in OA mice, while the expressions of aggrecan and COL2 were significantly decreased in TMJOA mice. RES treatment significantly upregulated the gene expressions of cartilage markers and reduced the gene expressions of COX-2, P65, and MMPs (Figure 4).

#### 4. Discussion

TMJOA is mainly characterized by the release of inflammatory cytokines, such as IL-1 and TNF- $\alpha$ , leading to the destruction of cartilage matrix. COX-2 is an important proinflammatory enzyme, whose abnormal expression is a significant marker of OA in joints [9, 14]. It is reported that normal human articular chondrocytes do not express measurable COX-2 mRNA, but inflammatory cytokines like IL-1 and TNF- $\alpha$  can induce articular chondrocytes expressing COX-2 mRNA [20, 21]. In TMJ, COX-2 plays an important part in condylar cartilage degeneration and progression of inflammation [5, 22]. When articular

chondrocytes and synoviocytes from TMJ were treated with exogenous IL-1 $\beta$ , the expression levels of COX-2/PGE2 were enhanced [23, 24]. On the other hand, COX inhibitors decreased the expression of COX-2 and PGE2 production in condylar chondrocytes and fibroblast-like synoviocytes from TMJ, showing the anti-inflammatory effect of COX inhibitors [21, 22]. The present study found that IL-1 could increase the protein expression of COX-2 and decrease the expression of cartilage markers, while inhibition of COX-2 by siRNA could suppress the NF- $\kappa$ B pathway by descending the expression of P65 and downstream factor MMP13. Meanwhile, inhibition of COX-2 could increase the expression of cartilage markers (SOX9 and COL2), which indicated that the COX-2 may be a potential therapeutic target against MCC degradation.

RES, which is known to have anti-inflammation and anti-oxidation effects, plays an important role in treating OA disease. And our study verified the therapeutic effect of RES on MCC cells by flow cytometry, which demonstrated that RES significantly reversed IL-1 $\beta$ -induced apoptosis in the chondrocytes. Some studies verified that RES exerted protective effects on OA through its anti-inflammatory property by the NF- $\kappa$ B pathway [25, 26]. The present study agreed with previous studies, which revealed the anti-inflammation of RES on TMJOA by inhibiting the COX-2 gene expression, NF- $\kappa$ B pathway, and downstream factors MMPs. MMPs are the key enzymes related to cartilage degradation in OA.

The proteolytic cleavage of collagens and proteoglycans by MMPs are responsible for temporomandibular disorders [27, 28]. The present study has implicated that RES could inhibit MMP1 and MMP13 in MCC and increase the expression of cartilage markers ACAN and COL2 in vitro, which is one of the mechanism responsible for RES therapeutic effect.

In TMJOA mice, the structure of the condylar articular cartilage was destroyed significantly by injection in the upper cavity of TMJ compared to control mice. After RES treatment, histological evaluation of the cartilage tissue revealed a significantly reduced cartilage destruction compared to the OA group, which indicated the protective effects of resveratrol against MCC. Many in vivo studies demonstrated that RES may exert an antiosteoarthritic effect by inhibiting COX-2 gene expression and enzyme activity [29]. It was reported that RES decreased AGEs-stimulated expressions of MMP13 and prevented AGEs-mediated destruction of collagen II [30]. In TMJOA mice, our study found that RES could suppress the expression of COX-2, NF- $\kappa$ B pathway, and MMPs and increase the expression of cartilage markers ACAN and COL2, which indicated that RES may be a promising agent in the treatment for TMJOA.

However, it should be realized that there are a few limitations of the experiments. More biological effects such as cell proliferation, more inflammatory mediators, and the mechanism through which COX-2 induced by inflammation were not demonstrated.

## 5. Conclusions

In conclusion, this study indicates the involvement of COX-2 on inflammation-induced condylar cartilage degeneration in temporomandibular osteoarthritis. The most intriguing aspect of this study is that the RES recovering MCC injury may be related to the inhibition of the expression of COX-2/NF- $\kappa$ B. In addition, RES could increase the expressions of chondrogenic markers, suggesting that RES plays an important role in the remodeling of the cartilage in TMJOA.

## Data Availability

Data used to support the findings of this study are available from the corresponding author upon request.

## Conflicts of Interest

The authors declare that there are no conflicts of interest regarding the publication of this paper.

## Authors' Contributions

Wen Li and Shiyu Hu contributed equally to this work.

## Acknowledgments

The authors are grateful to the Zhejiang Academy of Medical Sciences for biotechnical assistance. This work was financially supported by the Natural Science Foundation of Zhejiang Province (LY18H140001) and Zhejiang public welfare Technology Application Research Plan (LGF21H140003).

## References

- [1] G. A. Zarb and G. E. Carlsson, "Temporomandibular disorders: osteoarthritis," *Journal of Orofacial Pain*, vol. 13, no. 4, pp. 295–306, 1999.
- [2] W. Li, M. Wu, S. Jiang, W. Ding, Q. Luo, and J. Shi, "Expression of ADAMTs-5 and TIMP-3 in the condylar cartilage of rats induced by experimentally created osteoarthritis," *Archives of oral biology*, vol. 59, no. 5, pp. 524–529, 2014.
- [3] A. S. Marchev, P. A. Dimitrova, A. J. Burns, R. V. Kostov, A. T. Dinkova-Kostova, and M. I. Georgiev, "Oxidative stress and chronic inflammation in osteoarthritis: can NRF2 counteract these partners in crime?," *Annals of the New York Academy of Sciences*, vol. 1401, no. 1, pp. 114–135, 2017.
- [4] T. Izawa, H. Mori, T. Shinohara et al., "Rebamipide attenuates mandibular condylar degeneration in a murine model of TMJ-OA by mediating a chondroprotective effect and by downregulating RANKL-mediated osteoclastogenesis," *PLoS One*, vol. 11, no. 4, article e0154107, 2016.
- [5] C. Jiang, P. Luo, X. Li, P. Liu, Y. Li, and J. Xu, "Nrf2/ARE is a key pathway for curcumin-mediated protection of TMJ chondrocytes from oxidative stress and inflammation," *Cell Stress & Chaperones*, vol. 25, no. 3, pp. 395–406, 2020.
- [6] E. B. P. Lopes, A. Filiberti, S. A. Husain, and M. B. Humphrey, "Immune contributions to osteoarthritis," *Current osteoporosis reports*, vol. 15, no. 6, pp. 593–600, 2017.
- [7] S. Mitchell, J. Vargas, and A. Hoffmann, "Signaling via the NF $\kappa$ B system," *Wiley Interdisciplinary Reviews: Systems Biology and Medicine*, vol. 8, no. 3, pp. 227–241, 2016.
- [8] M. C. Choi, J. Jo, J. Park, H. K. Kang, and Y. Park, "NF- $\kappa$ B signaling pathways in osteoarthritic cartilage destruction," *Cells*, vol. 8, no. 7, p. 734, 2019.
- [9] P. Alstergren and S. Kopp, "Prostaglandin E2 in temporomandibular joint synovial fluid and its relation to pain and inflammatory disorders," *Journal of Oral & Maxillofacial Surgery*, vol. 58, no. 2, pp. 180–186, 2000.
- [10] B. Lyons-Giordano, M. A. Pratta, W. Galbraith, G. L. Davis, and E. C. Arner, "Interleukin-1 differentially modulates chondrocyte expression of cyclooxygenase-2 and phospholipase A2," *Experimental Cell Research*, vol. 206, no. 1, pp. 58–62, 1993.
- [11] S. C. Su, K. Tanimoto, Y. Tanne et al., "Celecoxib exerts protective effects on extracellular matrix metabolism of mandibular condylar chondrocytes under excessive mechanical stress," *Osteoarthritis and Cartilage*, vol. 22, no. 6, pp. 845–851, 2014.
- [12] S. S. Barbieri, S. Eligini, M. Brambilla, E. Tremoli, and S. Colli, "Reactive oxygen species mediate cyclooxygenase-2 induction during monocyte to macrophage differentiation: critical role of NADPH oxidase," *Cardiovascular Research*, vol. 60, no. 1, pp. 187–197, 2003.
- [13] L. Qiu, Y. Zhang, D. C. Do et al., "miR-155 modulates cockroach allergen- and oxidative stress-induced cyclooxygenase-2 in asthma," *The Journal of Immunology*, vol. 201, no. 3, pp. 916–929, 2018.
- [14] H. W. Fan, G. Y. Liu, C. F. Zhao, X. F. Li, and X. Y. Yang, "Differential expression of COX-2 in osteoarthritis and rheumatoid arthritis," *Genetics and Molecular Research*, vol. 14, no. 4, pp. 12872–12879, 2015.
- [15] W. Wang, L. Sun, P. Zhang, J. Song, and W. Liu, "An anti-inflammatory cell-free collagen/resveratrol scaffold for repairing osteochondral defects in rabbits," *Acta biomaterialia*, vol. 10, no. 12, pp. 4983–4995, 2014.

- [16] L. Malaguarnera, "Influence of resveratrol on the immune response," *Nutrients*, vol. 11, no. 5, p. 946, 2019.
- [17] G. Yang, C. C. Chang, Y. Yang et al., "Resveratrol alleviates rheumatoid arthritis via reducing ROS and inflammation, inhibiting MAPK signaling pathways, and suppressing angiogenesis," *Journal of Agricultural and Food Chemistry*, vol. 66, no. 49, pp. 12953–12960, 2018.
- [18] P. Yuce, H. Hosgor, S. F. Rencber, and Y. Yazir, "Effects of intra-articular resveratrol injections on cartilage destruction and synovial inflammation in experimental temporomandibular joint osteoarthritis," *Journal of Oral and Maxillofacial Surgery*, vol. 79, no. 2, pp. 344.e1–344.e12, 2021.
- [19] N. Rasheed, A. Alghasham, and Z. Rasheed, "Lactoferrin from *Camelus dromedarius* inhibits nuclear transcription factor-kappa B activation, cyclooxygenase-2 expression and prostaglandin E2 production in stimulated human chondrocytes," *Pharmacognosy research*, vol. 8, no. 2, pp. 135–141, 2016.
- [20] X. Li, P. He, Y. Hou et al., "Berberine inhibits the interleukin-1beta-induced inflammatory response via MAPK downregulation in rat articular chondrocytes," *Drug development research*, vol. 80, no. 5, pp. 637–645, 2019.
- [21] R. Y. Au, T. K. Al-Talib, A. Y. Au, P. V. Phan, and C. G. Frondoza, "Avocado soybean unsaponifiables (ASU) suppress TNF-alpha, IL-1beta, COX-2, iNOS gene expression, and prostaglandin E2 and nitric oxide production in articular chondrocytes and monocyte/macrophages," *Osteoarthritis and Cartilage*, vol. 15, no. 11, pp. 1249–1255, 2007.
- [22] N. Ouyang, Y. Zhao, Q. Chen et al., "The effect of celecoxib in traumatic heterotopic ossification around temporomandibular joint in mice," *Osteoarthritis and Cartilage*, vol. 28, no. 4, pp. 502–515, 2020.
- [23] K. Tanimoto, Y. Iwabuchi, Y. Tanne et al., "Interleukin-1 beta affects cyclooxygenase-2 expression and cartilage metabolism in mandibular condyle," *Archives of Oral Biology*, vol. 56, no. 11, pp. 1412–1418, 2011.
- [24] K. Satoh, N. Ogura, M. Akutsu et al., "Expression of cyclooxygenase-1 and -2 in IL-1 $\beta$ -induced synovitis of the temporomandibular joint," *Journal of Oral Pathology & Medicine*, vol. 38, no. 7, pp. 584–590, 2009.
- [25] X. Xu, X. Liu, Y. Yang et al., "Resveratrol Exerts Anti-Osteoarthritic Effect by Inhibiting TLR4/NF- $\kappa$ B Signaling Pathway via the TLR4/Akt/FoxO1 Axis in IL-1 $\beta$ -Stimulated SW1353 Cells," *Drug Design, Development and Therapy*, vol. 14, pp. 2079–2090, 2020.
- [26] H. Yi, W. Zhang, Z. M. Cui et al., "Resveratrol alleviates the interleukin-1 $\beta$ -induced chondrocytes injury through the NF- $\kappa$ B signaling pathway," *Journal of Orthopaedic Surgery and Research*, vol. 15, no. 1, p. 424, 2020.
- [27] K. Yoshida, S. Takatsuka, E. Hatada et al., "Expression of matrix metalloproteinases and aggrecanase in the synovial fluids of patients with symptomatic temporomandibular disorders," *Oral Pathology, Oral Radiology, and Endodontology*, vol. 102, no. 1, pp. 22–27, 2006.
- [28] Y. Asakawa-Tanne, S. Su, R. Kunimatsu et al., "Effects of enzymatic degradation after loading in temporomandibular joint," *Journal of Dental Research*, vol. 94, no. 2, pp. 337–343, 2015.
- [29] N. Elmali, I. Esenkaya, A. Harma, K. Ertem, Y. Turkoz, and B. Mizrak, "Effect of resveratrol in experimental osteoarthritis in rabbits," *Inflammation Research*, vol. 54, no. 4, pp. 158–162, 2005.
- [30] F. C. Liu, L. F. Hung, W. L. Wu et al., "Chondroprotective effects and mechanisms of resveratrol in advanced glycation end products-stimulated chondrocytes," *Arthritis research & therapy*, vol. 12, no. 5, p. R167, 2010.

## Research Article

# miR-125a-5p Regulates Osteogenic Differentiation of Human Adipose-Derived Mesenchymal Stem Cells under Oxidative Stress

Yongheng Ye <sup>1</sup>, Quan Liu,<sup>2</sup> Changzhao Li <sup>1</sup>, and Peiheng He <sup>1</sup>

<sup>1</sup>Department of Joint Surgery, The First Affiliated Hospital of Sun Yat-sen University, Guangzhou 510080, China

<sup>2</sup>Department of Orthopaedic Surgery, The First People's Hospital of Nankang, Ganzhou 341400, China

Correspondence should be addressed to Peiheng He; [hepeiheng@mail.sysu.edu.cn](mailto:hepeiheng@mail.sysu.edu.cn)

Received 12 January 2021; Revised 9 March 2021; Accepted 23 May 2021; Published 7 June 2021

Academic Editor: Xinhua Li

Copyright © 2021 Yongheng Ye et al. This is an open access article distributed under the Creative Commons Attribution License, which permits unrestricted use, distribution, and reproduction in any medium, provided the original work is properly cited.

Adipose-derived mesenchymal stem cells (ADSCs) are a well-recognized multilineage stem cell with vital clinical feasibility for tissue regeneration. Extensive evidence indicates that oxidative stress and microRNAs (miRNAs/miRs) play an important role in the osteoinduction of adipose-derived mesenchymal stem cells. In this study, we investigated the mechanism of miR-125a-5p in regulating the osteogenesis of human adipose-derived mesenchymal stem cells (hADSCs) under oxidative stress. The expression of miR-125a-5p lessened gradually during the osteogenic differentiation of hADSCs. Relative to the negative group, the expression levels of runt-related transcription factor 2 (RUNX2), alkaline phosphatase (ALP), osteocalcin (OCN), and osterix in the miR-125a-5p group were marked lower than those in the miR-125a-5p inhibitor group. The levels of p16, p21, p53, miR-125a-5p, and ROS during osteoinduction of hADSCs were assessed *in vitro* under oxidative stress and were observed to be upregulated. Further experiments showed that oxidative stress and miR-125a-5p together suppressed the expression of VEGF during osteogenic differentiation of hADSCs and that the inhibition of miR-125a-5p reversed the effect of oxidative stress. In short, our study indicated that miR-125a-5p is induced under oxidative stress and inhibits the expression of VEGF, leading to the reduction of osteogenic differentiation of hADSCs. Our outcomes showed that miR-125a-5p could be a potential clinical target for bone repairing.

## 1. Introduction

Bone loss caused by trauma, tumor, and age-related osteoporosis is a common problem in orthopedics. The balance of bone metabolism is a dynamic course influenced by osteoblasts, osteoclasts, and osteocytes. Oxidative stress, causing many reactive oxygen species (ROS) to form, plays an important role in the development of skeletal diseases [1–3]. The activity of oxidants has also been proven to enhance osteoclast differentiation [4]. With the need for more effective treatment, it is of great significance to find osteogenic methods for bone repair and regeneration.

Stem cells can differentiate into the bone, cartilage, and fat under the stimulation of certain factors, providing promising therapeutic applications with regard to the restoration of tissue defects [5–7]. Many researches have focused on efforts to utilize bone mesenchymal stem cells (BMSCs) for bone tissue engineering [8]. In addition, previous studies

have proven that VEGF regulates adipocyte and osteoblast differentiation in mesenchymal stem cells [9]. Adipose-derived mesenchymal stem cells (ADSCs) as seed cells are more readily available to that of BMSCs, but their osteogenic differentiation ability is limited [10]. Aging is the main factor leading to decreased activity and repair ability of mesenchymal stem cells [11]. Oxidative stress is one of the main causes of aging. There is evidence to show that oxidative stress suppresses osteogenic differentiation and weakens the stemness of MSCs, which causes bone formation defects [12–14]. In addition, oxidative stress can induce apoptosis, senescence, and death of MSCs [15]. Therefore, clarifying the regulating mechanisms of osteogenic differentiation of ADSCs is helpful for identifying their possible therapeutic applications in bone repair.

MicroRNA (miRNA) is a single stranded RNA molecule consisting of about 18–22 nucleotides, which play a key role in cell apoptosis, proliferation, tumorigenesis, and other physiological and pathological processes [16]. Several

investigations have shown that miRNAs are mentioned in the osteoblast differentiation of stem cells. For example, miR-199a-5p controls the osteogenic induction of bone marrow mesenchymal stem cells by targeting TET2 [17]. In addition, miR-450b promotes osteoblast induction in vitro and strength bone generation in vivo by targeting the BMP3 signaling pathway [18]. Prior studies indicate that the downregulation of miR-125a-5p was detected during osteogenic differentiation of hADSCs by microarray profiles of small RNA molecules [19]. However, by far, the regulating mechanism of miR-125a-5p in the osteogenic differentiation of hADSCs has not been reported.

Therefore, the purpose of this research was to investigate the specific mechanisms of miR-125a-5p controlling osteogenesis in hADSCs under oxidative stress. It is expected that our study will provide a beneficial groundwork for the application of miR-125a-5p in bone restoration.

## 2. Materials and Methods

**2.1. Isolation and Culture of Cells.** The human adipose-derived mesenchymal stem cells were purchased from Cyagen, USA (No. HUXMD-01001). The hADSCs were cultured in Dulbecco's Modified Eagle Medium: Nutrient Mixture F-12 (DMEM/F12, Gibco) medium, which includes 10% fetal bovine serum (FBS, Sigma), 100 U/mL penicillin, and 100  $\mu$ g/mL streptomycin, cultured incubated in a 5% CO<sub>2</sub> atmosphere at 37°C. The complete medium was changed in 48–72 h, and the cells were passaged when 70–90% confluence was reached. hADSCs were expanded until passage 3.

**2.2. hADSC Osteogenic Differentiation.** The cells (passage 3) were transplanted to 6-well cell culture plates. Cells were grown to 50–70% confluence in complete medium after 24–48 h [20]. The medium was completely replaced with an osteogenic differentiation medium, which consisted of human adipose-derived stem cell osteogenic differentiation basal medium, human adipose-derived stem cell osteogenic differentiation fetal bovine serum, penicillin-streptomycin, glutamine, ascorbate,  $\beta$ -glycerophosphate, and dexamethasone (Cyagen, USA). The cells were then cultured up to 21 days. The osteogenic medium was changed every 72 h.

**2.3. Reactive Oxygen Species (ROS) Measurement.** Cells were transplanted into  $2 \times 10^4$  cells/cm<sup>2</sup> in 6-well plates. After 24 h, 50, 100, and 200  $\mu$ M H<sub>2</sub>O<sub>2</sub> were added into the fresh medium to stimulate oxidative stress response, and cells were incubated for another 24 h. Then, the cells were incubated in a new solution without the FBS medium and including 10  $\mu$ M of the Reactive Oxygen Species Assay Kit (ROS Assay Kit, Beyotime, China) for 0.5 h. Finally, 1000  $\times$  g centrifugation of cells was conducted for 5 min and they were then washed with phosphate-buffered saline (PBS) for 2–3 times. The levels of dichlorofluorescein (DCF) were tested by flow cytometry (CytoFLEX, Beckman Coulter, USA) as prescribed by the manufacturer's instructions.

**2.4. Quantitative Real-Time Polymerase Chain Reaction (qRT-PCR).** hADSCs were lysed and gathered using the

TABLE 1: Primer sequences for qRT-PCR.

Gene or miRNA	Sequence(5' to 3')
miR-125a-5p	F: CGATTCCCTGAGACCCTTTAA
ALP	F: CGAGATACAAGCACTCCCACTTC R: CTGTTCAGCTCGTACTGCATGTC
Runx2	F: CAAGGACAGAGTCAGATTAC R: GTGGTAGAGTGGATGGAC
OCN	F: GGTGCAGCCTTTGTGTCCAAGC R: GTCAGCCAACCTCGTCACAGTCC
Osterix	F: TGCTTGAGGAGGAAGTTC R: CTTTGCCAGAGTTGTTG
p16	F: GATCCAGGTGGGTAGAAGGTC R: CCCCTGCAAACCTTCGTCTT
p21	F: TGTCCTCAGAACCCATGC R: AAAGTCGAAGTTCATCGCTC
p53	F: CAGCACATGACGGAGGTTGT R: TCATCCAAATACTCCACACGC
GAPDH	F: CCATCTTCCAGGAGCGAGATC R: GCCTTCTCCATGGTGGTGAA
U6	F: CTCGCTTCGGCAGCAC R: AACGCTTACGAATTTGCGT

TRIzol Reagent (Invitrogen, USA) according to the manufacturer's instructions. cDNA was synthesized using reverse transcription with a PrimeScript RT reagent kit (Takara, Dalian, China) and amplified using 2 $\times$ SYBR Green qPCR Master Mix (TOYOBO, Japan) as prescribed by the manufacturer's instructions. Primers of human osteoblastic marker genes, miR-125a-5p, and U6 were compounded by RIBOBIO (Guangzhou, China). The primers for qRT-PCR are shown in Table 1. U6 and GAPDH were the reference genes of miRNA and mRNA, respectively. Relative expression levels were quantified by the 2<sup>- $\Delta\Delta$ CT</sup> method. Each experiment was repeated 3 times, and each assay was performed in triplicate.

**2.5. Cell Counting Kit-8 (CCK-8) Assay.** Cell viability was measured by the CCK-8 colorimetric assay. hADSCs ( $3 \times 10^3$ /well) were cultured to confluence on 96-well culture plates and incubated with increasing concentrations of H<sub>2</sub>O<sub>2</sub> (50, 100, and 200  $\mu$ M) and increasing time (4, 6, 8, and 24 h). After treatment, the cells were incubated with 10  $\mu$ L CCK-8 for 0.5–4 h, and the absorbance was measured at 450 nm using a microplate reader (Sunrise, TECAN, Austria).

**2.6. Western Blotting.** The target protein productions were gathered in RIPA lysis buffer (Solarbio, China), including the protease inhibitor, and put on ice for 15 min. After processing through electrophoresis and membrane transferring, the membranes were incubated by the anti-VEGF (1:1000 dilution, ab32152, Abcam, Cambridge, UK) antibody. After washing, the membranes were incubated with the corresponding secondary antibody (Proteintech, Wuhan, China) as prescribed by the manufacturer's instructions. Protein bands were quantified using the ImageJ software (National Institutes of Health, Bethesda, MD).

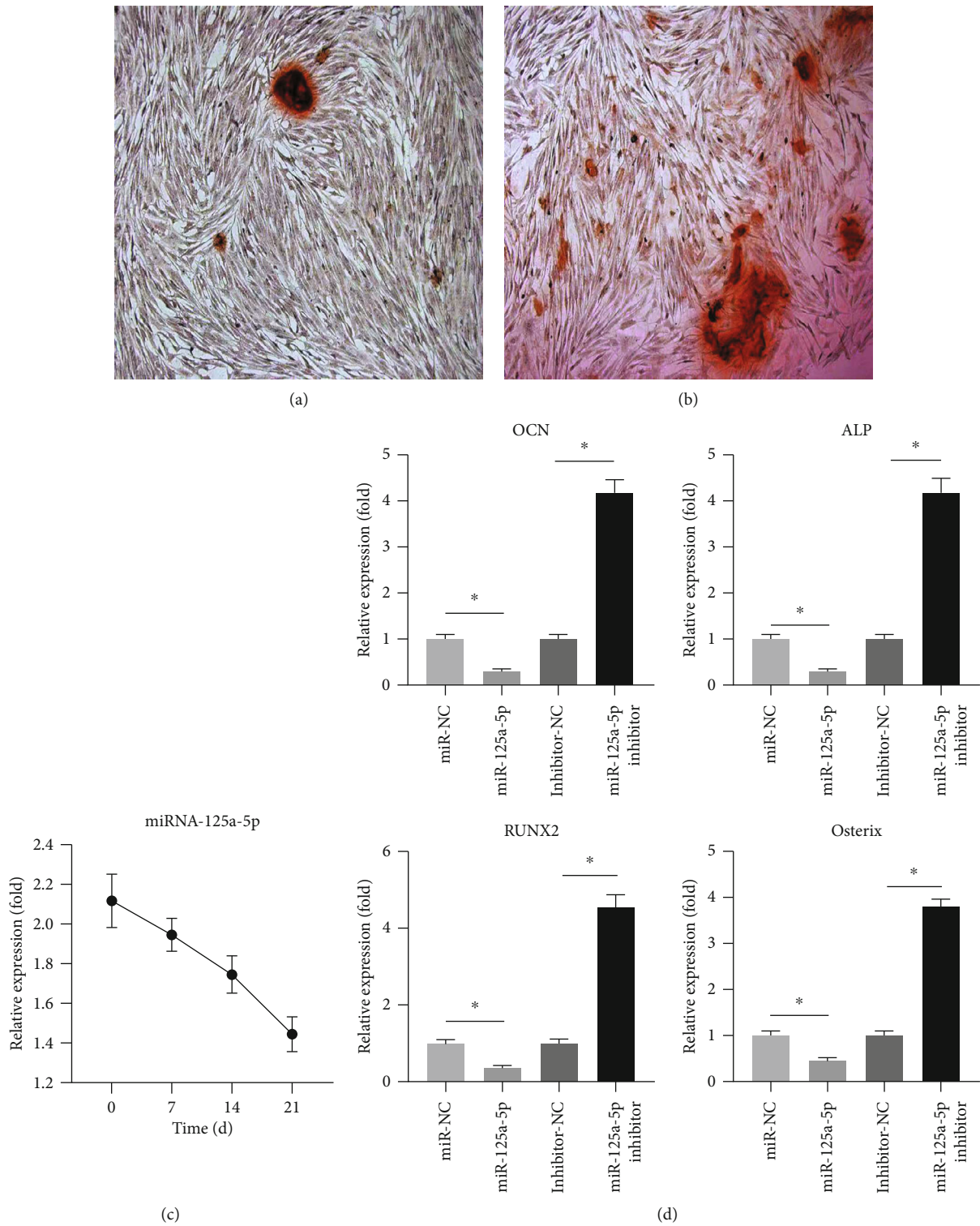


FIGURE 1: miR-125a-5p inhibits the osteogenic differentiation of hADSCs. (a, b) Osteogenic differentiation was induced in hADSCs on days 14 and 21 and was then processed with Alizarin red staining. (c) After the induction of osteogenic differentiation, the relative expression of miRNA-125a-5p was measured on days 0, 7, 14, and 21. (d) mRNA relative expression of the osteoblastic marker genes OCN, ALP, RUNX2, and osterix were measured after being transfected with miRNA-125a-5p and miRNA-125a-5p inhibitor.  $N = 3$ ; \* means  $p < 0.05$ ; \*\* means  $p < 0.01$ .

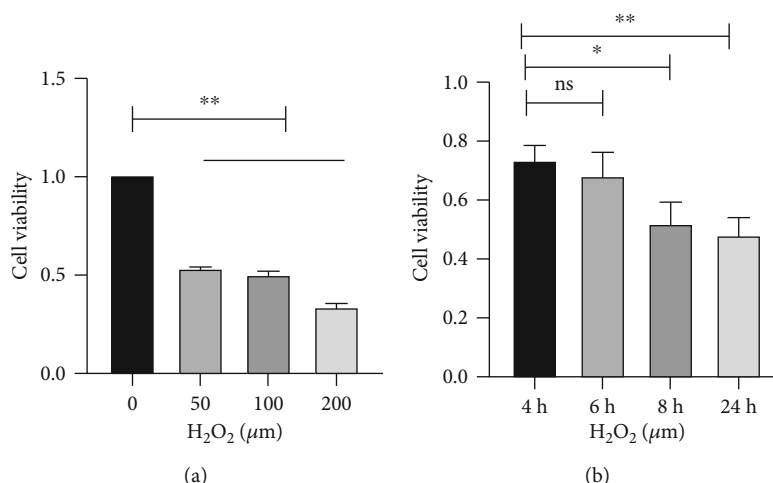


FIGURE 2: Effects of H<sub>2</sub>O<sub>2</sub> on the viability of hADSCs. (a, b) Cell viability was measured by the CCK-8 colorimetric assay in different concentrations of H<sub>2</sub>O<sub>2</sub> and induction times.  $N = 3$ ;  $^{ns}p > 0.05$ ;  $^*p < 0.05$ ;  $^{**}p < 0.01$ .

**2.7. Cell Transfection.** After 24 h of seeding, the miR-125a-5p mimics and miR-125a-5p inhibitor were transfected into the cells by the Lipofectamine™ 2000 transfection reagent as prescribed by the manufacturer's instructions (Gibco Life Technologies, USA); miR-NC and inhibitor-NC were used as the control and negative control, respectively. The medium was replaced after 24 h, and the cells were gathered for subsequent experiments.

**2.8. Alizarin Red Staining (ARS).** hADSCs or hADSCs transfected with miR-125a-5p mimic (50 nM), miR-125a-5p inhibitor (50 nM), and corresponding negative control were seeded into 24-well plates, respectively. After reaching 75–90% density, the hADSCs were induced using the osteogenic differentiation medium for a further 3 weeks. After 14 and 21 days, the hADSCs were fixed by the 4% Paraformaldehyde and stained with ARS for 15 min at  $23 \pm 2^\circ\text{C}$ , followed by analysis under an inverted microscope (Leica DMI4000B, Leica, Germany).

**2.9. Statistical Analysis.** SPSS 19.0 software (IBM Corporation, Armonk, NY, USA) was used for the statistical analysis. Data are presented as the mean  $\pm$  standard deviation (mean  $\pm$  SD). Comparisons between groups were used one-way analysis of variance followed by Tukey's post hoc test. A  $p$  value  $< 0.05$  was treated as significant.

### 3. Results

**3.1. miR-125a-5p Inhibits Osteogenic Differentiation of hADSCs.** The presence of calcium deposition in hADSCs indicates that osteogenic differentiation was induced in hADSCs (Figures 1(a) and 1(b)). We first detected the expression level of miR-125a-5p in hADSCs by qRT-PCR in the osteogenic differentiation of hADSCs. The change of miR-125a-5p was reduced on day 7 compared with day 0 and continuously decreased to day 21 (Figure 1(c)). This suggested that miR-125a-5p might negatively regulate the osteogenic differentiation of hADSCs. hADSCs were transfected

with the miR-125a-5p mimic and the miR-125a-5p inhibitor. The expression level of osteogenic marker genes was evaluated by qRT-PCR for osteogenic differentiation in 21 days. The results show that the mRNA level of the osteogenic marker genes was reduced after being transfected with the miR-125a-5p mimic, whereas the level expression of the osteogenic marker genes was increased after being transfected with the miR-125a-5p inhibitor (Figure 1(d)). It can be seen from these results that miR-125a-5p negatively regulated the osteogenic differentiation of hADSCs.

**3.2. Effects of H<sub>2</sub>O<sub>2</sub> on Cell Viability.** The cytotoxic effect of H<sub>2</sub>O<sub>2</sub> on hADSC viability was evaluated at 50, 100, and 200  $\mu\text{M}$  for 4, 6, 8, and 24 h using a CCK-8 assay. As shown in Figure 2, the cell viability was decreased by 50% with the 100  $\mu\text{M}$  H<sub>2</sub>O<sub>2</sub> and for 24 h.

**3.3. Oxidative Stress Induces Senescence of hADSCs and miR-125a-5p Expression.** hADSCs were stimulated by different doses of H<sub>2</sub>O<sub>2</sub> for 24 h to simulate the environment of oxidative stress response. As can be seen in Figures 3(a)–3(c), the three-cell senescence-related markers p16, p21, and p53 were significantly increased along with the dose of H<sub>2</sub>O<sub>2</sub> and induction time. Furthermore, we can find that the level of ROS was increased along with the dose of H<sub>2</sub>O<sub>2</sub>, which was marked at 100  $\mu\text{M}$  and 200  $\mu\text{M}$ , and 100  $\mu\text{M}$  H<sub>2</sub>O<sub>2</sub> was chosen for subsequent experiments (Figure 3(d)). The expression level of miR-125a-5p was increased following an increase in the concentration of H<sub>2</sub>O<sub>2</sub> (Figure 3(e)). These data suggested that hADSCs exhibit an obvious increase in senescence with oxidative stress, which was the trigger to increase the expression level of miRNA-125a-5p.

**3.4. Oxidative Stress Increases miR-125a-5p Expression during Osteogenic Differentiation of hADSCs.** It was observed that the osteogenic marker genes continually increased when osteogenic differentiation was induced in hADSCs from day 0 to day 21. However, when osteogenic differentiation was induced in hADSCs in the presence of 100  $\mu\text{M}$  H<sub>2</sub>O<sub>2</sub>, the

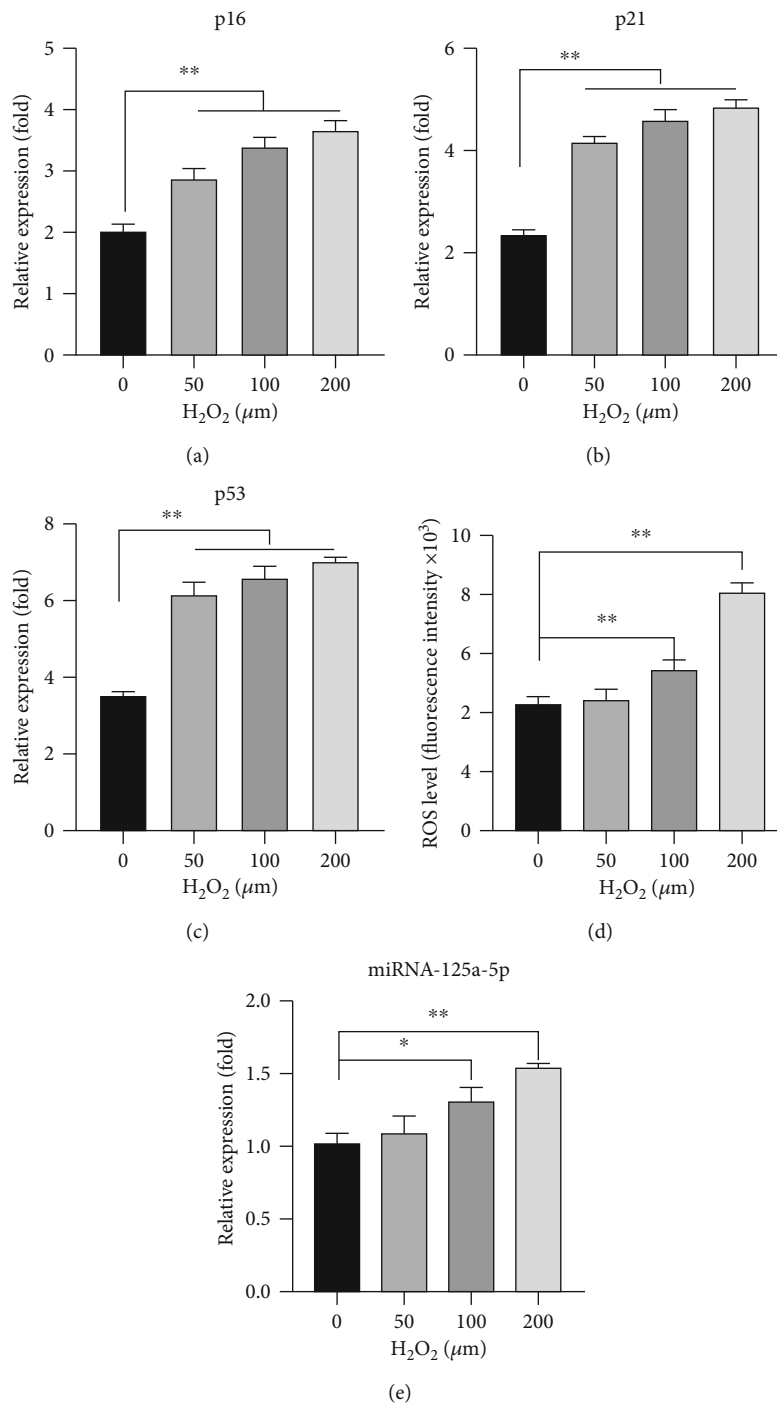


FIGURE 3: Oxidative stress induces senescence of hADSCs and miR-125a-5p expression. (a–c) mRNA expression levels of p16, p21, and p53 were evaluated by qRT-PCR. (d) The ROS level of the cells was measured by exposure to different concentrations of H<sub>2</sub>O<sub>2</sub>. (e) The expressions of miRNA-125a-5p were measured by exposure to different concentrations of H<sub>2</sub>O<sub>2</sub>. N = 3; \*p < 0.05; \*\*p < 0.01.

expression level of osteogenic marker genes decreased (Figure 4(a)). The level of miRNA-125a-5p was reduced in osteogenic differentiation, but the level in the medium with H<sub>2</sub>O<sub>2</sub> was higher than that in the medium without H<sub>2</sub>O<sub>2</sub> (Figure 4(b)). These results show that oxidative stress increased miR-125a-5p and concomitantly reduced osteogenic differentiation during the osteogenic differentiation of hADSCs.

**3.5. miR-125a-5p Mediates the VEGF-Regulated Osteogenic Differentiation of hADSCs under Oxidative Stress.** By using the web-based bioinformatics tool, miRBase (<http://mirtarbase.cuhk.edu.cn>), a predictor gene is considered a target gene of miRNA when it met software’s requirement. It was found that miR-125a-5p’s regulated target gene is VEGF. Thus, we first analyzed VEGF levels in transfected cells and found that the VEGF proteins were significantly declined with transfected

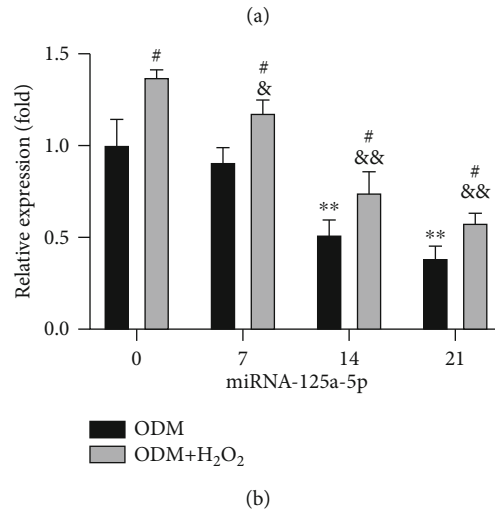
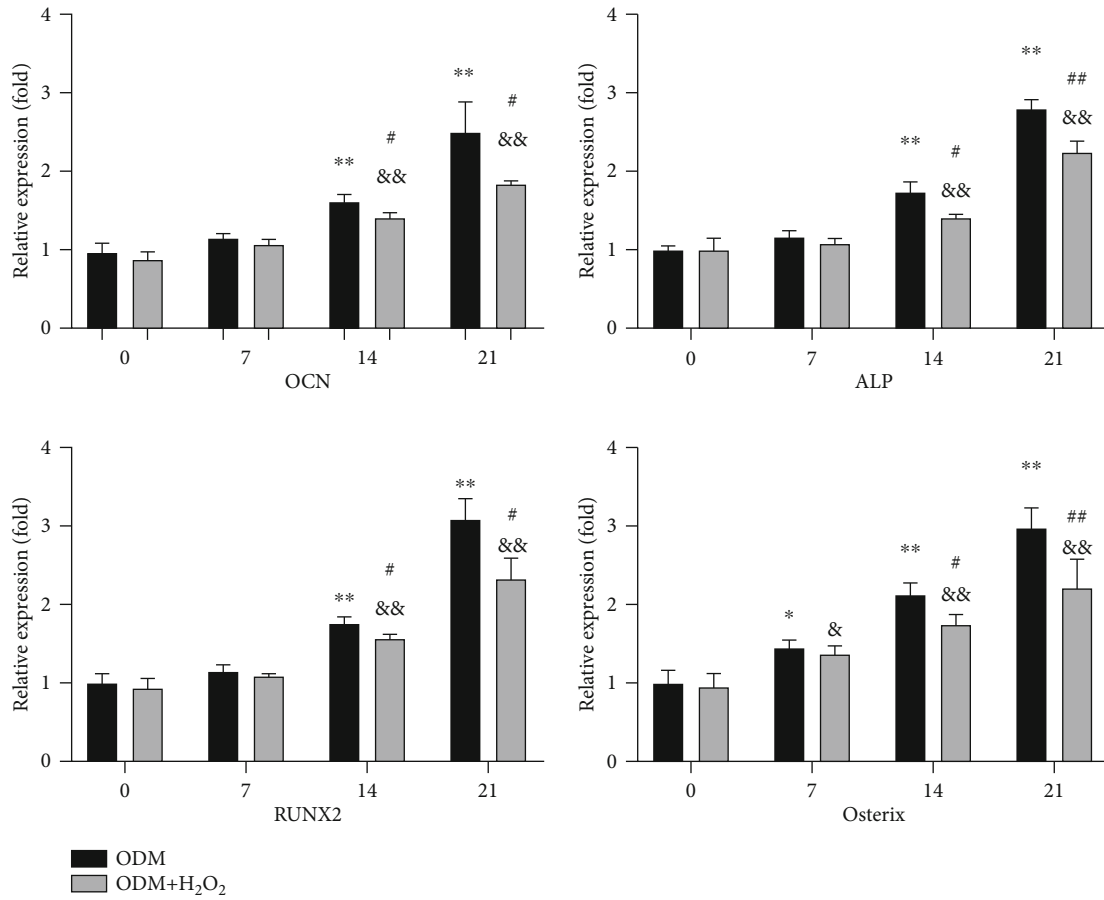


FIGURE 4: Oxidative stress increases miR-125a-5p expression during osteogenic differentiation of hADSCs. (a, b) The expression levels of the osteoblastic marker genes and the miRNA-125a-5p were measured with or without H<sub>2</sub>O<sub>2</sub> in the condition of osteogenic differentiation medium (ODM). N = 3; \*p < 0.05, \*\*p < 0.01 vs. day 0 (ODM group); #p < 0.05, ##p < 0.01 vs. day 0 (ODM+H<sub>2</sub>O<sub>2</sub> group); &p < 0.05, &&p < 0.01 (ODM+H<sub>2</sub>O<sub>2</sub> group vs. ODM group).

miR-125a-5p mimic and rose with transfected miR-125a-5p inhibitor (Figure 5(a)). Then, hADSCs were cultured under osteogenic conditions with 100 μM H<sub>2</sub>O<sub>2</sub>, and the mRNA level of VEGF was evaluated by qRT-PCR at different time points during osteogenic differentiation. Although the mRNA level of VEGF showed marked increase during osteogenic differentiation up to 21 days, the VEGF levels were decreased

when H<sub>2</sub>O<sub>2</sub> stimulated the oxidative stress response (Figure 5(b)). Furthermore, under the conditions of oxidative stress, the overexpression of miRNA-125a-5p could suppress the expression of VEGF while the overexpression of miRNA-125a-5p inhibitor could promote the expression of VEGF (Figure 5(c)). These results provide strong evidence that miR-125a-5p could mediate the expression level of VEGF.

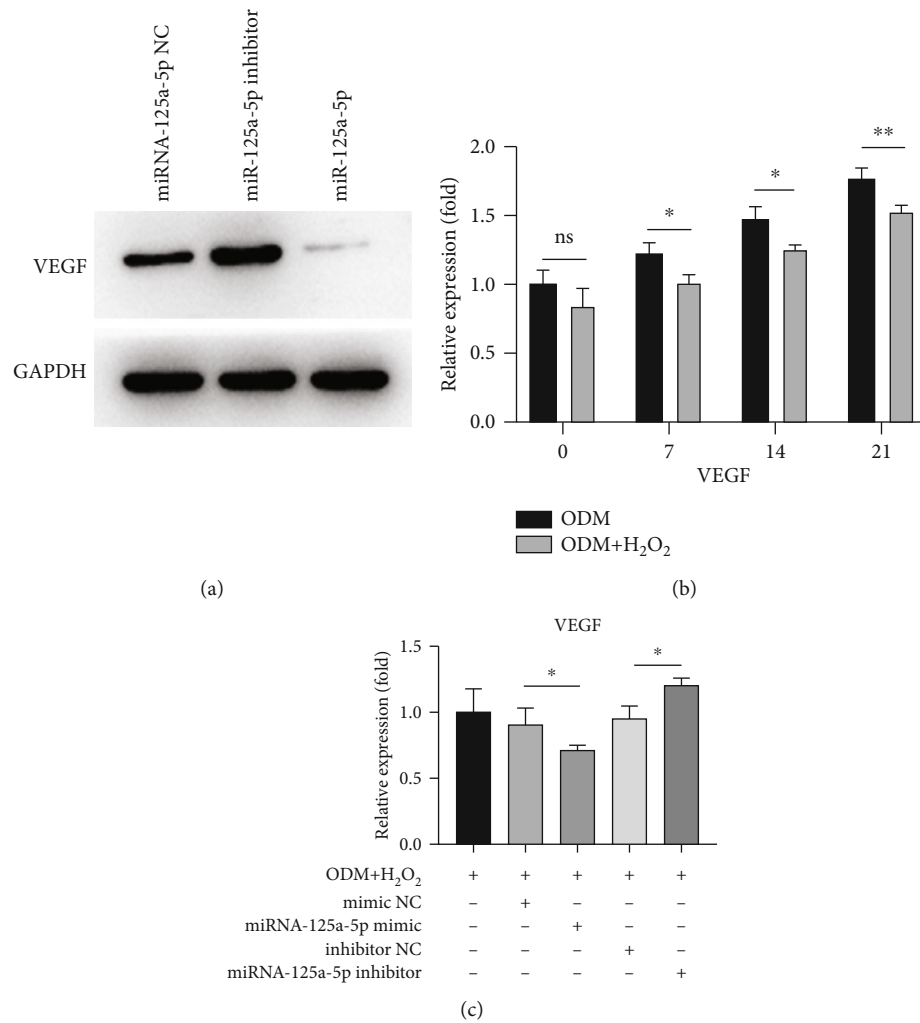


FIGURE 5: miR-125a-5p mediates the VEGF-regulated osteogenic differentiation of hADSCs under oxidative stress. (a) The expression level of VEGF protein in hADSCs infected by miRNA-125a-5p or infected with miRNA-125a-5p inhibitor was measured by western blotting. (b) The expression level of VEGF was evaluated at different time points during osteoinduction with or without H<sub>2</sub>O<sub>2</sub>. (c) The expression level of VEGF was measured by qRT-PCR on day 21, and after that, the cells were induced by the osteogenic differentiation medium (ODM) and, with the H<sub>2</sub>O<sub>2</sub> stimulation, infected by miRNA-125a-5p or infected with miRNA-125a-5p inhibitor. *N* = 3; <sup>ns</sup>*p* > 0.05; \**p* < 0.05.

#### 4. Discussion

ADSCs are found largely and can be obtained readily, and they have the ability to differentiate into numerous cell lineages, including hepatocytes, endothelial cells, smooth muscle cells, cardiomyocytes, neurons, adipocytes, osteocytes, and chondrocytes. Therefore, ADSCs are known as a tool for repairing, replacing, and regenerating damaged tissue, but the limited osteogenic differentiation ability greatly impedes the clinical application of ADMSCs in bone repair [21].

Specific regulatory factors and multiple signaling pathways are involved in the progression of osteogenesis [22, 23]. miRNAs have been shown to have a vital role in osteogenic differentiation and may become vital for regulating bone repair [24, 25]. The role of miR-125a-5p has been researched in a variety of cell lineages. As a functional microRNA, miR-125a-5p regulates the progression of bladder cancer by effecting on FUT4 [26]. Recently, a study has revealed that increased miR-125a-5p decreases the expression of

TNFRSF1B and increases osteoclast differentiation [27]. The outcomes of previous studies suggest that miR-125a-5p affects the osteogenic differentiation of ADSCs [19]. This current study further explored the specific mechanism of miR-125a-5p in the osteogenic differentiation of hADSCs. We show an obvious decrease in miR-125a-5p expressions during the osteogenic differentiation of hADSCs. Meanwhile, the overexpression of miR-125a-5p suppressed osteogenic induction of hADSCs, and the inhibition of miR-125a-5p by transfecting inhibitor oligonucleotide increased osteogenesis. Taken together, these outcomes show that miR-125a-5p is a negative regulator of the osteogenic differentiation of hADSCs.

Senescence of MSCs can be caused by different stimuli, including oxidative stress, radiation, chemicals (inducing acute senescence), or replication failure (inducing chronic senescence) [28]. Oxidative stress is induced by an imbalance between an excessive reactive oxygen species (ROS) and lacking antioxidant defense mechanisms [29]. The properties and their linked differentiation of ADSCs are regulated by

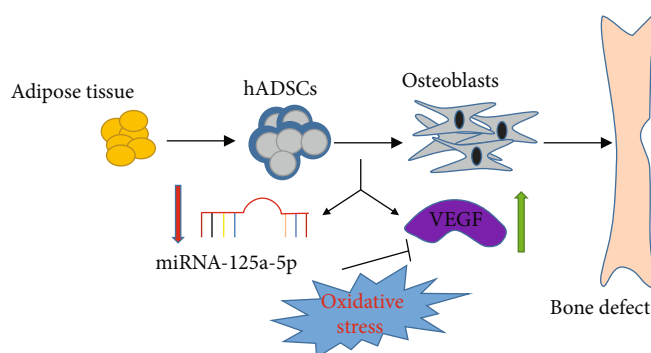


FIGURE 6: Schematic illustration of miRNA-125a-5p as it regulates osteogenic differentiation of hADSCs under oxidative stress by inhibiting the expression of VEGF.

reactive oxygen species in some degree [30]. In this study, hADSCs were treated with  $100\ \mu\text{M}$   $\text{H}_2\text{O}_2$  to mimic the environment of oxidative stress and induce the generation of ROS. When hADSCs were grown in osteogenic differentiation medium, the levels of osteogenic genes exhibited a time-dependent increase. However, the osteogenic genes tended to be reduced by oxidative stress stimulation. Meanwhile, under oxidative stress, ROS, the senescence of hADSCs, and miR-125a-5p were increased over time, suggesting that oxidative stress suppresses the osteogenic differentiation of hADSCs, induces the senescence of hADSCs, and is important for miR-125a-5p production.

Researchers have shown that VEGF has dual activities of angiogenesis and osteogenesis, which can significantly promote the growth of osteoblasts and accelerate bone formation [31]. Previous studies have also found that lamin A/C regulates the transcription factors Runx2 and PPAR $\gamma$ 2 by VEGF to control the osteogenic or adipogenic differentiation of mesenchymal stem cells. Moreover, the reduction of osteogenic differentiation of MSCs caused by VEGF gene deletion could only be restored by retrovirus-mediated VEGF expression, rather than by the exogenous recombination of VEGF [9]. In this study, it was proven using western blotting that miR-125a-5p controls the expression of VEGF in hADSCs. Meanwhile, we also showed that oxidative stress has a key role in regulating VEGF during the osteogenic differentiation of hADSCs. Oxidative stress and miR-125a-5p together suppressed the production of VEGF in the course of osteogenic differentiation of hADSCs, and the effect of oxidative stress could be reversed by the inhibition of miR-125a-5p.

In conclusion, our study pointed out that miR-125a-5p is induced under oxidative stress and inhibits the expression of VEGF, leading to the reduction of osteogenic differentiation of hADSCs (Figure 6). This demonstrates that miR-125a-5p could be a potential clinical target for bone repairing.

## Data Availability

All experiment methods and the result generated or used during the study appear in the submitted article.

## Conflicts of Interest

The authors have declared that no competing interest exists.

## Authors' Contributions

Yongheng Ye and Quan Liu contributed equally to this work.

## Acknowledgments

This work was supported by the Guangdong Natural Science Foundation (No. 2016A030313259).

## References

- [1] A. J. Serra, J. R. Pinto, M. D. Prokić, G. Arsa, and A. Vasconsuelo, "Oxidative stress in muscle diseases: current and future therapy 2019," *Oxidative Medicine and Cellular Longevity*, vol. 2020, Article ID 6030417, 4 pages, 2020.
- [2] S. F. Vatner, J. Zhang, M. Oydanich, T. Berkman, R. Naftalovich, and D. E. Vatner, "Healthful aging mediated by inhibition of oxidative stress," *Ageing Research Reviews*, vol. 64, p. 101194, 2020.
- [3] C. Wilson, "Oxidative stress and osteoporosis," *Nature Reviews Endocrinology*, vol. 10, no. 1, p. 3, 2014.
- [4] J. Lean, B. Kirstein, Z. Urry, T. Chambers, and K. Fuller, "Thioredoxin-1 mediates osteoclast stimulation by reactive oxygen species," *Biochemical and Biophysical Research Communications*, vol. 321, no. 4, pp. 845–850, 2004.
- [5] A. M. Craft, J. S. Rockel, Y. Nartiss, R. A. Kandel, B. A. Alman, and G. M. Keller, "Generation of articular chondrocytes from human pluripotent stem cells," *Nature Biotechnology*, vol. 33, no. 6, pp. 638–645, 2015.
- [6] W. K. Ong and S. Sugii, "Adipose-derived stem cells: fatty potentials for therapy," *The International Journal of Biochemistry & Cell Biology*, vol. 45, no. 6, pp. 1083–1086, 2013.
- [7] D. Rana, S. Kumar, T. J. Webster, and M. Ramalingam, "Impact of induced pluripotent stem cells in bone repair and regeneration," *Current Osteoporosis Reports*, vol. 17, no. 4, pp. 226–234, 2019.
- [8] X. Fu, G. Liu, A. Halim, Y. Ju, Q. Luo, and A. G. Song, "Mesenchymal stem cell migration and tissue repair," *Cell*, vol. 8, no. 8, p. 784, 2019.
- [9] Y. Liu, A. D. Berendsen, S. Jia et al., "Intracellular VEGF regulates the balance between osteoblast and adipocyte differentiation," *The Journal of Clinical Investigation*, vol. 122, no. 9, pp. 3101–3113, 2012.
- [10] D. Zhang, N. Ni, Y. Wang et al., "CircRNA-vgl3 promotes osteogenic differentiation of adipose-derived mesenchymal stem cells via modulating miRNA-dependent integrin  $\alpha 5$

- expression," *Cell Death and Differentiation*, vol. 28, no. 1, pp. 283–302, 2021.
- [11] S. Neri and R. Borzi, "Molecular mechanisms contributing to mesenchymal stromal cell aging," *Biomolecules*, vol. 10, no. 2, p. 340, 2020.
- [12] M. C. Gómez-Puerto, L. P. Verhagen, A. K. Braat, E. W. F. Lam, P. J. Coffey, and M. J. Lorenowicz, "Activation of autophagy by FOXO3 regulates redox homeostasis during osteogenic differentiation," *Autophagy*, vol. 12, no. 10, pp. 1804–1816, 2016.
- [13] R. Yang, J. Chen, J. Zhang et al., "1,25-Dihydroxyvitamin D protects against age-related osteoporosis by a novel VDR-Ezh2-p16 signal axis," *Aging Cell*, vol. 19, no. 2, article e13095, 2020.
- [14] W. Sun, W. Qiao, B. Zhou et al., "Overexpression of Sirt1 in mesenchymal stem cells protects against bone loss in mice by FOXO3a deacetylation and oxidative stress inhibition," *Metabolism*, vol. 88, pp. 61–71, 2018.
- [15] F. Zhang, W. Peng, J. Zhang et al., "P53 and Parkin co-regulate mitophagy in bone marrow mesenchymal stem cells to promote the repair of early steroid-induced osteonecrosis of the femoral head," *Cell Death & Disease*, vol. 11, no. 1, p. 42, 2020.
- [16] T. X. Lu and M. E. Rothenberg, "MicroRNA," *The Journal of Allergy and Clinical Immunology*, vol. 141, no. 4, pp. 1202–1207, 2018.
- [17] X. B. Qi, B. Jia, W. Wang et al., "Role of miR-199a-5p in osteoblast differentiation by targeting TET2," *Gene*, vol. 726, p. 144193, 2020.
- [18] L. Fan, J. Fan, Y. Liu et al., "miR-450b promotes osteogenic differentiation in vitro and enhances bone formation in vivo by targeting BMP3," *Stem Cells and Development*, vol. 27, no. 9, pp. 600–611, 2018.
- [19] Z. J. Zhang, H. Zhang, Y. Kang et al., "miRNA expression profile during osteogenic differentiation of human adipose-derived stem cells," *Journal of Cellular Biochemistry*, vol. 113, no. 3, pp. 888–898, 2012.
- [20] E. K. Moiola, L. Hong, and J. J. Mao, "Inhibition of osteogenic differentiation of human mesenchymal stem cells," *Wound Repair and Regeneration*, vol. 15, no. 3, pp. 413–421, 2007.
- [21] R. T. Qomi and M. Sheykhasan, "Adipose-derived stromal cell in regenerative medicine: a review," *World Journal of Stem Cells*, vol. 9, no. 8, pp. 107–117, 2017.
- [22] S. Mollazadeh, B. S. Fazly Bazzaz, V. Neshati et al., "T-Box20 inhibits osteogenic differentiation in adipose-derived human mesenchymal stem cells: the role of T-Box20 on osteogenesis," *Journal of Biological Research (Thessaloniki)*, vol. 26, no. 1, 2019.
- [23] E. Chiarella, A. Aloisio, B. Codispoti et al., "ZNF521 has an inhibitory effect on the adipogenic differentiation of human adipose-derived mesenchymal stem cells," *Stem Cell Reviews and Reports*, vol. 14, no. 6, pp. 901–914, 2018.
- [24] A. Narayanan, N. Srinaath, M. Rohini, and N. Selvamurugan, "Regulation of Runx2 by microRNAs in osteoblast differentiation," *Life Sciences*, vol. 232, p. 116676, 2019.
- [25] Z. Yuan, Q. Li, S. Luo et al., "PPAR $\gamma$  and Wnt signaling in adipogenic and osteogenic differentiation of mesenchymal stem cells," *Current Stem Cell Research & Therapy*, vol. 11, no. 3, pp. 216–225, 2016.
- [26] Y. Zhang, D. Zhang, J. Lv, S. Wang, and Q. Zhang, "MiR-125a-5p suppresses bladder cancer progression through targeting FUT4," *Biomedicine & Pharmacotherapy*, vol. 108, pp. 1039–1047, 2018.
- [27] L. Sun, J. X. Lian, and S. Meng, "MiR-125a-5p promotes osteoclastogenesis by targeting TNFRSF1B," *Cellular & Molecular Biology Letters*, vol. 24, no. 1, p. 23, 2019.
- [28] S. Capasso, N. Alessio, T. Squillaro et al., "Changes in autophagy, proteasome activity and metabolism to determine a specific signature for acute and chronic senescent mesenchymal stromal cells," *Oncotarget*, vol. 6, no. 37, pp. 39457–39468, 2015.
- [29] Y. B. Zhang, Z. M. Zhong, G. Hou, H. Jiang, and J. T. Chen, "Involvement of oxidative stress in age-related bone loss," *The Journal of Surgical Research*, vol. 169, no. 1, pp. e37–e42, 2011.
- [30] L. Rochette, L. Mazini, G. Malka, M. Zeller, Y. Cottin, and C. Vergely, "The crosstalk of adipose-derived stem cells (ADSC), oxidative stress, and inflammation in protective and adaptive responses," *International Journal of Molecular Sciences*, vol. 21, no. 23, p. 9262, 2020.
- [31] R. M. H. Rumney, S. A. Lanham, J. M. Kanczler et al., "In vivo delivery of VEGF RNA and protein to increase osteogenesis and intraosseous angiogenesis," *Scientific Reports*, vol. 9, no. 1, article 17745, 2019.

## Research Article

# Identification of Critical Genes and lncRNAs in Osteolysis after Total Hip Arthroplasty and Osteoarthritis by RNA Sequencing

Guang Yang<sup>1</sup>, Kai Tang<sup>2</sup>, Li Qiao<sup>3</sup>, Yixin Li<sup>4</sup>, and Shui Sun<sup>1</sup>

<sup>1</sup>Department of Joint Surgery, Shandong Provincial Hospital Affiliated to Shandong First Medical University, Jinan 250000, China

<sup>2</sup>Department of Orthopaedics, Shandong Provincial Hospital (Group) Ludong Hospital, Yantai 264000, China

<sup>3</sup>Department of Orthopedics, Yantaishan Hospital, Yantai 264000, China

<sup>4</sup>Department of Surgical Osteoarthritis, Jinan Central Hospital Affiliated to Shandong University, China

Correspondence should be addressed to Guang Yang; mayayangguang@163.com and Shui Sun; sunshui@sdfmu.edu.cn

Received 1 January 2021; Revised 20 February 2021; Accepted 1 March 2021; Published 15 March 2021

Academic Editor: Dongliang Xu

Copyright © 2021 Guang Yang et al. This is an open access article distributed under the Creative Commons Attribution License, which permits unrestricted use, distribution, and reproduction in any medium, provided the original work is properly cited.

Total hip arthroplasty (THA) is a cost-effective treatment for osteoarthritis (OA), and osteolysis is a common complication of THA. This study was aimed at exploring the relevant molecular biomarkers for osteolysis after THA. We performed RNA sequence to identify and characterize expressed mRNAs and lncRNAs in OA and osteolysis. Differentially expressed mRNAs (DEmRNAs) and lncRNAs (DElncRNAs) in OA and osteolysis were acquired, as well as shared DEmRNAs/DElncRNAs in OA and osteolysis and osteolysis-specific DEmRNAs/DElncRNAs. Then, shared and osteolysis-specific DElncRNA-DEmRNA coexpression networks were constructed to further investigate the function of DElncRNAs and DEmRNAs in OA and osteolysis. In total, 343 DEmRNAs and 25 DElncRNAs in OA, 908 DEmRNAs and 107 DElncRNAs in osteolysis, and 406 DEmRNAs and 46 DElncRNAs between OA and osteolysis were acquired. A total of 136 shared DEmRNAs and 9 shared DElncRNAs in OA and osteolysis and 736 osteolysis-specific DEmRNAs and 103 osteolysis-specific DElncRNAs were acquired. Then, 128 shared DElncRNA-DEmRNA coexpression pairs and 522 osteolysis-specific DElncRNA-DEmRNA coexpression pairs were identified. The present study highlighted the roles of four interaction pairs, including two shared lncRNA-mRNA interaction pairs in OA and osteolysis (AC111000.4 and AC016831.6), which may function in the immune process of OA and osteolysis by regulating CD8A and CD8B, respectively, and two osteolysis-specific interaction pairs (AC090607.4-FOXO3 and TAL1-ABALON), which may play an important role in osteoclastogenesis.

## 1. Introduction

Osteoarthritis (OA) is a leading cause of chronic disability in old people. For the treatment, the total hip arthroplasty (THA) is a cost-effective way, which can reduce joint pain, restore joint function, and increase the quality of life of patients [1]. Despite the improvement of the quality of polyethylene, osteolysis remains a risk for older designs and younger, active patients. Osteolysis is a progressive, active, biologic cascade, a phenomenon due to a foreign body response to particulate wear debris from the prosthetic joint [2]. Increased wear particles activate osteoclast formation, and overweight osteoclasts caused much bone resorption, which eventually led to osteolysis [3]. Osteolysis, as a complication of THA, leads to prosthesis failure

and bringing about additional suffering and burden for patients [4].

Long noncoding RNAs (lncRNAs), as a type of noncoding RNA, have been recognized as key regulatory molecules with diverse roles in gene expression, epigenetic modification, and protein activity [5]. Recently, lncRNA has been revealed to be involved in osteolysis. lncRNA TSIX was involved in particle-induced osteolysis by regulating miR-30a-5p to promote osteoblast apoptosis [6]. lncRNA DANCR inhibits osteoblast differentiation in osteolysis after THA through regulating FOXO1 [7]. lncRNA KCNQ1OT1 could ameliorate particle-induced osteolysis, by inhibiting miR-21a-5p to induce macrophage polarization [8]. However, more studies focused on the role of lncRNAs in osteolysis after THA need to be performed.

In this study, we, respectively, investigated the gene expression profiles of lncRNAs and mRNAs in patients with osteolysis after THA and OA, attempting to screen out differentially expressed mRNAs (DEmRNAs) and lncRNAs (DElncRNAs) associated with osteolysis after THA and OA. The objective of this study was to explore the underlying mechanism and the relevant molecular biomarkers for osteolysis after THA.

## 2. Materials and Methods

**2.1. Subjects and Samples.** The cohort subjected to RNA-Seq comprised 3 patients with OA, 3 patients with osteolysis after THA, and 3 healthy individuals. Inclusion criteria for patients with osteolysis after THA: (1) with current radiographic evidence of osteolysis and (2) received a THA after failure to improve function and pain after at least 6 months of conservative treatment. Subjects were excluded if they had any history of inflammatory arthropathy or known secondary causes of hip arthritis such as trauma, avascular necrosis, or developmental or childhood hip disease. Subjects were also excluded if they had taken courses of immunosuppressant agents or bisphosphonates for a continuous period of greater than 6 months since THA. OA was diagnosed according to the criteria of the American College of Rheumatology. Healthy individuals with no personal or family history of OA, no symptoms or signs of OA, or any other type of arthritis, or any painful condition of the joints, were included as controls. The participants with history of joint diseases, including inflammatory arthritis (rheumatoid arthritis or any other autoimmune disease), posttraumatic or postseptic arthritis, poliomyelitis, and skeletal dysplasia, were excluded. Table 1 described the characteristics of all these participants. All samples were collected after obtaining written informed consent from every participant. This study was approved by the Ethics Committee of Shandong Provincial Hospital (No. 2020-123) and performed in accordance with the Declaration of Helsinki. Peripheral whole blood (2.5 mL) drawn from each subject was collected in PAXgene® RNA blood tubes and stored at  $-80^{\circ}\text{C}$  prior to processing. RNA isolation was performed with PAXgene blood RNA kit. RNA integrity and concentration were evaluated with an Agilent 2100 Bioanalyzer (Agilent RNA 6000 Nano Kit). Total RNA samples used in subsequent experiments fulfilled the following requirements: RNA integrity number (RIN)  $> 7.0$  and  $28\text{S}/18\text{S} \geq 1$ . In brief, total RNA was subjected to ribosomal RNA (rRNA) removal using Ribo-Zero. A total amount of  $3\ \mu\text{g}$  RNA was used for library preparation. Libraries for sequencing were constructed according to the manufacturer's protocol. The quality of the libraries was determined using an Agilent 2100 Bioanalyzer and ABI StepOnePlus Real-Time PCR System. Based on the BGISEQ platform, sequencing was performed. The raw sequencing data were submitted to sequencing quality control by FastQC to assess whether they will be used for subsequent data analysis. Reads with low quality (adaptor sequences, sequences with a quality score  $< 20$ , and sequences with an  $N$  base rate of raw reads  $> 10\%$ ) were removed. Clean reads were aligned with the human reference genome, Ensemble GRCh38.p7.

**2.2. Identification of DEmRNAs and Functional Annotation.** StringTie software was used to compare the results to the known transcriptome and calculate the transcriptional abundance. Then, Ballgown was used for quantification of gene expression levels, as well as analysis of intergroup differential expression of genes. DESeq2 was applied to identify DEmRNAs in OA vs. control and osteolysis after THA vs. control with a  $p$  value  $< 0.05$ . DEmRNAs between OA and osteolysis after THA were obtained with a  $p$  value  $< 0.05$  as well. Hierarchical clustering analysis of DEmRNAs was performed with R package "pheatmap." Then, shared DEmRNAs in OA and osteolysis after THA and osteolysis-specific DEmRNAs (DEmRNAs in osteolysis after THA but no differences in OA) were further identified with Venny 2.1.0. The Database for Annotation, Visualization and Integrated Discovery (DAVID), which is a web-based tool, provides integrated solutions for the annotation and analysis of genome-scale datasets from high-throughput sequencing. DAVID 6.8 was used to perform GO and KEGG enrichment analysis for shared DEmRNAs in OA and osteolysis after THA and osteolysis-specific DEmRNAs. The lower the  $p$  value, the more significant are the GO term and the pathway. A value of  $p < 0.05$  was considered to be represented statistically significant.

**2.3. Identification of DElncRNAs.** DESeq2 was applied to identify DElncRNAs in OA vs. control and osteolysis after THA vs. control with a  $p$  value  $< 0.05$  and  $|\log_2\text{FC}| > 1.5$ . DElncRNAs between OA and osteolysis after THA were obtained with a  $p$  value  $< 0.05$  and  $|\log_2\text{FC}| > 1.5$  as well. Hierarchical clustering analysis of DElncRNAs was performed with R package "pheatmap." Then, shared DElncRNAs in OA and osteolysis after THA and osteolysis-specific DElncRNAs (DElncRNAs in osteolysis after THA but no differences in OA) were further identified with Venny 2.1.0.

**2.4. DElncRNA-DEmRNA Coexpression Network and Functional Annotation.** The shared and osteolysis-specific DElncRNA-DEmRNA coexpression networks were constructed to further investigate the potential functions of lncRNAs and mRNAs in OA and osteolysis. Pearson correlation coefficients were calculated between the expression values of DElncRNAs and DEmRNAs. The pairs with  $|\text{PCC}| > 0.8$  and  $p < 0.01$  in shared DElncRNA-DEmRNA pairs and pairs with  $|\text{PCC}| > 0.95$  and  $p < 0.01$  in osteolysis-specific DElncRNA-DEmRNA pairs were defined as coexpressed DElncRNA-DEmRNA pairs, respectively. Then coexpressed networks were visualized by using Cytoscape. DAVID 6.8 was used to perform GO and KEGG enrichment analysis for DEmRNAs in shared and osteolysis-specific DElncRNA-DEmRNA coexpression network. A value of  $p < 0.05$  was considered to be represented statistically significant.

**2.5. Statistical Analysis.** Statistical analyses were performed using R software v3.5.3 (R Foundation for Statistical Computing, Vienna, Austria). All tests were two-tailed, and  $p$  values  $< 0.05$  were considered statistically significant. In addition, the GraphPad Prism Software, version 7.0, was used for the statistical analysis of experimental data. The results

TABLE 1: Patient characteristics.

Group	Age (years)	Gender	<i>p</i> value	BMI (kg/m <sup>2</sup> )	<i>p</i> value	Years after THA	Kellgren-Lawrence grade ( <i>n</i> )	WBC (cells/mL)	<i>p</i> value	PLT (cells/mL)	<i>p</i> value	ESR (mm/h)	<i>p</i> value	CRP (mg/L)	<i>p</i> value	Part
Osteolysis	59	Male		24.2		15	—	7.3		276		19		4.2		Left
	42	Male		25.4		15	—	5.89		210		19		4.2		Right
	70	Female		25.4		17	—	7.42		278		22		9.5		Right
OA	55	Female		30.5		—	3	4.1		225		10		2.1		Right
	40	Female	0.64	28.1	0.05	—	4	5.77	0.11	270	0.56	10	0.03	2.2	0.41	Right
	67	Male		29.8		—	3	5.65		187		10		6.6		Right
Controls	30	Male		26.1		—	—	6.62		233		15		7.7		Left
	29	Male		27.1		—	—	4.45		221		10		2.1		Right
	18	Female		30		—	—	6.85		253		11		1.3		Right

BMI: body mass index; THA: total hip arthroplasty; WBC: white blood cell; PLT: blood platelet; ESR: erythrocyte sedimentation ratio; CRP: C-reactive protein; OA: osteoarthritis.

TABLE 2: Top 10 up- and downregulated DEmRNAs.

Symbol	$\log_2FC$	$p$ value	FDR	Regulation
OA vs. control				
HIST2H4A	2.017903	1.45E-12	1.86E-08	Up
ZNF778	2.30578	2.34E-09	1.50E-05	Up
RAB8A	1.084187	4.61E-07	0.001473	Up
MYOM2	3.614517	1.16E-05	0.021164	Up
PI3	1.77021	4.16E-05	0.05915	Up
VASH1	1.031837	0.000207	0.203576	Up
SNHG28	1.440766	0.000309	0.263506	Up
LILRB3	1.133152	0.000349	0.27883	Up
UPRT	1.107994	0.000428	0.322295	Up
UNC13B	1.407436	0.000467	0.331741	Up
CD8A	-1.49304	2.03E-07	0.000865	Down
AL157935.2	-3.11394	2.71E-06	0.006946	Down
AL121594.1	-3.12822	4.34E-06	0.00926	Down
EPHB4	-2.33741	1.40E-05	0.022395	Down
F11R	-1.30037	6.96E-05	0.080899	Down
YPEL2	-1.41993	0.000184	0.196205	Down
CHKB-CPT1B	-1.48977	0.00028	0.255821	Down
ZNF80	-1.53824	0.000671	0.393542	Down
EEF1AKMT3	-1.76553	0.000677	0.393542	Down
CD8B	-1.42735	0.000767	0.426828	Down
Osteolysis vs. control				
ZNF778	2.261961	6.77E-08	0.000222	Up
LILRB3	1.396428	1.23E-06	0.003224	Up
MYOM2	3.476227	3.33E-06	0.00575	Up
BCORL1	2.051727	1.40E-05	0.018296	Up
RTL5	1.812327	1.85E-05	0.022092	Up
FOSL2	1.834524	3.50E-05	0.026994	Up
CNTNAP3	2.346929	7.26E-05	0.047612	Up
MGAM2	2.714451	9.47E-05	0.049807	Up
ERV3-1	1.398861	9.50E-05	0.049807	Up
TMEM164	1.378476	0.000107	0.053473	Up
TMEM56-RWDD3	-3.54683	9.81E-12	1.29E-07	Down
AC013489.1	-4.17415	3.51E-06	0.00575	Down
PLVAP	-2.61008	2.39E-05	0.026097	Down
PPDPF	-2.88183	2.75E-05	0.026397	Down
RPS26	-2.22182	2.82E-05	0.026397	Down
HBB	-2.40451	3.29E-05	0.026994	Down
RGS6	-2.33305	4.89E-05	0.035625	Down
EVPL	-3.08781	5.28E-05	0.036452	Down
RIOK3	-2.15799	7.94E-05	0.049573	Down
LRRN3	-2.13595	8.98E-05	0.049807	Down
Osteolysis vs. OA				
EPHB4	3.187856	9.59E-07	0.003135	Up
RASSF5	1.444879	1.47E-05	0.023969	Up
FAM118A	1.406201	4.97E-05	0.064931	Up
AL354822.1	2.9104	0.000364	0.250326	Up
AL121594.1	2.129941	0.0004	0.259591	Up

TABLE 2: Continued.

Symbol	log <sub>2</sub> FC	p value	FDR	Regulation
ZNF587	1.181929	0.000736	0.320854	Up
SERPING1	1.589099	0.002698	0.608048	Up
LRP1	1.363794	0.004148	0.796847	Up
CASP10	1.098776	0.004527	0.796847	Up
REC8	1.074025	0.004665	0.796847	Up
MTURN	-1.58117	1.09E-05	0.021921	Down
HBB	-2.3627	1.17E-05	0.021921	Down
CISD2	-1.29668	6.10E-05	0.07251	Down
AC093668.3	-2.78122	6.93E-05	0.073252	Down
DDA1	-1.3542	8.91E-05	0.08323	Down
AC013489.1	-3.94451	0.000133	0.11567	Down
ARL4A	-1.83919	0.00018	0.147286	Down
EPB41	-1.62564	0.000288	0.221659	Down
CRIL	-1.61874	0.000353	0.250326	Down
DLGAP5	-2.34576	0.000426	0.259591	Down

FC: fold change; FDR: false discovery rate; OA: osteoarthritis.

are expressed as means  $\pm$  standard deviations (SDs). In addition, we used Shapiro-Wilk to test the normal distribution of data. However, the statistical analysis of clinical data showed that the data are not normal distribution. Therefore, we choose the Kruskal-Wallis test for statistical analysis. Pearson correlation coefficients were calculated between the expression values of DElncRNAs and DEMRNAs.  $p < 0.05$  was considered to indicate a significant difference between the groups.

### 3. Results

**3.1. Identification of DEMRNAs and Functional Annotation.** DESeq2 was applied to identify DEMRNAs, and our results showed that a total of 343 DEMRNAs (184 up- and 159 downregulated) in OA vs. control, 908 DEMRNAs (429 up- and 479 downregulated) in osteolysis vs. control, and 406 DEMRNAs (112 up- and 294 downregulated) in OA vs. osteolysis were identified. Of these, HIST2H4A and CD8A, ZNF778 and TMEM56-RWDD3, and EPHB4 and MTURN were the most up- and downregulated DEMRNAs in OA vs. control, osteolysis vs. control, and OA vs. osteolysis, respectively (Table 2). The heatmap of the top 100 up- and downregulated DEMRNAs was shown in Figures 1(a)–1(c). The volcano plots of DEMRNAs are shown in Figures S1A–C. A total of 136 shared DEMRNAs (71 up- and 65 downregulated) in OA vs. control and osteolysis vs. control and 736 osteolysis-specific DEMRNAs (381 up- and 355 downregulated) were acquired (Figure 1(d)).

To investigate the functions of shared and osteolysis-specific DEMRNAs, DAVID 6.8 was used to perform GO and KEGG enrichment analysis. For shared DEMRNAs, cell activation ( $p = 2.81E - 03$ ), leukocyte activation ( $p = 5.20E - 03$ ), integral to plasma membrane ( $p = 3.17E - 04$ ), and protein homodimerization activity ( $p = 1.93E - 02$ ) were several significantly enriched GO terms, and mTOR signal-

ing pathway ( $p = 1.89E - 02$ ) and cell cycle ( $p = 3.81E - 02$ ) were significantly enriched KEGG pathways (Figures S2, S4 A and B). For osteolysis-specific DEMRNAs, intracellular signaling cascade ( $p = 1.80E - 02$ ), cell adhesion ( $p = 8.45E - 04$ ), plasma membrane ( $p = 9.54E - 05$ ), and cytoskeletal protein binding ( $p = 1.08E - 02$ ) were several significantly enriched GO terms, and hematopoietic cell lineage ( $p = 1.35E - 02$ ), cell adhesion molecules (CAMs) ( $p = 2.29E - 02$ ), porphyrin and chlorophyll metabolism ( $p = 3.40E - 02$ ), and systemic lupus erythematosus ( $p = 4.86E - 02$ ) were significantly enriched KEGG pathways (Figures S3, S4 C–F).

**3.2. Identification of DElncRNAs.** DESeq2 was applied to identify DElncRNAs, and our results showed that a total of 25 DElncRNAs (15 up- and 10 downregulated) in OA vs. control, 107 DElncRNAs (58 up- and 49 downregulated) in osteolysis vs. control, and 46 DElncRNAs (17 up- and 29 downregulated) in OA vs. osteolysis were identified. Of these, NEAT1 and AC005726.2, FLJ42393 and AC123912.4, and AC016737.1 and AC123912.4 were the most up- and downregulated DElncRNAs in OA vs. control, osteolysis vs. control, and OA vs. osteolysis, respectively (Table 3). The heatmap of DElncRNAs is shown in Figures 2(a)–2(c). The volcano plots of DEMRNAs are shown in Figure S1D–F. A total of 9 shared DElncRNAs (6 up- and 3 downregulated) in OA vs. control and osteolysis vs. control and 103 osteolysis-specific DElncRNAs (52 up- and 51 downregulated) were acquired (Figure 2(d)).

**3.3. DElncRNA-DEMNA Coexpression Network and Functional Annotation.** To further investigate the potential functions of lncRNAs and mRNAs in OA and osteolysis, the shared and osteolysis-specific DElncRNA-DEMNA coexpression networks were constructed. A total of 128 shared DElncRNA-DEMNA coexpression pairs including 9 DElncRNAs and 81 DEMRNAs were obtained (Figure 3(a)).

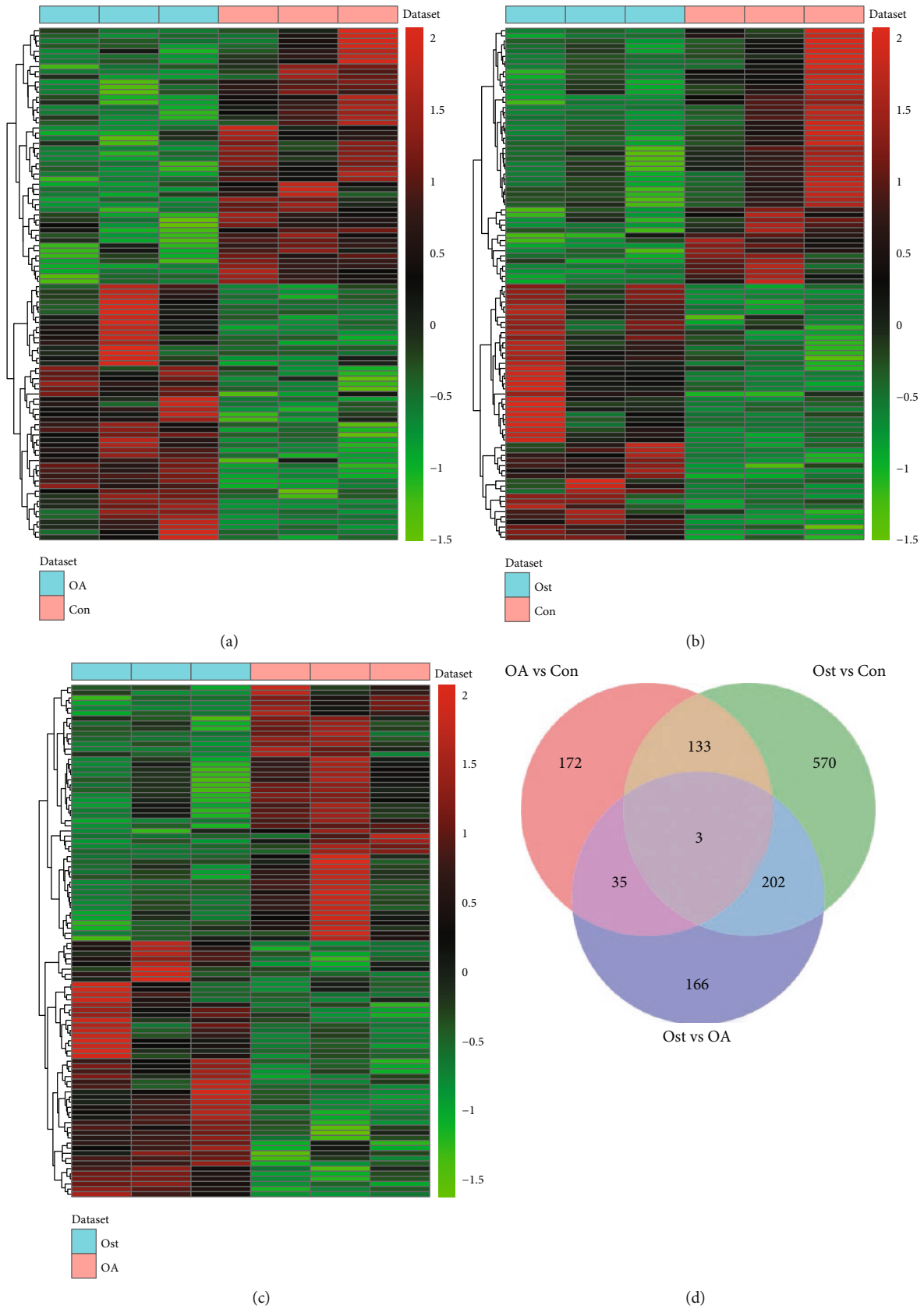


FIGURE 1: Identification of DEMRNAs: (a) heatmap of top 100 DEMRNAs between OA and normal controls; (b) heatmap of top 100 DEMRNAs between osteolysis after THA and normal controls; (c) heatmap of top 100 DEMRNAs between OA and osteolysis after THA; (d) Venn diagram of DEMRNAs in OA and osteolysis after THA. Con: controls; Ost: osteolysis.

TABLE 3: Top 10 up- and downregulated DElncRNAs.

Symbol	$\log_2FC$	$p$ value	FDR	Regulation
OA vs. control				
NEAT1	5.1159	1.85E-18	1.12E-14	Up
AL512625.3	2.570376	3.24E-05	0.065224	Up
AC016831.6	1.728574	5.90E-05	0.088885	Up
AC111000.4	2.064848	0.001215	0.563632	Up
LINC01341	2.02527	0.005032	0.92186	Up
AC018445.3	1.654176	0.010542	0.999047	Up
AC004231.1	1.894872	0.01745	0.999047	Up
AC114752.2	1.692437	0.020267	0.999047	Up
AP003117.2	1.771314	0.023032	0.999047	Up
AC096642.1	1.589585	0.025643	0.999047	Up
AC005726.2	-1.66485	4.64E-08	0.00014	Down
PITRM1-AS1	-2.72439	0.000346	0.348099	Down
OVCH1-AS1	-2.18336	0.000714	0.478621	Down
AC005082.1	-2.31905	0.002001	0.670439	Down
AL162457.1	-1.71468	0.002791	0.701277	Down
AC126755.7	-1.50226	0.004787	0.92186	Down
AP006545.1	-1.89154	0.011714	0.999047	Down
AC020659.1	-1.60564	0.013616	0.999047	Down
AC007541.1	-1.69387	0.031639	0.999047	Down
AC068870.2	-1.90393	0.039154	0.999047	Down
Osteolysis vs. control				
FLJ42393	1.62292	7.39E-05	0.067195	Up
AC007272.1	2.182036	0.000975	0.279887	Up
AC016831.6	1.690991	0.001091	0.285274	Up
AL359532.1	1.86552	0.001529	0.335756	Up
AL359183.1	1.921891	0.001606	0.340963	Up
AC091185.1	1.772238	0.001807	0.359718	Up
AC018946.1	1.549455	0.002757	0.427746	Up
AC015871.4	1.542564	0.00288	0.427746	Up
AC100788.2	1.613121	0.003089	0.427746	Up
LINC02288	1.673173	0.003444	0.429946	Up
AC123912.4	-3.00991	2.78E-10	1.77E-06	Down
AC010615.2	-3.72122	1.34E-06	0.004253	Down
DDIT4-AS1	-1.59273	1.65E-05	0.033738	Down
AC092490.1	-2.67119	2.42E-05	0.033738	Down
AC100810.1	-2.2893	5.65E-05	0.059947	Down
SLC2A1-AS1	-2.12909	0.000292	0.191562	Down
AC100835.2	-2.25064	0.000369	0.195639	Down
AC097478.1	-2.43982	0.000553	0.242589	Down
LINC00570	-2.3716	0.000559	0.242589	Down
MIR9-3HG	-2.61167	0.000581	0.242589	Down
Osteolysis vs. OA				
AC016737.1	2.007544	0.000286	0.459454	Up
AC124319.2	1.591514	0.003026	0.999986	Up
AL357078.3	1.935801	0.005568	0.999986	Up
AL139020.1	2.119999	0.007539	0.999986	Up
AC004263.1	1.824237	0.015321	0.999986	Up

TABLE 3: Continued.

Symbol	$\log_2FC$	$p$ value	FDR	Regulation
AC018653.3	1.519922	0.020607	0.999986	Up
AC099521.2	1.851515	0.024567	0.999986	Up
AC110801.1	2.016041	0.0264	0.999986	Up
AL022328.1	1.56358	0.02739	0.999986	Up
AL844908.2	1.529839	0.03055	0.999986	Up
AC123912.4	-3.68915	3.62E-08	0.000233	Down
AC010615.2	-3.84396	5.84E-06	0.018749	Down
AL356489.2	-3.8055	0.000598	0.654803	Down
AC092821.3	-1.68773	0.001213	0.866219	Down
KRT73-AS1	-1.77092	0.002183	0.999986	Down
FP236383.2	-1.99999	0.002243	0.999986	Down
AL159978.1	-2.32724	0.003423	0.999986	Down
TPM1-AS	-1.77588	0.003634	0.999986	Down
MIR9-3HG	-1.88441	0.004272	0.999986	Down
LINC00570	-1.98324	0.005975	0.999986	Down

FC: fold change; FDR: false discovery rate; OA: osteoarthritis.

Among them, AC018761.2 (degree = 49), AC090607.4 (degree = 46), and ABALON (degree = 42) were the top 3 DElncRNAs that covered the most DEmRNAs. Then, to investigate the functions of DEmRNAs in shared and osteolysis-specific DElncRNA-DEmRNA coexpression network, DAVID 6.8 was used to perform GO and KEGG enrichment analysis. For DEmRNAs in shared DElncRNA-DEmRNA coexpression network, T cell activation ( $p = 1.53E - 02$ ), leukocyte differentiation ( $p = 1.69E - 02$ ), leukocyte activation ( $p = 1.77E - 02$ ), immune system development ( $p = 2.72E - 02$ ), T cell differentiation ( $p = 2.96E - 02$ ), and mTOR signaling pathway ( $p = 2.85E - 02$ ) were several significantly enriched pathways (Figure 3(b)).

A total of 522 osteolysis-specific DElncRNA-DEmRNA coexpression pairs including 36 DElncRNAs and 194 DEmRNAs were obtained (Figure 4(a)). Among them, AC111000.4 (degree = 38), OVCH1-AS1 (degree = 24), and AC016831.6 (degree = 19) were the top 3 DElncRNAs that covered the most DEmRNAs. For DEmRNAs in osteolysis-specific DElncRNA-DEmRNA coexpression network, myeloid cell differentiation ( $p = 4.50E - 04$ ), immune system development ( $p = 7.00E - 04$ ), cell proliferation ( $p = 2.27E - 03$ ), and positive regulation of myeloid cell differentiation ( $p = 4.73E - 02$ ) were several significantly enriched pathways (Figure 4(b)).

#### 4. Discussion

Osteolytic lesions may develop after THA from a biologic reaction to particulate debris [9]. It is a major complication of THA, causing additional suffering and burden for patients. Aggravating evidence indicates that lncRNAs regulate gene expression via cis- and/or transregulation mechanisms and participate in various biological processes, including chromatin modification, DNA synthesis, cell proliferation, differentiation, and apoptosis [10]. In this present study, we screened

out critical genes and lncRNAs correlated with OA and osteolysis by RNA sequencing and bioinformatics analysis.

Due to the close interaction between immune cells and bone cells, immune disorders can lead to abnormal bone metabolism [11]. T lymphocyte differentiation could be made by the “clusters of differentiation” (CD), and the common receptors are CD4 and CD8. CD8, a cell surface glycoprotein, is predominantly expressed on the surface of cytotoxic T killer cells and implicated in the immune system. The CD8 antigen is a specifically recognized antigen displayed by the class major histocompatibility complex I molecules. Long et al. identified a 16-gene biomarker panel to differentiate RA from OA and indicated the lower expression level of CD8A in OA than in RA [12]. Landgraeber et al. reported that the  $CD4^+/CD8^+$  ratio was associated with the stage of osteolysis in aseptic loosening [13]. In this study, both CD8A and CD8B were significantly decreased in OA vs. control and osteolysis vs. control. Functional annotation revealed that CD8A and CD8B were enriched in immune-related pathways, such as T cell activation, leukocyte differentiation, leukocyte activation, immune system development, and T cell differentiation. In addition, CD8A was coexpressed with AC111000.4, and CD8B was coexpressed with AC016831.6 in shared the DElncRNA-DEmRNA coexpression network. Taken together, we speculated that AC111000.4 and AC016831.6 may function in the immune process of OA and osteolysis by regulating CD8A and CD8B, respectively.

The FOXO proteins are an evolutionarily conserved family of transcription factors which comprised FOXO1, FOXO3, FOXO4, and FOXO6 in mammals [14]. The four FOXO members share obvious sequence homology and are ubiquitously expressed in various organs, including bone [15]. FOXOs regulate diverse cellular processes, including oxidative stress, metabolism, apoptosis, and inflammation [16]. In addition, FOXOs have been revealed to regulate bone

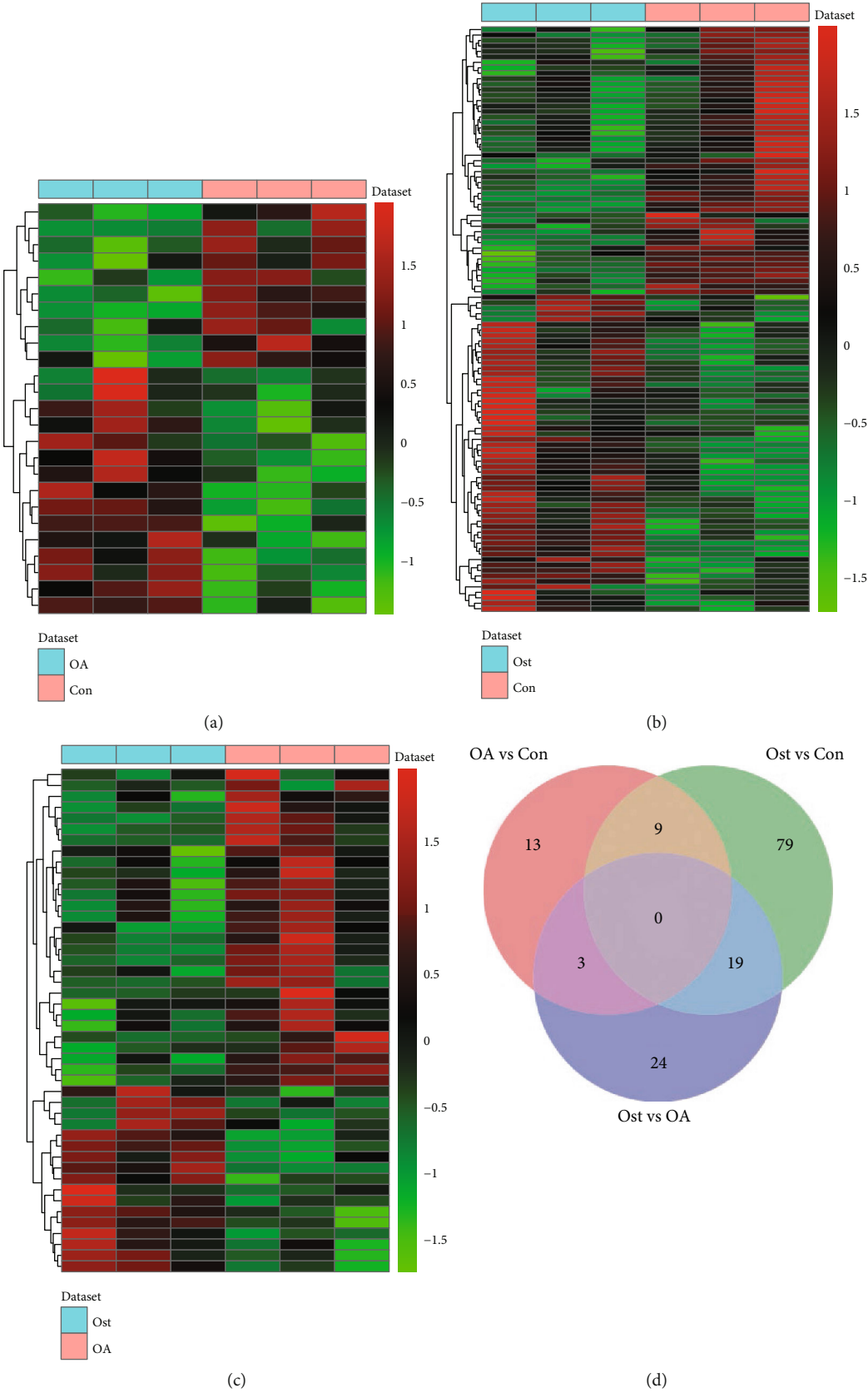


FIGURE 2: Identification of DElncRNAs: (a) heatmap of DElncRNAs between OA and normal controls; (b) heatmap of DElncRNAs between osteolysis after THA and normal controls; (c) heatmap of DElncRNAs between OA and osteolysis after THA; (d) Venn diagram of DElncRNAs in OA and osteolysis after THA. Con: controls; Ost: osteolysis.

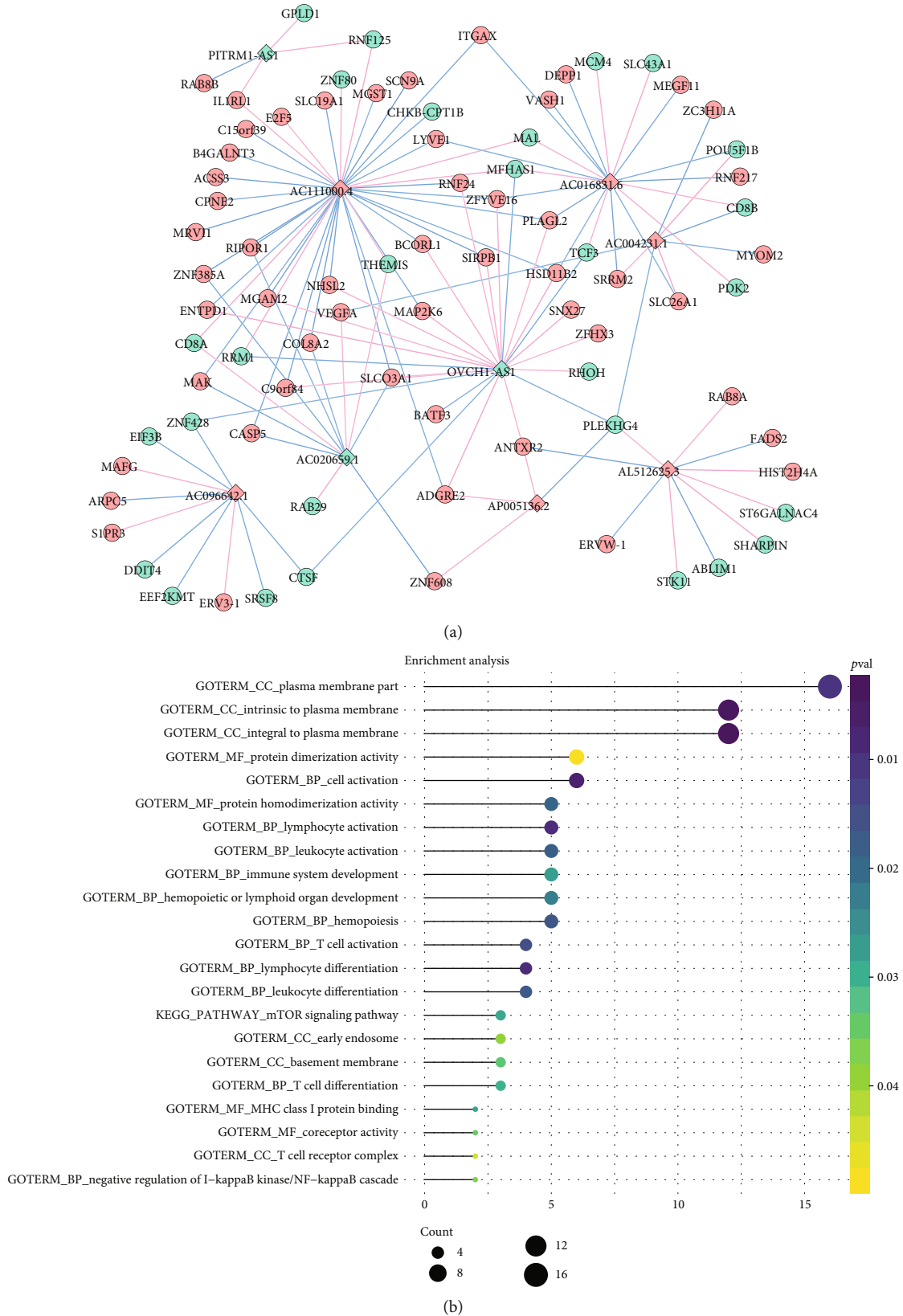
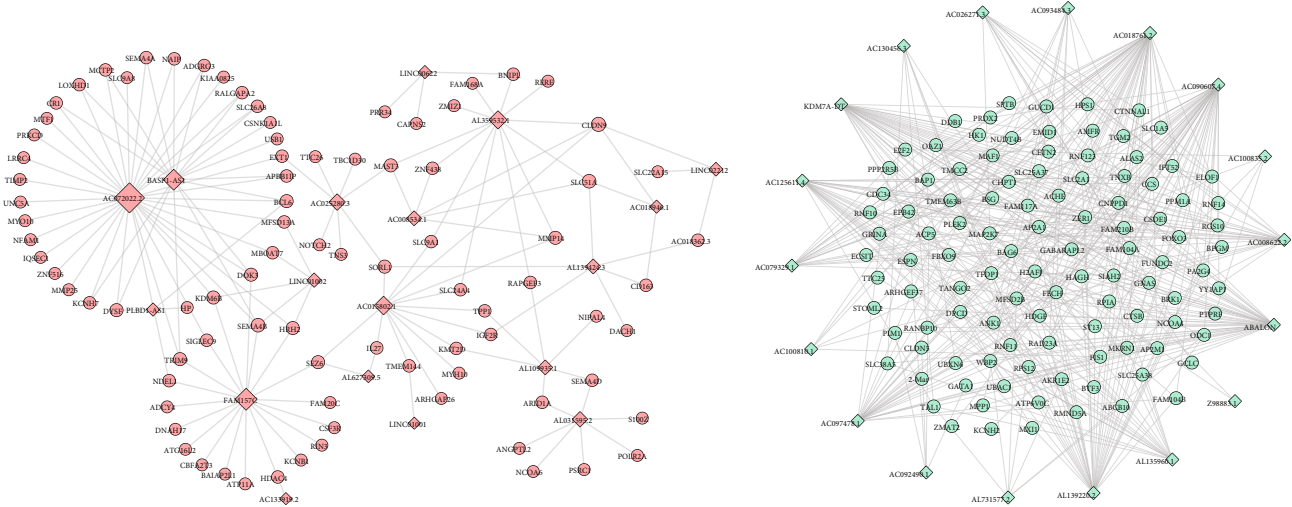
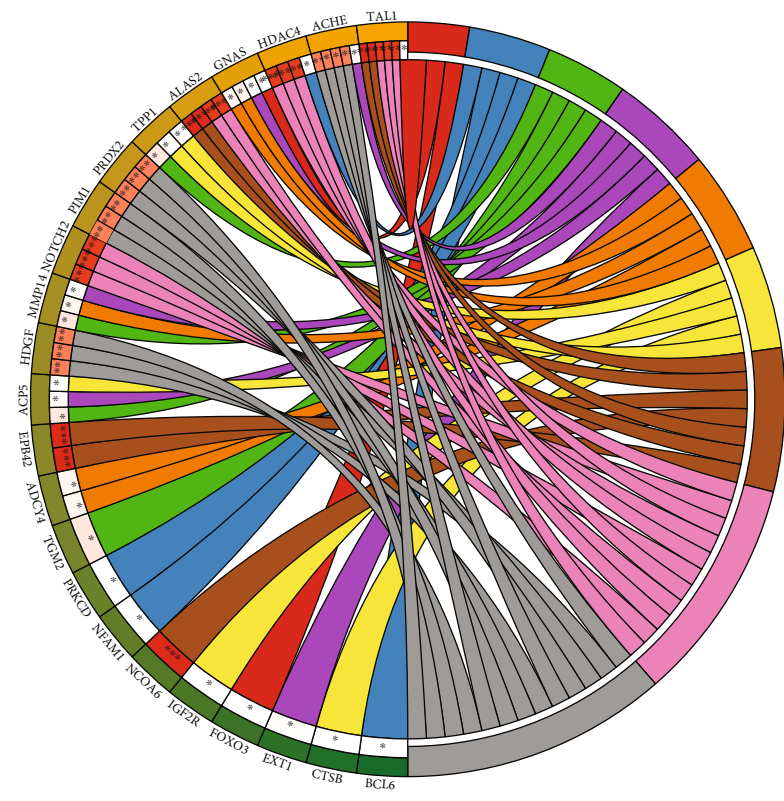


FIGURE 3: Shared DElncRNA-DEmRNA coexpression network and functional annotation. (a) Shared DElncRNA-DEmRNA co-expression network in OA and osteolysis after THA. The rhombus and ellipses represent DElncRNAs and DEmRNAs, respectively. Red and blue colors represent up- and downregulation, respectively. Red and blue edges represent positively and negatively correlated lncRNA-mRNA pairs, respectively. (b) Function enrichment.



(a)



- Term
- BP:positive regulation of myeloid cell differentiation
  - BP:B cell activation
  - BP:tissue remodeling
  - BP:bone development
  - KEGG:GnRH signaling pathway
  - KEGG:lysosome
  - BP:myeloid cell differentiation
  - BP:immune system development
  - BP:cell proliferation

(b)

FIGURE 4: Osteolysis-specific DElncRNA-DEmRNA coexpression network and functional annotation. (a) Osteolysis-specific DElncRNA-DEmRNA coexpression network. The rhombus and ellipses represent DElncRNAs and DEMRNAs, respectively. Red and blue color represent up- and downregulation, respectively. (b) Function enrichment.

cell functions, osteoblast differentiation, and the maintenance of skeletal homeostasis [17]. Bartell et al. suggested that FOXO3 regulate receptor activator of NF- $\kappa$ B ligand-(RANKL-) induced osteoclast differentiation [18]. Miller et al. reported that FOXO3 play important inhibitory roles in TNF- $\alpha$ -mediated osteoclastogenesis and bone resorption [19]. Ambrogini et al. found that overexpression of FOXO3 in osteoblasts may reduce osteoclast numbers [20]. Increased osteoclastogenesis leads to osteolysis. Here, FOXO3 was determined to be a significantly decreased osteolysis-specific DEmRNA and coexpressed with AC090607.4, which indicated the importance of AC090607.4 in osteolysis by targeting FOXO3.

TAL1, also known as SCL, plays a crucial role in hematopoiesis and is causally connected to T cell acute lymphatic leukemia [21, 22]. The fact that embryonic stem cells of Tal1-knockout mice did not develop into osteoclasts *in vitro* supported that Tal1 plays a role in osteoclast differentiation [23]. The maintenance of bone homeostasis mainly depends on the balance between bone-forming osteoblasts and bone-resorbing osteoclasts. The transcription factor TAL1 was of great importance in cell cycle progression and proliferation in differentiating murine bone marrow monocyte precursors [24]. Knockdown of Tal1 in osteoclast progenitors leads to larger osteoclasts, containing more nuclei, and altered expression of a large number genes [25]. Wang et al. found that TAL1 was a differentially expressed transcription factor in osteoporosis [26]. In this study, TAL1 was coexpressed with ABALON in the osteolysis-specific DElncRNA-DEmRNA coexpression network. Therefore, the role of TAL1-BALON in osteolysis should be paid attention.

## 5. Conclusions

In conclusion, we highlighted the roles of four interaction pairs, including two shared lncRNA-mRNA interaction pairs in OA and osteolysis (AC111000.4-CD8A and AC016831.6-CD8B) and two osteolysis-specific interaction pairs (AC090607.4-FOXO3 and TAL1-BALON) in this present work. Taken as a whole, our work made contribution to understanding the pathophysiology of osteolysis. Our study also had a limitation. The sample size for RNA sequencing in this study was small, and further studies with larger sample size are warranted to confirm these results.

## Data Availability

The clinical data used to support the findings of this study are restricted by the Ethics Committee of Shandong Provincial Hospital (No. 2020-123) in order to protect patient privacy. Data are available from Guang Yang (mayayangguang@163.com) for researchers who meet the criteria for access to confidential data.

## Conflicts of Interest

The authors declare that there is no conflict of interest regarding the publication of this paper.

## Acknowledgments

This work was supported by the Natural Science Foundation of Shandong (No. ZR2020QH073) and National Natural Science Foundation of China (No. 81972056).

## Supplementary Materials

Figure S1: the volcano plots of DEmRNAs in OA (A), osteolysis (B), OA vs osteolysis (C), DElncRNAs in OA (D), osteolysis (E), and OA vs osteolysis (F). Figure S2: significantly enriched GO terms (A) and KEGG (B) pathways of shared DEmRNAs in OA and osteolysis after THA. Figure S3: significantly enriched GO terms (A) and KEGG (B) pathways of osteolysis-specific DEmRNAs. Figure S4: mTOR signaling pathway and cell cycle were significantly enriched KEGG pathways of shared DEmRNAs (A, B). Hematopoietic cell lineage, cell adhesion molecules (CAMs), porphyrin and chlorophyll metabolism, and systemic lupus erythematosus were significantly enriched KEGG pathways of osteolysis-specific DEmRNAs (C–F). (*Supplementary Materials*)

## References

- [1] J. M. Wilkinson, A. G. Wilson, I. Stockley et al., "Variation in the TNF gene promoter and risk of osteolysis after total hip arthroplasty," *Journal of Bone and Mineral Research*, vol. 18, no. 11, pp. 1995–2001, 2003.
- [2] N. P. Sheth, J. C. Rozell, and W. G. Paprosky, "Evaluation and treatment of patients with acetabular osteolysis after total hip arthroplasty," *The Journal of the American Academy of Orthopaedic Surgeons*, vol. 27, no. 6, pp. e258–e267, 2019.
- [3] I. Roato, D. Caldo, L. D'Amico et al., "Osteoclastogenesis in peripheral blood mononuclear cell cultures of periprosthetic osteolysis patients and the phenotype of T cells localized in periprosthetic tissues," *Biomaterials*, vol. 31, no. 29, pp. 7519–7525, 2010.
- [4] M. Attinger and K. Siebenrock, "Total hip replacement: between normal rehabilitation and complication," *Praxis (Bern 1994)*, vol. 103, no. 24, pp. 1439–1446, 2014.
- [5] A. Fatica and I. Bozzoni, "Long non-coding RNAs: new players in cell differentiation and development," *Nature Reviews. Genetics*, vol. 15, no. 1, pp. 7–21, 2014.
- [6] Y. Bu, D. Zheng, L. Wang, and J. Liu, "LncRNA TSIX promotes osteoblast apoptosis in particle-induced osteolysis by down-regulating miR-30a-5p," *Connective Tissue Research*, vol. 59, no. 6, pp. 534–541, 2018.
- [7] Z. Tang, Z. Gong, and X. Sun, "LncRNA DANCR involved osteolysis after total hip arthroplasty by regulating FOXO1 expression to inhibit osteoblast differentiation," *Journal of Biomedical Science*, vol. 25, no. 1, p. 4, 2018.
- [8] X. Gao, J. Ge, W. Li, W. Zhou, and L. Xu, "LncRNA KCNQ1OT1 ameliorates particle-induced osteolysis through inducing macrophage polarization by inhibiting miR-21a-5p," *Biological Chemistry*, vol. 399, no. 4, pp. 375–386, 2018.
- [9] M. D. Ries and T. M. Link, "Monitoring and risk of progression of osteolysis after total hip arthroplasty," *The Journal of Bone and Joint Surgery. American Volume*, vol. 94, no. 22, pp. 2097–2105, 2012.
- [10] J. T. Lee, "Epigenetic regulation by long noncoding RNAs," *Science*, vol. 338, no. 6113, pp. 1435–1439, 2012.

- [11] L. Li, Y. Wang, N. Zhang et al., "Heterozygous deletion of LRP5 gene in mice alters profile of immune cells and modulates differentiation of osteoblasts," *Bioscience Trends*, vol. 12, no. 3, pp. 266–274, 2018.
- [12] N. P. Long, S. Park, N. H. Anh et al., "Efficacy of integrating a novel 16-gene biomarker panel and intelligence classifiers for differential diagnosis of rheumatoid arthritis and osteoarthritis," *Journal of Clinical Medicine*, vol. 8, no. 1, p. 50, 2019.
- [13] S. Landgraeber, M. von Knoch, F. Löer et al., "Association between apoptotic and CD4(+)/CD8(+) T-lymphocyte ratio in aseptic loosening after total hip replacement," *International Journal of Biological Sciences*, vol. 5, no. 2, pp. 182–191, 2009.
- [14] D. A. Salih and A. Brunet, "FoxO transcription factors in the maintenance of cellular homeostasis during aging," *Current Opinion in Cell Biology*, vol. 20, no. 2, pp. 126–136, 2008.
- [15] D. Tsitsipatis, L. O. Klotz, and H. Steinbrenner, "Multifaceted functions of the forkhead box transcription factors FoxO1 and FoxO3 in skin," *Biochimica et Biophysica Acta (BBA) - General Subjects*, vol. 1861, no. 5, pp. 1057–1064, 2017.
- [16] C. Xu, G. J. Vitone, K. Inoue, C. Ng, and B. Zhao, "Identification of a novel role for Foxo3 isoform2 in osteoclastic inhibition," *Journal of Immunology*, vol. 203, no. 8, pp. 2141–2149, 2019.
- [17] M. F. Siqueira, S. Flowers, R. Bhattacharya et al., "FOXO1 modulates osteoblast differentiation," *Bone*, vol. 48, no. 5, pp. 1043–1051, 2011.
- [18] S. M. Bartell, H.-N. Kim, E. Ambrogini et al., "FoxO proteins restrain osteoclastogenesis and bone resorption by attenuating H<sub>2</sub>O<sub>2</sub> accumulation," *Nature Communications*, vol. 5, no. 1, 2014.
- [19] C. H. Miller, S. M. Smith, M. Elguindy et al., "RBP-J-regulated miR-182 promotes TNF- $\alpha$ -induced osteoclastogenesis," *Journal of Immunology*, vol. 196, no. 12, pp. 4977–4986, 2016.
- [20] E. Ambrogini, M. Almeida, M. Martin-Millan et al., "FoxO-mediated defense against oxidative stress in osteoblasts is indispensable for skeletal homeostasis in mice," *Cell Metabolism*, vol. 11, no. 2, pp. 136–146, 2010.
- [21] A. J. Bloor, M. J. Sanchez, A. R. Green, and B. Gottgens, "The role of the stem cell leukemia (SCL) gene in hematopoietic and endothelial lineage specification," *Journal of Hematotherapy & Stem Cell Research*, vol. 11, no. 2, pp. 195–206, 2002.
- [22] E. Lecuyer and T. Hoang, "SCL: from the origin of hematopoiesis to stem cells and leukemia," *Experimental Hematology*, vol. 32, no. 1, pp. 11–24, 2004.
- [23] T. Yamane, T. Kunisada, H. Yamazaki, T. Nakano, S. H. Orkin, and S. I. Hayashi, "Sequential requirements for SCL/tal-1, GATA-2, macrophage colony-stimulating factor, and osteoclast differentiation factor/osteoprotegerin ligand in osteoclast development," *Experimental Hematology*, vol. 28, no. 7, pp. 833–840, 2000.
- [24] S. Dey, D. J. Curtis, S. M. Jane, and S. J. Brandt, "The TAL1/SCL transcription factor regulates cell cycle progression and proliferation in differentiating murine bone marrow monocyte precursors," *Molecular and Cellular Biology*, vol. 30, no. 9, pp. 2181–2192, 2010.
- [25] N. Courtial, J. J. Smink, O. N. Kuvardina, A. Leutz, J. R. Göthert, and J. Lausen, "Tal1 regulates osteoclast differentiation through suppression of the master regulator of cell fusion DC-STAMP," *The FASEB Journal*, vol. 26, no. 2, pp. 523–532, 2012.
- [26] C. Wang, T. Yu, L. Tan, and J. Cheng, "Bioinformatics analysis of gene expression profile in callus tissues of osteoporotic phenotype mice induced by osteoblast-specific Krm2 overexpression," *International Journal of Rheumatic Diseases*, vol. 19, no. 12, pp. 1263–1271, 2016.

## Research Article

# Icariin Promotes the Osteogenesis of Bone Marrow Mesenchymal Stem Cells through Regulating Sclerostin and Activating the Wnt/ $\beta$ -Catenin Signaling Pathway

Jianliang Gao, Shouyu Xiang, Xiao Wei, Ram Ishwar Yadav, Menghu Han, Weihao Zheng, Lili Zhao, Yichuan Shi, and Yanming Cao 

Department of Orthopedics, The Second Affiliated Hospital of Guangzhou Medical University, Guangzhou, China

Correspondence should be addressed to Yanming Cao; 13729813888@126.com

Received 4 December 2020; Revised 21 December 2020; Accepted 2 January 2021; Published 23 January 2021

Academic Editor: Chaohong Li

Copyright © 2021 Jianliang Gao et al. This is an open access article distributed under the Creative Commons Attribution License, which permits unrestricted use, distribution, and reproduction in any medium, provided the original work is properly cited.

Osteoporosis (OP) is a metabolic disease characterized by decreased bone mass and increased risk of fragility fractures, which significantly reduces the quality of life. Stem cell-based therapies, especially using bone marrow mesenchymal stem cells (BMSCs), are a promising strategy for treating OP. Nevertheless, the survival and differentiation rates of the transplanted BMSCs are low, which limits their therapeutic efficiency. Icariin (ICA) is a traditional Chinese medicine formulation that is prescribed for tonifying the kidneys. It also promotes the proliferation and osteogenic differentiation of BMSCs, although the specific mechanism remains unclear. Based on our previous research, we hypothesized that ICA promotes bone formation via the sclerostin/Wnt/ $\beta$ -catenin signaling pathway. We isolated rat BMSCs and transfected them with sclerostin gene (*SOST*) overexpressing or knockdown constructs and assessed osteogenic induction in the presence or absence of ICA. Sclerostin significantly inhibited BMSC proliferation and osteogenic differentiation, whereas the presence of ICA not only increased the number of viable BMSCs but also enhanced ALP activity and formation of calcium nodules during osteogenic induction. In addition, the osteogenic genes including Runx2,  $\beta$ -catenin, and *c-myc* as well as antioxidant factors (Prdx1, Cata, and Nqo1) were downregulated by sclerostin and restored by ICA treatment. Mechanistically, ICA exerted these effects by activating the Wnt/ $\beta$ -catenin pathway. In conclusion, ICA can promote the proliferation and osteogenic differentiation of BMSCs in situ and therefore may enhance the therapeutic efficiency of BMSC transplantation in OP.

## 1. Introduction

Osteoporosis (OP) is a common skeletal disease characterized by reduced bone mineral density (BMD), bone microstructure deterioration, and an increased risk of fragility fractures [1, 2]. The incidence of OP has risen sharply with the aging of the global population, and currently, one-third of women and one-fifth of men are afflicted worldwide [3]. The antiosteoporosis drugs approved at present are bone resorption inhibitors [4], and their long-term intake can increase the risk of jaw osteonecrosis and atypical femoral fractures, thereby limiting their clinical application [5]. Therefore, it is necessary to develop novel treatment strategies for OP.

Recent studies show that bone marrow mesenchymal stem cells (BMSCs) can repair bone defects in several animal models [6] and are a promising tool for bone regeneration in OP [7]. However, the survival and differentiation rates of the transplanted BMSCs are low, which significantly reduces the efficacy of BMSC-based regenerative therapy [8]. Therefore, enhancing the proliferation and osteogenesis differentiation of BMSCs in situ can significantly improve therapeutic efficacy. Sclerostin is an osteoinhibitory protein encoded by the *SOST* gene that is secreted by bone cells [9] and inhibits osteoblast activity by inactivating the Wnt/ $\beta$ -catenin pathway [10]. The *SOST*<sup>-/-</sup> mice show accelerated osteoblast differentiation via  $\beta$ -catenin activation [11], which suggests that knocking down the

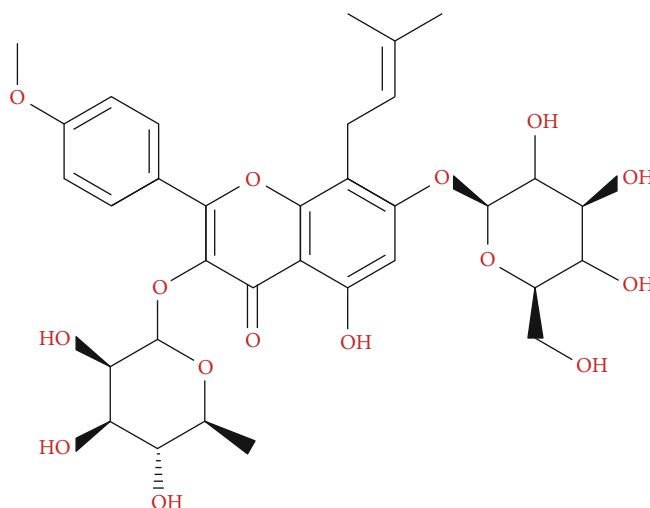


FIGURE 1: The chemical structure of ICA.

*SOST* gene may enhance osteogenic differentiation of BMSCs and promote bone renewal.

Icariin (ICA, chemical structure shown in Figure 1) is the main active flavonoid glycoside in the Chinese herbal medicine *Herba Epimedii*, which is used to treat renal disorders and prevent bone loss [12]. Recent studies show that ICA can effectively treat postmenopausal OP and promote bone formation [13] by stimulating BMSC proliferation and osteogenic differentiation [14]. In addition, the Chinese medicinal formulation Zuogui pills can also regulate BMSC osteogenic differentiation via the Wnt/ $\beta$ -catenin signaling pathway [15]. The aim of this study was to elucidate the mechanistic basis of the proosteogenic function of ICA, with specific focus on the sclerostin-Wnt/ $\beta$ -catenin signaling pathway. To this end, we isolated rat BMSCs and transfected them with *SOST* overexpression or knockdown constructs and treated them with ICA during osteogenic induction.

## 2. Materials and Methods

**2.1. Animals and Ethics.** Twelve-week-old female Sprague-Dawley (SD) rats weighing 200–300 g were purchased from the Experimental Animal Center of Sun Yat-sen University (Guangzhou, China, Certificate SCXK (Guangdong) 2016-0029). Animal experiments were performed in accordance with the guidelines of the Regulations of the People's Republic of China on the Administration of Experimental Animals and approved by the Animal Ethics Committee of the Second Hospital Affiliated with Guangzhou Medical University.

**2.2. Chemical Reagents and Drugs.** Dulbecco minimum essential medium (DMEM), fetal bovine serum (FBS), potassium phosphate buffer saline (PBS), and penicillin-streptomycin were purchased from Hyclone (Logan, Utah, USA). Icariin (ICA, purity > 94%) and dimethyl sulfoxide (DMSO) were obtained from Sigma (Steinheim, Germany). The alkaline phosphatase (ALP) staining kit (BCIP/NBT kit) was obtained from Beyotime Biotechnology (Shanghai, China) and the ALP activity measurement kit from Nanjing Jiancheng Biotech (Nanjing, China). Anti- $\beta$ -catenin anti-

body was purchased from GeneTex (Southern California, USA) and the antibodies targeting GSK- $\beta$  and p-GSK- $\beta$  from GST (Hangzhou, China). Secondary antibodies were obtained from Abcam (Shanghai, China).

**2.3. BMSC Extraction and Culture.** The animals were euthanized by cervical dislocation, and the tibia and femurs were removed. The bone marrow cavities were flushed repeatedly with 10% FBS-supplemented DMEM using a sterile 10 ml syringe to prepare a single cell suspension. The cells were seeded into a 25 cm<sup>2</sup> flask and cultured at 37°C under 5% CO<sub>2</sub> [16]. The medium was changed every 3 days, and the cells were observed regularly under an inverted microscope. After culturing for 7–10 days, the 80%–90% confluent monolayer was harvested with 0.25% EDTA-trypsin, washed at 1000 rpm for 5 minutes, and resuspended in complete DMEM for subculturing at 1:2 ratio.

**2.4. Flow Cytometry.** BMSCs ( $1 \times 10^6$  cells/ml) were incubated with phycoerythrin-labeled anti-CD90, anti-CD44, anti-CD31, or anti-CD34 antibodies at room temperature in the dark. After washing twice with PBS at 800 rpm for 5 minutes, the cells were acquired by flow cytometry [17].

**2.5. Vector Construction and Lentivirus Production.** The *SOST* overexpression and shRNA lentiviruses were constructed by Suzhou Genewiz. The *SOST* gene was amplified using the following primers: *SOST* forward ATGCAGCTC TCACTAGCCCCTTGCC and *SOST* reverse CTAGTA GCGTTCCTCCAGCTCCGCTGG. The *SOST* shRNA sequences were as follows: forward GGCCTCCTCAGGAA CTAGAGAATTCAAGAGATTCTCTAGTTCTCCTGAGGA GGCTTTTT and reverse AAAAAGCCTCCTCAGGAA CTAGAGAATCTCTTGAATTCTCTAGTTCTCCTGAGGAG GCC. The sequences were cloned into L303-CMV.Gene.EF1.GFP-T2A-Puro and L202-CMV.CopGFP.2A.Puro H1 plasmids, which were transiently transfected into 293T packaging cells (Invitrogen, Thermo Fisher Scientific Inc.). The serum-free medium was replaced after 8 hours with complete medium. The cells were cultured for 48 hours,

TABLE 1: Primers used for target amplification in this study.

Name	Accession number	Primer	Sequence (5'-3')
Runx2	NM_053470.1	Forward	GATGCCTTAGTGCCCAATGT
		Reverse	GGCTGAAGGGTGAAGAAAGC
$\beta$ -catenin	NM_053357.2	Forward	TGAGAAACTTGTCCGATGCA
		Reverse	CACTTGGCACACCATCATCT
c-myc	NM_012603.2	Forward	TGTAGTAATTCCAGCGAGAG
		Reverse	CGCAGATTGTAAGTTCCAG
Prdx1	NM_057114.1	Forward	GGATTGGGACCCATGAACAT
		Reverse	GAACCTGGAAGGCCTGGACTA
Cata	NM_012520.2	Forward	CCATCGCCAGTGGCAATTAC
		Reverse	AGTCCTTGTGAGGCCAAACC
Nqo1	NM_017000.3	Forward	TGTGGCTTCCAGGTCTTAGA
		Reverse	TGACTCCTCCAGACAGTCT
GAPDH	NM_017008.3	Forward	CCCATTCTCCACCTTTGAT
		Reverse	CAACTGAGGGCCTCTCTCT

and the supernatant was collected and concentrated. The virus titer was measured, and the transduction rate was measured by PCR [18].

**2.6. BMSC Transfection and Osteogenic Induction.** The BMSCs were transduced with the *SOST* overexpression or shRNA lentiviruses and cultured in osteogenic induction medium with or without 0.1  $\mu$ M ICA. Nontransfected and normal controls were also included. After predetermined time points, osteogenic differentiation was assessed by specific tests.

**2.7. CCK-8 Assay.** BMSCs were seeded into 96-well plates at the density of  $1 \times 10^4$  per well, and 10  $\mu$ l CCK-8 reagent (Keki Bio, Cat. No. KGA317) was added to each well after 24, 48, and 72 h of culture. After incubating for 2 hours, the absorbance was measured at 450 nm using a microplate reader (Thermo Fisher Scientific, Vantaa, Finland).

**2.8. Alkaline Phosphatase (ALP) Staining and Activity Assay.** The suitable cells were fixed with 10% formaldehyde for 15 minutes, rinsed with distilled water for 30 seconds, and stained with NBT-BCIP solution (Beyotime Biotechnology, China) at 37°C in the dark for 15 minutes [19]. After washing with distilled water for 30 seconds, the stained cells were viewed under a microscope. For the ALP activity assay, the cells were digested with 0.25% pancrease at room temperature for 2 to 3 minutes and centrifuged. After washing once with PBS, the lysate was analyzed using the ALP assay kit according to the manufacturer's instructions.

**2.9. Alizarin Red Staining.** The differentiated BMSCs were transferred to a six-well plate and fixed with 2 ml 4% neutral formaldehyde solution for 30 min. After rinsing twice with PBS, 1 ml Alizarin red solution was added to each well, and the cells were stained for 3–5 min. The cells were rinsed 2–3 times and observed under a microscope.

**2.10. RT-qPCR.** Total RNA was extracted using Trizol reagent (Invitrogen, USA) and quantified using a Thermo Scientific Microplate Reader (Thermo, USA). RT-qPCR was

conducted using SYBR Green qPCR SuperMix (Invitrogen, California, USA) on the ABI PRISM® 7500 Sequence Detection System (Applied Biosystems; Thermo Fisher Scientific, Inc.). The primer sequences are listed in Table 1.

**2.11. Western Blotting.** Western blotting was performed according to standard protocols [20]. Briefly, the proteins were loaded onto 10% SDS-PA gels, electrophoresed, and transferred onto polyvinylidene difluoride membranes (Millipore, USA). The blots were probed overnight with anti- $\beta$ -catenin, anti-GSK-3 $\beta$ , and anti-p-GSK-3 $\beta$  primary antibodies at 4°C, followed by secondary antibody (1:2000 Southern Biotech) at room temperature for 1 hour. GAPDH (1:1000, Aksomics, China) was used as the internal control [21]. The positive bands were visualized using an Enhanced Chemiluminescence Western Blot Substrate Kit (Keygen, Nanjing) and analyzed using ImageJ software (National Institutes of Health, Bethesda, MD).

**2.12. Statistical Analysis.** Data are presented as mean  $\pm$  standard deviation (SD). Statistical analyses were performed using SPSS version 16.0 software (SPSS Inc., Chicago, IL, USA). One-way analysis of variance (ANOVA) or Student's *t*-test was used to compare different groups. *P* values less than 0.05 were considered statistically significant.

### 3. Results

**3.1. Characterization of BMSCs.** The initial BMSC cultures exhibited adherent cells, colonies, and floating cells (Figure 2(a), A), and the latter disappeared completely by the fifth passage (Figure 2(a), B). Immunophenotypic analysis showed that 99.83% and 99.78% of the cells expressed CD90 and CD44, and only 1.15% and 1.43% expressed CD31 and CD34, respectively (Figures 2(b)–2(e)), indicating that most cells were BMSCs.

**3.2. ICA Promotes Proliferation and Osteogenic Differentiation of BMSCs.** As shown in Figure 3, 0.1  $\mu$ M ICA significantly increased proliferation of the BMSCs compared to the untreated controls. Osteogenic differentiation of the BMSCs

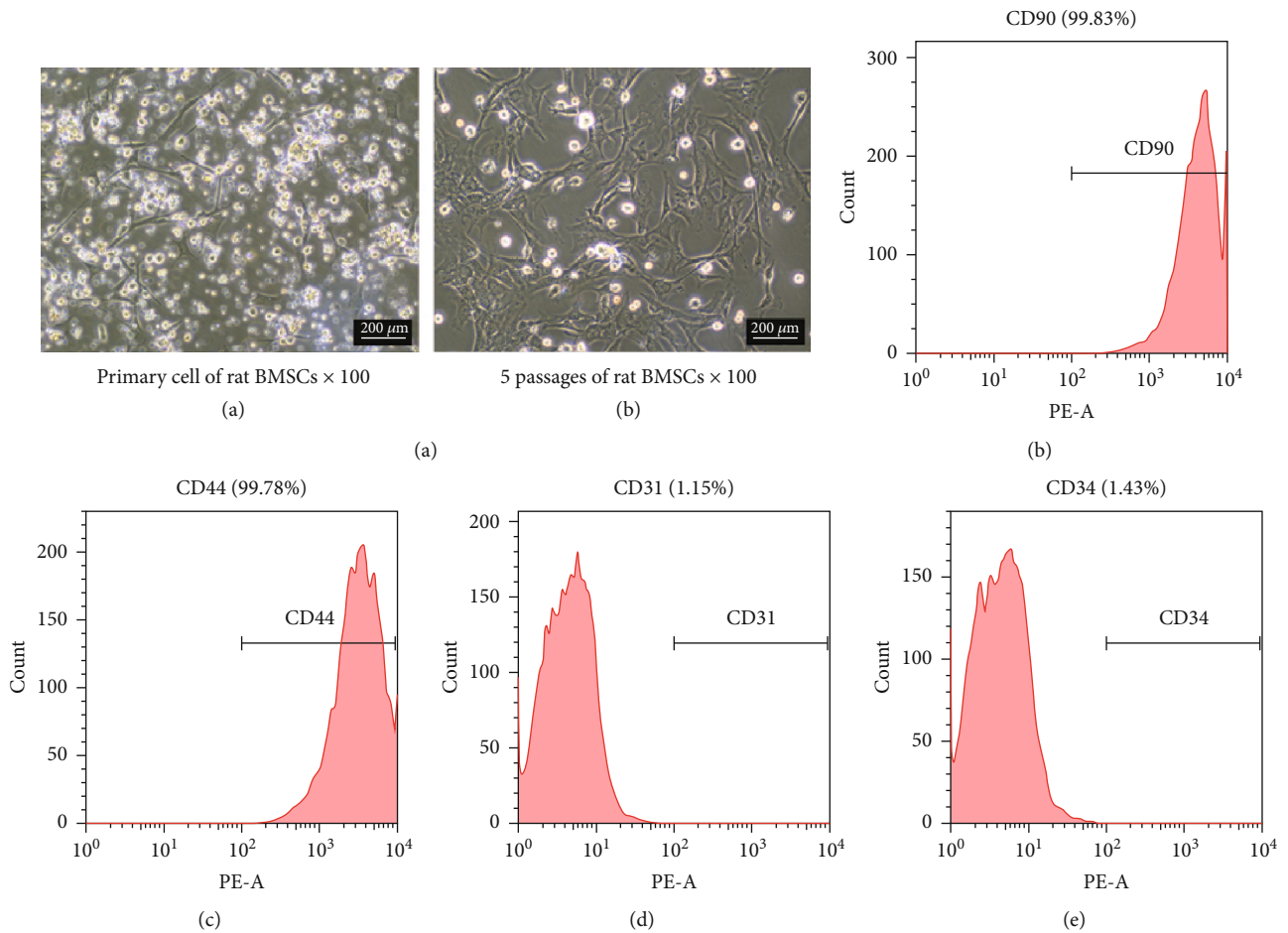


FIGURE 2: Morphology and phenotypic characterization of BMSCs. (a) Representative images of cultured rBMSCs at the primary passage (A) and passage 5 (B). Flow cytometry plots showing percentage of cells expressing (b) CD90, (c) CD44, (d) CD31, and (e) CD34.

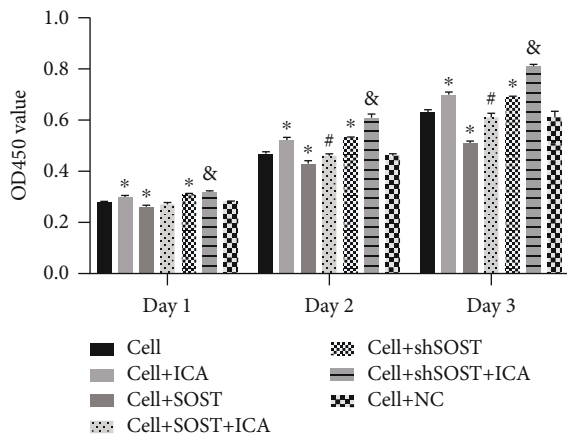


FIGURE 3: Effects of ICA and sclerostin on BMSC proliferation. Percentage of viable cells in the indicated groups at days 1, 2, and 3 postinduction. All data are presented as mean ± SEM. \* $P < 0.05$  compared to the control group, # $P < 0.05$  compared to the sclerostin overexpression group, and & $P < 0.05$  compared to the sclerostin knockdown group.

was assessed by ALP staining and activity and Alizarin red staining. ICA significantly enhanced ALP levels and activity in the BMSCs compared to the control (Figure 4), which is indicative of early osteoblast differentiation. Furthermore, intense Alizarin red staining in the ICA-treated cells indicated formation of calcified nodules and osteogenic differentiation (Figure 4). Taken together, ICA significantly promoted BMSC proliferation and osteogenic differentiation *in vitro*.

**3.3. ICA Reverses the Inhibitory Effect of Sclerostin on Osteogenic Gene Expression.** To ascertain the involvement of sclerostin in ICA-induced osteogenic differentiation of BMSCs, we transfected the cells with SOST overexpression and shRNA constructs prior to ICA treatment. As shown in Figures 3 and 4, SOST overexpression inhibited BMSC proliferation and ALP activity compared to the control group, whereas SOST knockdown had the opposite effect. However, ICA treatment restored proliferative and osteogenic capacity of the SOST-overexpressing BMSCs, which underscores the proosteogenic activity of ICA. Consistent with this, ICA significantly increased the expression levels of osteogenic genes including Runx2,  $\beta$ -catenin, and c-myc after 4, 7, and 14 days. Similar results were observed in the SOST-knockdown BMSCs as well. In addition, the osteogenic genes were also

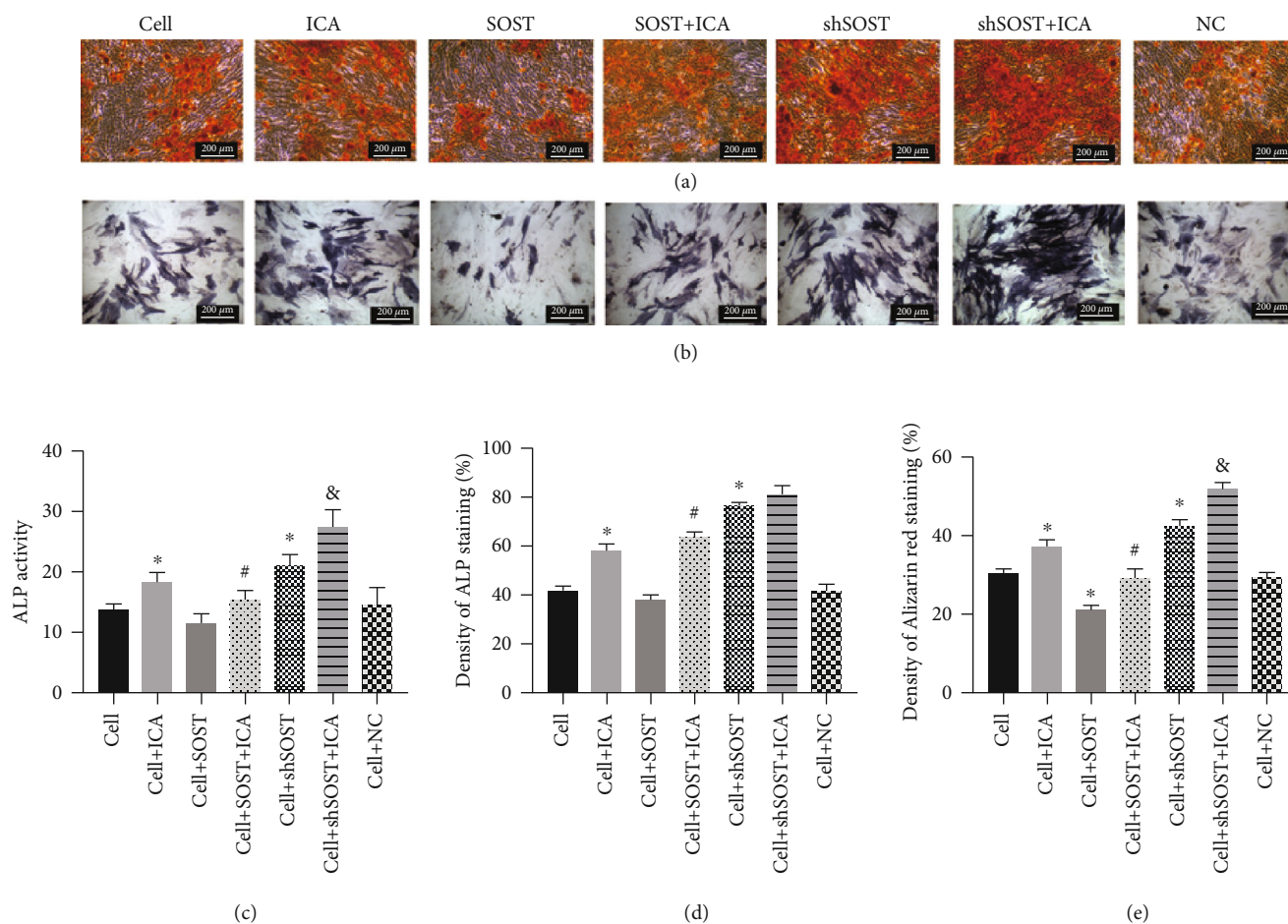


FIGURE 4: Effects of ICA and sclerostin on the osteogenic differentiation of BMSCs. (a) Alizarin red staining, (b) alkaline phosphatase staining, (c) ALP activity in the indicated groups, and (d, e) ratio of control in ALP staining and Alizarin red staining. All data are presented as mean  $\pm$  SEM. \* $P < 0.05$  compared to the control group, # $P < 0.05$  compared to the sclerostin overexpression group, and & $P < 0.05$  compared to the sclerostin knockdown group.

upregulated in the *SOST*-overexpressing and *SOST*-knockdown cells following ICA treatment (Figure 5). Taken together, sclerostin inhibits the osteogenic potential of BMSCs, which can be reversed by ICA.

**3.4. ICA Enhances the Antioxidant Response in BMSCs.** Oxidative stress is one of the underlying causes of OP and is known to inhibit osteogenesis [22]. To determine whether ICA modulates oxidative stress in the BMSCs, we analyzed the expression levels of antioxidant factors including *Prdx1*, *Cata*, and *Nqo1* in the differentially treated cells. As shown in Figure 6, both ICA treatment and *SOST* knockdown significantly upregulated *Prdx1*, *Cata*, and *Nqo1* mRNA levels on days 4 and 7 postosteogenic induction compared to the control group, whereas *SOST* overexpression had the opposite effect. Furthermore, ICA treatment augmented the antioxidant response in the *SOST*-knockdown BMSCs and restored the same in cells overexpressing *SOST*. Taken together, ICA promotes the osteogenic differentiation of BMSCs by mitigating oxidative stress.

**3.5. ICA Promotes Osteogenesis via the Sclerostin/Wnt/ $\beta$ -Catenin Signaling Pathway.** To further elucidate the mecha-

nistic basis of ICA action, we next analyzed the expression levels of key Wnt/ $\beta$ -catenin pathway intermediates, such as  $\beta$ -catenin, GSK-3 $\beta$ , and p-GSK-3 $\beta$ . As shown in the immunoblots in Figure 7, both ICA and *SOST*-shRNA significantly upregulated  $\beta$ -catenin and p-GSK-3 $\beta$  proteins on days 4 and 7 of culture compared to the control group. In contrast, *SOST* overexpression downregulated these factors at the same time points. Consistent with the findings so far, ICA increased the expression of Wnt/ $\beta$ -catenin pathway factors in BMSCs regardless of the *SOST* expression status. Taken together, ICA reverses the antiosteogenic activity of sclerostin by activating the Wnt/ $\beta$ -catenin signaling pathway.

#### 4. Discussion

The incidence of osteoporotic fractures is steadily increasing due to a globally aging population and is associated with reduced quality of life as well as significant socioeconomic burden [23]. Therefore, it is vital to explore novel treatment options for OP that are highly effective and have minimal side effects. We found that sclerostin inhibited BMSC proliferation and osteogenic differentiation, which was reversed by ICA treatment. ICA not only upregulated osteogenesis-

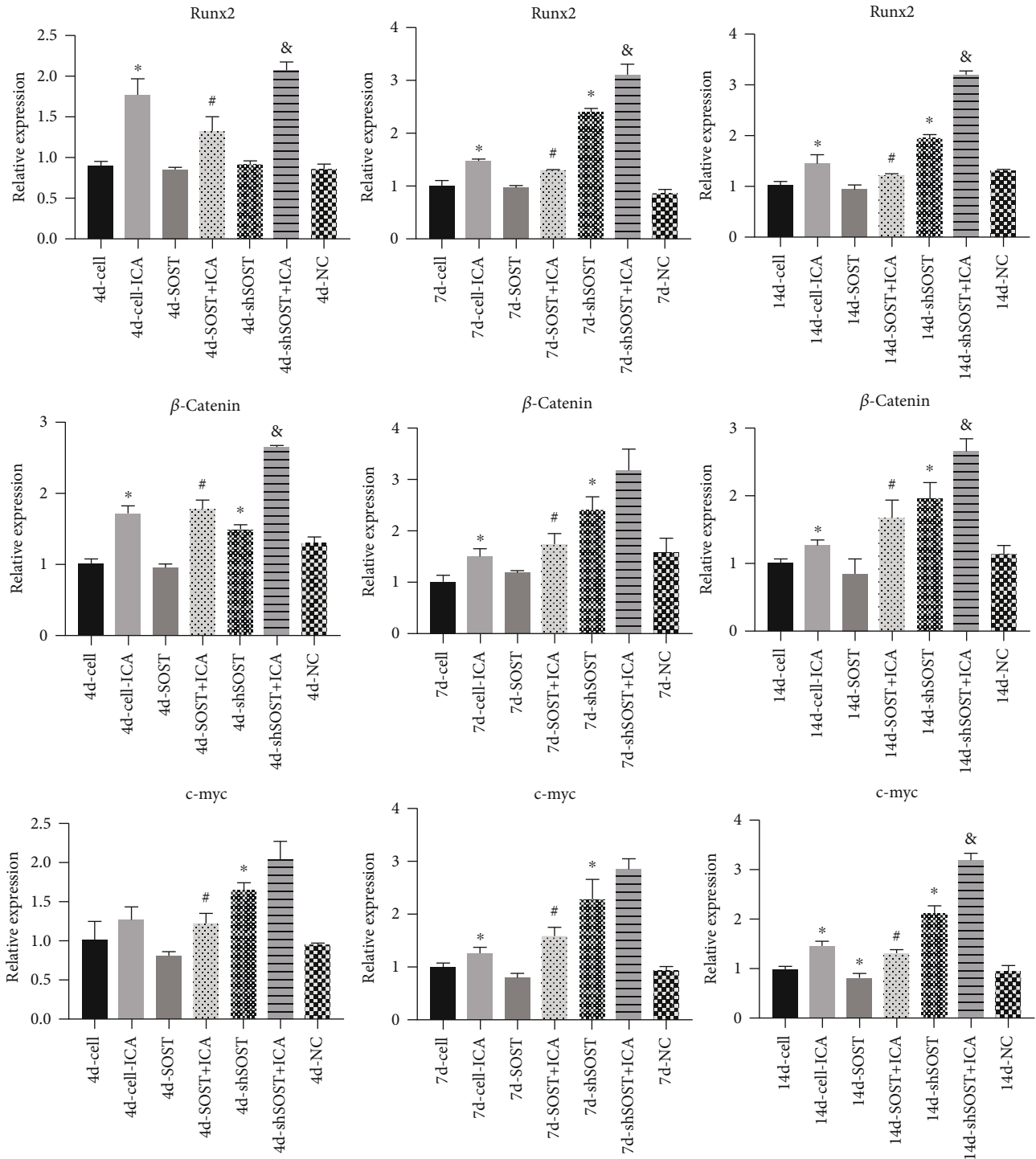


FIGURE 5: The expression of Runx2,  $\beta$ -catenin, and c-myc mRNAs at the different time points (4, 7, and 14 days) of osteogenic induction in the indicated groups. All data are presented as mean  $\pm$  SEM. \* $P$  < 0.05 compared to the control group, # $P$  < 0.05 compared to the sclerostin overexpression group, and & $P$  < 0.05 compared to the sclerostin knockdown group.

related genes including Runx2,  $\beta$ -catenin, and c-myc but also increased the expression of antioxidant factors (Prdx1, Cata, and Nqo1). Furthermore, ICA activated the Wnt/ $\beta$ -catenin pathway in *SOST*-overexpressing BMSCs. Thus, ICA may promote osteogenic differentiation of BMSCs by activating the sclerostin/Wnt/ $\beta$ -catenin signaling pathway.

Sclerostin is secreted by bone cells and inhibits differentiation of osteoblasts [24]. *SOST*<sup>-/-</sup> mice display accelerated bone formation, as well as increased bone mass and strength [25]. Furthermore, blocking sclerostin with specific antibodies can restore bone mass during estrogen deficiency [26]. To the best of our knowledge, this is the

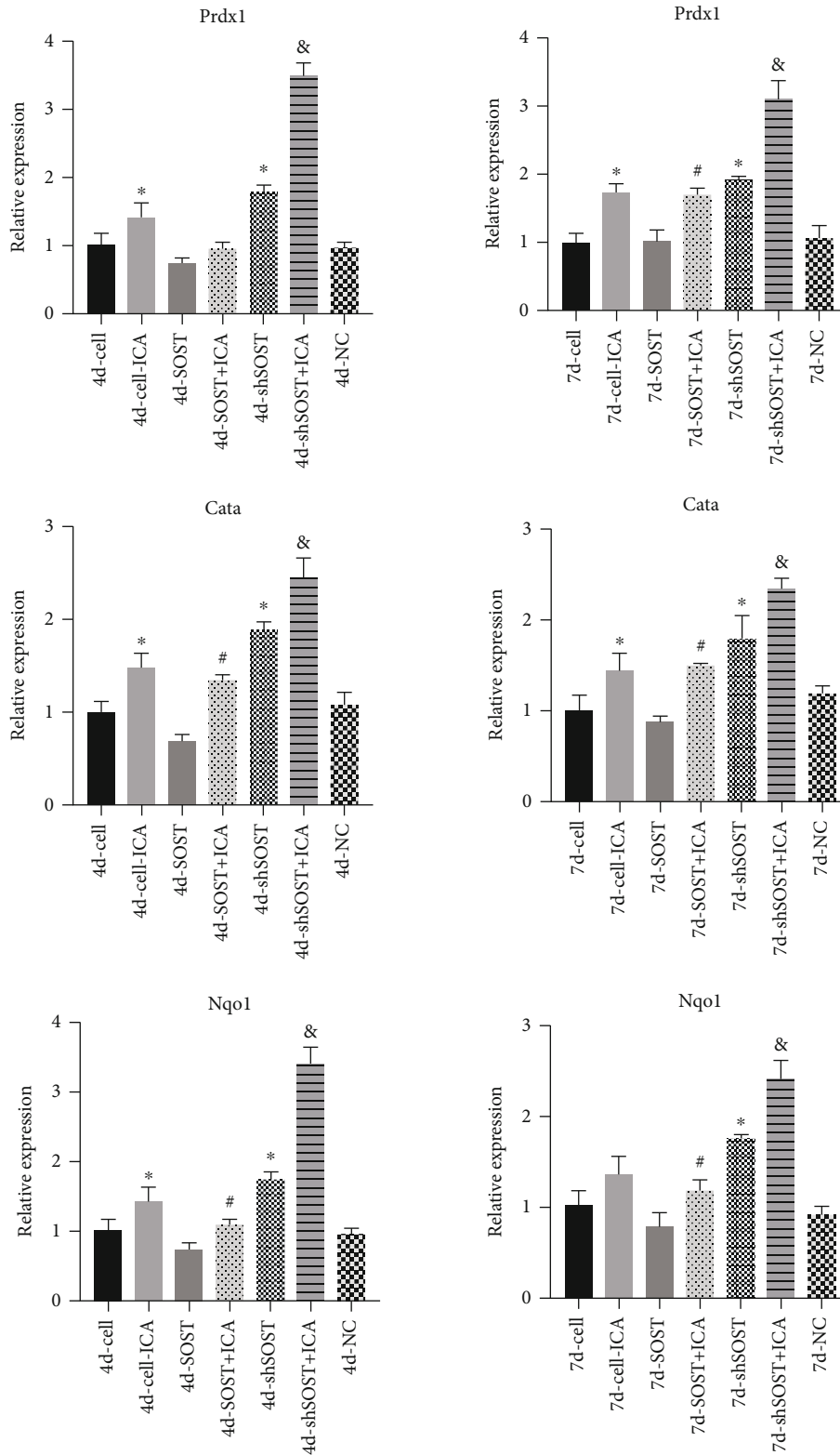


FIGURE 6: Prdx1, Cata, and Nqo1 mRNA levels in the BMSCs at the different time points (4 and 7 days) of osteogenesis in the indicated groups. All data are presented as mean  $\pm$  SEM. \* $P < 0.05$  compared to the control group, # $P < 0.05$  compared to the sclerostin overexpression group, and & $P < 0.05$  compared to the sclerostin knockdown group.

first study to directly assess the role of sclerostin in the osteogenic differentiation of BMSCs *in vitro*. Sclerostin overexpression significantly inhibited the proliferation of

rBMSCs and downregulated osteogenic factors, which was neutralized by ICA, indicating a novel regulatory pathway of osteogenic differentiation.

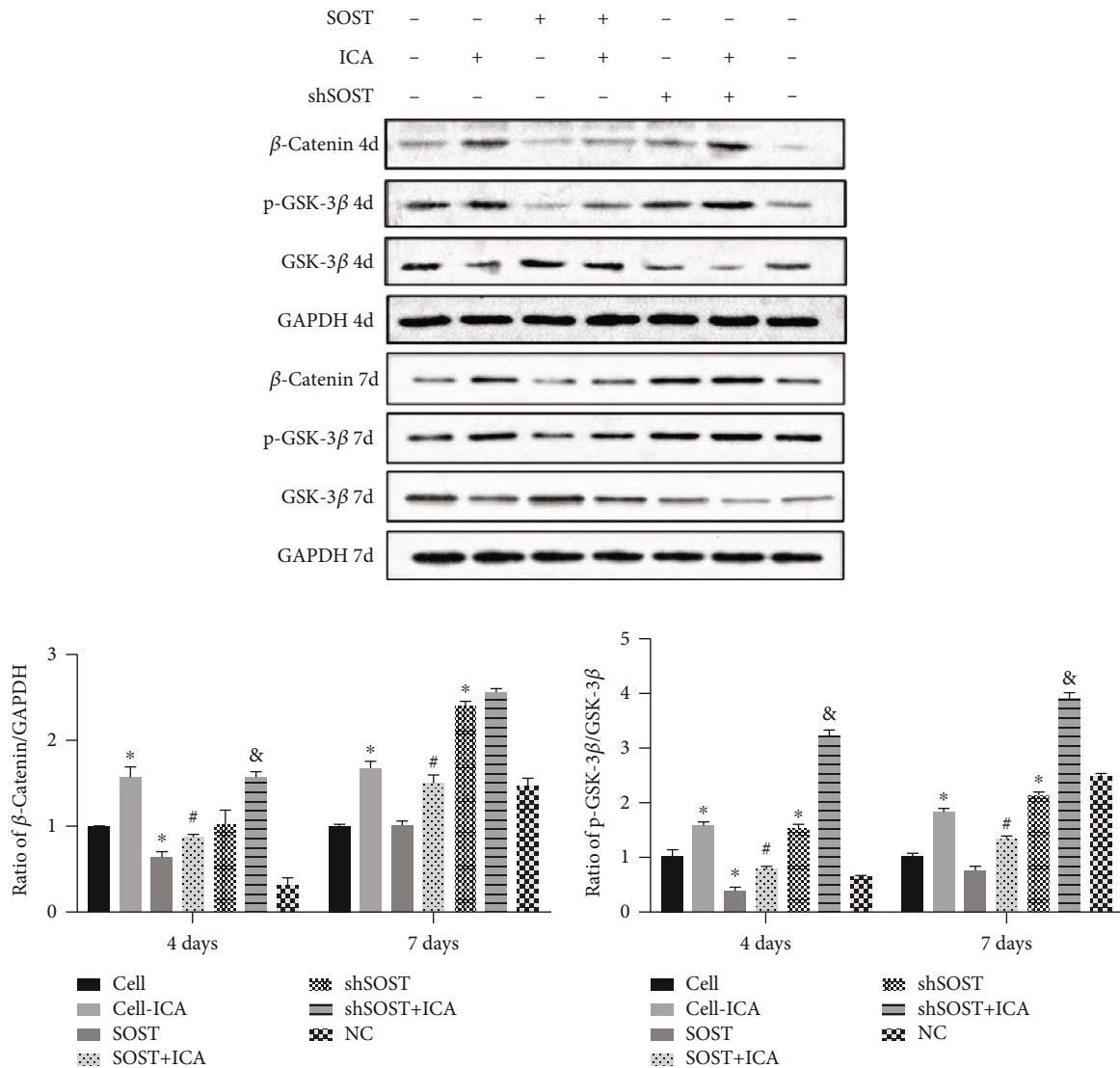


FIGURE 7: Immunoblot showing  $\beta$ -catenin, GSK-3 $\beta$ , and p-GSK-3 $\beta$  protein levels in the BMSCs cultured for 4 and 7 days. All data are presented as mean  $\pm$  SEM. \* $P < 0.05$  compared to the control group, # $P < 0.05$  compared to the sclerostin overexpression group, and & $P < 0.05$  compared to the sclerostin knockdown group.

The transcription factor Runx2 is necessary for osteoblast differentiation and bone formation and is an early indicator of the same [27]. Previous studies have shown that Runx2 induces differentiation and migration of osteoblasts and chondrocytes via the PI3K-Akt signaling pathway [28]. c-myc is a key downstream component of the Wnt/ $\beta$ -catenin pathway and mediates cell proliferation. Indo et al. [29] reported that the inhibition of c-myc in mature osteoclasts reduces bone-resorbing activity and downregulates the neutral amino acid transporter (B0), which in turn suppresses osteoclastogenesis. We found that sclerostin significantly downregulated Runx2 and c-myc, whereas ICA restored the expression of both. Thus, ICA promotes osteogenic differentiation of BMSCs by regulating the expression of sclerostin.

Oxidative stress plays an important role in osteoporosis [30] by accelerating apoptosis of BMSCs, osteoblasts, and osteoclasts as well as promoting the proliferation and differ-

entiation of osteoclasts [31]. Prdx1, Cata, and Nqo1 are antioxidants [32] that clear ROS and suppress oxidative stress [33]. In the present study, sclerostin significantly downregulated the above factors and ICA had the opposite effect, indicating that inhibition of oxidative stress is one of the mechanisms through which ICA may promote osteogenic differentiation of BMSCs.

The Wnt/ $\beta$ -catenin signaling pathway mediates BMSC proliferation and osteoblast differentiation. Following interaction of the Wnt glycoprotein with frizzled (FZD) and low-density lipoprotein receptor-related protein 5/6 (LRP5/6) [34], axin is recruited to the receptor complex and binds to the phosphorylation site of LRP. This leads to complex dissociation and phosphorylation of glycogen synthase kinase 3 $\beta$  (p-GSK3 $\beta$ ), resulting in the cytosolic accumulation of  $\beta$ -catenin and nuclear translocation, eventually leading to the transcriptional activation of the target genes

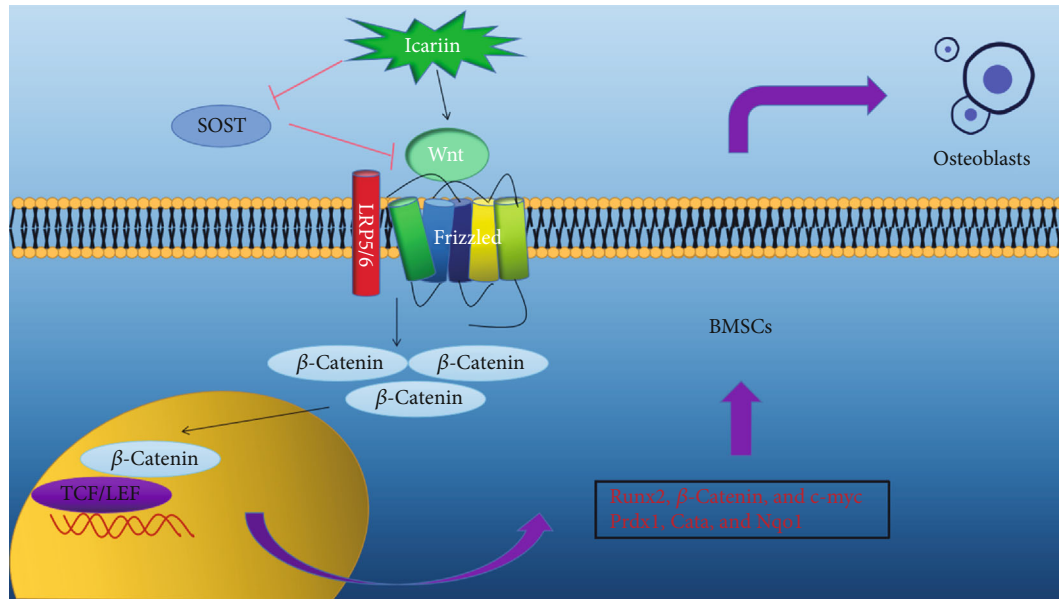


FIGURE 8: Schematic diagram.

[35]. Sclerostin downregulated the expression of  $\beta$ -catenin and p-GSK-3 $\beta$ , which were increased by ICA treatment. Thus, ICA promotes osteogenesis via the sclerostin/Wnt/ $\beta$ -catenin signaling pathway (schematic diagram shown in Figure 8).

## 5. Conclusions

In summary, ICA promotes osteogenic differentiation of BMSCs by inhibiting the action of sclerostin by activating the Wnt/ $\beta$ -catenin pathway. It can potentially enhance the survival and differentiation of transplanted BMSCs in situ and improve the efficacy of BMSC-based regenerative therapy for OP.

## Data Availability

The data used to support the results of this study can be obtained from the corresponding author according to the requirements.

## Conflicts of Interest

All the authors declare they have no competing interests.

## Authors' Contributions

Jianliang Gao and Shouyu Xiang contributed equally to this work.

## Acknowledgments

This work was supported by the National Natural Science Foundation of China (No. 81574002) and Guangzhou Municipal Science and Technology Fund (No. 201704020032).

## References

- [1] K. E. Ensrud and C. J. Crandall, "Osteoporosis," *Annals of Internal Medicine*, vol. 167, no. 3, pp. ITC17–ITC32, 2017.
- [2] I. Reid, "A broader strategy for osteoporosis interventions," *Nature Reviews Endocrinology*, vol. 16, no. 6, pp. 333–339, 2020.
- [3] S. Abtahi, J. H. M. Driessen, P. Vestergaard et al., "Secular trends in major osteoporotic fractures among 50+ adults in Denmark between 1995 and 2010," *Osteoporosis International*, vol. 30, no. 11, pp. 2217–2223, 2019.
- [4] N. B. Watts, J. T. Grbic, N. Binkley et al., "Invasive oral procedures and events in postmenopausal women with osteoporosis treated with denosumab for up to 10 years," *The Journal of Clinical Endocrinology and Metabolism*, vol. 104, no. 6, pp. 2443–2452, 2019.
- [5] P. J. Voss, D. Steybe, P. Poxleitner et al., "Osteonecrosis of the jaw in patients transitioning from bisphosphonates to denosumab treatment for osteoporosis," *Odontology*, vol. 106, no. 4, pp. 469–480, 2018.
- [6] A. Qadir, S. Liang, Z. Wu, Z. Chen, L. Hu, and A. Qian, "Senile osteoporosis: the involvement of differentiation and senescence of bone marrow stromal cells," *International Journal of Molecular Sciences*, vol. 21, no. 1, p. 349, 2020.
- [7] Y. Liu, L. Ming, H. Luo et al., "Integration of a calcined bovine bone and BMSC-sheet 3D scaffold and the promotion of bone regeneration in large defects," *Biomaterials*, vol. 34, no. 38, pp. 9998–10006, 2013.
- [8] Z.-W. Luo, F.-X.-Z. Li, Y.-W. Liu et al., "Aptamer-functionalized exosomes from bone marrow stromal cells target bone to promote bone regeneration," *Nanoscale*, vol. 11, no. 43, pp. 20884–20892, 2019.
- [9] J. Delgado-Calle, A. Y. Sato, and T. Bellido, "Role and mechanism of action of sclerostin in bone," *Bone*, vol. 96, pp. 29–37, 2017.
- [10] K. Maeda, Y. Kobayashi, M. Koide et al., "The regulation of bone metabolism and disorders by Wnt signaling,"

- International Journal of Molecular Sciences*, vol. 20, no. 22, p. 5525, 2019.
- [11] Z. C. Ryan, T. A. Craig, M. McGee-Lawrence, J. J. Westendorf, and R. Kumar, "Alterations in vitamin D metabolite, parathyroid hormone and fibroblast growth factor-23 concentrations in sclerostin-deficient mice permit the maintenance of a high bone mass," *The Journal of Steroid Biochemistry and Molecular Biology*, vol. 148, pp. 225–231, 2015.
  - [12] Y. Liu, X. Wang, H. Chang et al., "Mongolian medicine echinops prevented postmenopausal osteoporosis and induced ER/AKT/ERK pathway in BMSCs," *Bioscience Trends*, vol. 12, no. 3, pp. 275–281, 2018.
  - [13] H. Sheng, X.-f. Rui, C.-J. Sheng et al., "A novel semisynthetic molecule icaritin stimulates osteogenic differentiation and inhibits adipogenesis of mesenchymal stem cells," *International Journal of Medical Sciences*, vol. 10, no. 6, pp. 782–789, 2013.
  - [14] J. Jiang, J. Li, and X. Jia, "The antiosteoporotic activity of central-icaritin (CIT) on bone metabolism of ovariectomized rats," *Molecules*, vol. 19, no. 11, pp. 18690–18704, 2014.
  - [15] A. Yang, C. Yu, F. You, C. He, and Z. Li, "Mechanisms of Zuogui pill in treating osteoporosis: perspective from bone marrow mesenchymal stem cells," *Evidence-Based Complementary and Alternative Medicine*, vol. 2018, Article ID 3717391, 8 pages, 2018.
  - [16] H. Zhao, X. Li, D. Zhang et al., "Integrative Bone Metabolomics–Lipidomics Strategy for Pathological Mechanism of Postmenopausal Osteoporosis Mouse Model," *Scientific Reports*, vol. 8, no. 1, article 16456, 2018.
  - [17] X. Li, J. Zhan, Y. Hou et al., "Coenzyme Q10 Regulation of Apoptosis and Oxidative Stress in H<sub>2</sub>O<sub>2</sub> Induced BMSC Death by Modulating the Nrf-2/NQO-1 Signaling Pathway and Its Application in a Model of Spinal Cord Injury," *Oxidative Medicine and Cellular Longevity*, vol. 2019, Article ID 6493081, 15 pages, 2019.
  - [18] Q. Wei, B. Wang, H. Hu et al., "Icaritin promotes the osteogenesis of bone marrow mesenchymal stem cells via the regulation of sclerostin expression," *International Journal of Molecular Medicine*, vol. 45, no. 3, pp. 816–824, 2020.
  - [19] X.-J. Chen, Y.-S. Shen, M.-C. He et al., "Polydatin promotes the osteogenic differentiation of human bone mesenchymal stem cells by activating the BMP2-Wnt/ $\beta$ -catenin signaling pathway," *Biomedicine & Pharmacotherapy*, vol. 112, article 108746, 2019.
  - [20] Y. Cao, B. Wang, D. Wang et al., "Expression of Sclerostin in Osteoporotic Fracture Patients Is Associated with DNA Methylation in the CpG Island of the SOST Gene," *International journal of genomics*, vol. 2019, Article ID 7076513, 8 pages, 2019.
  - [21] A. Y. H. Ng, Z. Li, M. M. Jones et al., "Regulator of G protein signaling 12 enhances osteoclastogenesis by suppressing Nrf2-dependent antioxidant proteins to promote the generation of reactive oxygen species," *eLife*, vol. 8, 2019.
  - [22] Q. Zhou, L. Zhu, D. Zhang et al., "Oxidative stress-related biomarkers in postmenopausal osteoporosis: a systematic review and meta-analyses," *Disease Markers*, vol. 2016, Article ID 7067984, 12 pages, 2016.
  - [23] P. Alejandro and F. Constantinescu, "A review of osteoporosis in the older adult: an update," *Rheumatic Diseases Clinics of North America*, vol. 44, no. 3, pp. 437–451, 2018.
  - [24] X. Li, M. S. Ominsky, K. S. Warmington et al., "Sclerostin antibody treatment increases bone formation, bone mass, and bone strength in a rat model of postmenopausal osteoporosis," *Journal of Bone and Mineral Research*, vol. 24, no. 4, pp. 578–588, 2009.
  - [25] J. Jürimäe, V. Karvelyte, L. Rimmel et al., "Sclerostin, preadipocyte factor-1 and bone mineral values in eumenorrheic adolescent athletes with different training patterns," *Journal of Bone and Mineral Metabolism*, 2020.
  - [26] S. Thiele, A. Hannemann, M. Winzer et al., "Regulation of sclerostin in glucocorticoid-induced osteoporosis (GIO) in mice and humans," *Endocrine Connections*, vol. 8, no. 7, pp. 923–934, 2019.
  - [27] Q. Yin, J. Wang, Q. Fu, S. Gu, and Y. Rui, "CircRUNX2 through has-miR-203 regulates RUNX2 to prevent osteoporosis," *Journal of Cellular and Molecular Medicine*, vol. 22, no. 12, pp. 6112–6121, 2018.
  - [28] N. Cai, C. Li, and F. Wang, "Silencing of LncRNA-ANCR promotes the osteogenesis of osteoblast cells in postmenopausal osteoporosis via targeting EZH2 and RUNX2," *Yonsei Medical Journal*, vol. 60, no. 8, pp. 751–759, 2019.
  - [29] Y. Indo, S. Takeshita, K.-A. Ishii et al., "Metabolic regulation of osteoclast differentiation and function," *Journal of Bone and Mineral Research*, vol. 28, no. 11, pp. 2392–2399, 2013.
  - [30] C. Cervellati, G. Bonaccorsi, E. Cremonini et al., "Oxidative stress and bone resorption interplay as a possible trigger for postmenopausal osteoporosis," *BioMed Research International*, vol. 2014, Article ID 569563, 8 pages, 2014.
  - [31] K. H. Baek, K. W. Oh, W. Y. Lee et al., "Association of oxidative stress with postmenopausal osteoporosis and the effects of hydrogen peroxide on osteoclast formation in human bone marrow cell cultures," *Calcified Tissue International*, vol. 87, no. 3, pp. 226–235, 2010.
  - [32] Y. Kumar, T. Biswas, G. Thacker et al., "BMP signaling-driven osteogenesis is critically dependent on Prdx-1 expression-mediated maintenance of chondrocyte prehypertrophy," *Free Radical Biology & Medicine*, vol. 118, pp. 1–12, 2018.
  - [33] X. Li, J. Zhan, Y. Hou et al., "Coenzyme Q10 suppresses oxidative stress and apoptosis via activating the Nrf-2/NQO-1 and NF- $\kappa$ B signaling pathway after spinal cord injury in rats," *American Journal of Translational Research*, vol. 11, no. 10, pp. 6544–6552, 2019.
  - [34] Y. Zhu, Y. Wang, Y. Jia, J. Xu, and Y. Chai, "Catalpol promotes the osteogenic differentiation of bone marrow mesenchymal stem cells via the Wnt/ $\beta$ -catenin pathway," *Stem Cell Research & Therapy*, vol. 10, no. 1, p. 37, 2019.
  - [35] L. D. Antika, E.-J. Lee, Y.-H. Kim et al., "Dietary phlorizin enhances osteoblastogenic bone formation through enhancing  $\beta$ -catenin activity via GSK-3  $\beta$  inhibition in a model of senile osteoporosis," *The Journal of Nutritional Biochemistry*, vol. 49, pp. 42–52, 2017.